The Holistic Analysis of Gamma-ray Spectra in Instrumental Neutron Activation Analysis

Menno Blaauw

The Holistic Analysis
of Gamma-ray Spectra
in
Instrumental Neutron
Activation Analysis

Menno Blaauw

The Holistic Analysis
of Gamma-ray Spectra
in
Instrumental Neutron
Activation Analysis

(met een samenvatting in het Nederlands)

Proefschrift   .

ter verkrijging van
de graad van doctor aan
de Technische Universiteit Delft,
op gezag van de Rector Magnificus,
prof. ir. K.F. Wakker, in het openbaar
te verdedigen ten overstaan van een
commissie aangewezen door het
College van Dekanen op maandag 15 november 1993
te 16.00 uur door

Menno Blaauw   .

doctorandus in de natuurkunde
geboren te Utrecht

Dit proefschrift is goedgekeurd door
de promotoren: prof.dr.ir. M. de Bruin en prof.dr.ir. W. Lourens

.

Dirk Gently: "I believe, as you know, Mrs Sauskind, in the fundamental interconnectedness of all things. Furthermore, I have plotted and triangulated the vectors of the inter-connectedness of all things and traced them to a beach in Bermuda which it is therefore necessary for me to visit from time to time in the course of my investigations. I wish it were not the case, since, sadly, I am allergic to both the sun and rum punches, but then we all have our crosses to bear, do we not, Mrs Sauskind?"

(Douglas Adams, Dirk Gently's holistic detective agency, Pan Books, 1987)

Opgedragen aan Corine en ter nagedachtenis aan haar vader Wim

.

Contents

Chapter 1
General Introduction

1.1. Introduction to Neutron Activation Analysis

Activation analysis is a method to measure amounts of chemical elements, irrespective of their chemical and physical state. Stable nuclides in the sample are activated to radionuclides by irradiation with high energy photons or various types of particles (e.g. neutrons, protons, deuterons). Gamma-ray spectrometry can subsequently be used for the simultaneous measurement of the activities of different radionuclides. Knowing which radionuclides are the result of the activation of the elements, the identity of the radionuclide indicates which element was activated, and its activity is a measure of the amount of the element present in the sample.

In Neutron Activation Analysis (NAA), neutron radiation is used to convert the nuclei in the sample. A distinction is made between instrumental neutron activation analysis (INAA), where the sample is irradiated and measured directly, and radiochemical neutron activation analysis (RNAA), where the sample is subjected to chemical separations prior to the activity measurement.

The subject of this thesis is INAA with a nuclear reactor as a source of neutrons.

1.2. Theoretical introduction to INAA

1.2.1. Activation

Each nucleus can capture a neutron during irradiation. Directly after the capture, particles and excess energy in the form of kinetic energy of the particles and/or photons may be emitted. The most common reaction used in NAA is the (n,γ)-reaction, where only photons are emitted, but (n,n')-, (n,p)-, (n,α)- and (n,2n)-reactions are important as well. Some nuclei, e.g. ^{235}U, are fissionable by neutron capture (the (n,f)-reaction), yielding the so-called fission products.

The probability of a nucleus capturing a neutron is the neutron capture cross section, expressed in m^2 or barns (1 barn = 10^{-28} m^2). It depends on the reaction involved and the energy of the neutron. (n,f)- and (n,γ)-reactions in general have the highest cross section for slow neutrons (energies of less than 1 eV), whereas the other, so-called threshold reactions mainly occur with fast neutrons (energies of 1 MeV or higher).

The probability R of a nucleus capturing a neutron in a unit of time is given by

$$R = \int_0^\infty \sigma(v) \Phi(v) dv \qquad (1.1)$$

where

v = the neutron velocity [m.s⁻¹];

$\sigma(v)$ = the neutron cross section [m²] for neutrons with velocity v;

$\Phi(v)$ = the neutron density [m⁻³] of neutrons with velocities between v and $v+dv$, considered to be constant in time.

For a specific type of neutron source, it is sometimes possible to simplify this relationship using so-called conventions, where $\sigma(v)$ and $\Phi(v)$ are characterized by only a few parameters.

Nuclear research reactors are the most intense sources of thermal neutron radiation available to perform NAA with. The energy distribution of the neutrons released by the fission of ^{235}U ranges from 1 to 25 MeV with a maximum at 2 MeV. In a thermal fission reactor, these so-called fission or fast neutrons are slowed down by interaction with a moderator (H_2O, D_2O, graphite) to enhance the probability of them causing another fission reaction. After sufficient interaction, they reach thermal equilibrium with the moderator. The energy distribution of the thermal neutrons is Maxwellian with a maximum of 0.025 eV at room temperature. Neutrons in the process of slowing down are called epithermal neutrons. Several conventions, e.g. the Høgdahl[1,2] and the Westcott[3] convention, are available to describe the (n,γ) reaction rate for the neutron energy distribution as obtained from these reactors.

If the neutron flux can be considered homogeneous over the volume of the sample, the rate $(dN_1/dt)_{act}$ of production of activated nuclei is approximated by

$$(\frac{dN_1}{dt})_{act} = RN_0 \qquad (1.2)$$

N_0 = the number of target nuclei in the sample

N_1 = the number of activated nuclei in the sample

This approximation is valid only if the number of target nuclei does not significantly decrease during irradiation, i.e. $N_0(t) = N_0$. For most reactions, neutron fluxes and irradiation durations, this so-called burnup is negligible. Also, the neutron flux may significantly decrease from the outside to the centre of the sample because of absorption of neutrons in the sample itself. This effect is called self-shielding.

1.2.2. Decay

The nucleus that has captured a neutron may have become unstable. This means that it has a constant probability λ per unit of time to transform spontaneously into

another, possibly stable nucleus. The rate $(dN_l/dt)_{dis}$ of disintegration of unstable nuclei is given by

$$(\frac{dN_l(t)}{dt})_{dis} = -\lambda N_l(t) \qquad (1.3)$$

where
λ = the probablity of disintegration per unit time [s^{-1}].
The half life $t_{1/2}$ and the decay probability λ are related as follows:

$$\lambda = \frac{\ln(2)}{t_{1/2}} \qquad (1.4)$$

where
$t_{1/2}$ = the time that must elapse before half of the nuclei has disintegrated [s].

The simultaneous occurence of activation and decay during irradiation is described by

$$\frac{dN_l(t)}{dt} = (\frac{dN_l(t)}{dt})_{act} + (\frac{dN_l(t)}{dt})_{dis} = RN_0 - \lambda N_l(t) \qquad (1.5)$$

and the number of activated nuclei present after irradiation time t_{ir} is approximated by

$$N_l(t_{ir}) = \frac{RN_0}{\lambda}(1 - e^{-\lambda t_{ir}}) \qquad (1.6)$$

After irradiation, the number of activated nuclei will decrease exponentially in time. The number of activated nuclei $N_l(t_d)$ present at the start of the measurement is given by

$$N_l(t_{ir},t_d) = \frac{RN_0}{\lambda}(1 - e^{-\lambda t_{ir}})(e^{-\lambda t_d}) \qquad (1.7)$$

where
t_d = the decay time, i.e. the time between irradiation and measurement.

The representation given here is correct only for the simplest of cases. In practice, complications may arise e.g. if the number of activated nucleus decreases not only by decay but also by significantly capturing neutrons, or if the activated nucleus decays to another unstable nucleus of which the activity is measured. Also, the neutron flux must be constant in time and homogeneous over the volume of the sample.

1.2.3. Measurement

As a result of the irradiation with neutrons, a mixture of radionuclides is formed in the sample. The nuclei may disintegrate by alpha-decay, beta-decay and/or electron capture. In each case, photons (gamma-radiation, X-radiation) may be emitted. Because the photons emitted have discrete energies which usually are characteristic for the decaying nucleus and can pass through matter without energy degradation, gamma-ray spectrometry is the method of choice to detect and identify the disintegrating nuclei. For this purpose, Ge semiconductor detectors are used that convert the energy deposited by an incident photon to an electric pulse of proportional height. The pulse heights are digitized, classified according to their heights and counted, resulting in a histogram, showing both gamma- and X-ray signals, which is called a gamma-ray spectrum.

The number of nuclei ΔN_l disintegrating during the measurement is given by

$$\Delta N_l(t_{ir}, t_d, t_m) = \frac{RN_0}{\lambda}(1 - e^{-\lambda t_{ir}})(e^{-\lambda t_d})(1 - e^{-\lambda t_m}) \tag{1.8}$$

where

t_m = the duration of the measurement.

The resulting net area A of the so-called photopeak for a given photon energy in the spectrum is approximated by

$$A = \Delta N_l \gamma \epsilon \tag{1.9}$$

where

γ = the gamma-ray abundance, i.e. the probability of the disintegrating nucleus emitting a photon of this energy;

ϵ = the photopeak efficiency of the detector, i.e. the probability of the emitted photon contributing to the photopeak in the spectrum.

Allthough the photons emitted by decaying nuclei have detectable energies ranging from tens of keVs to MeVs and have high penetrating power, they can be absorbed or scattered in the sample itself, depending on sample size and composition. This effect is called self-absorption. Also, two or more photons may simultaneously deposit energy in the detector. This effect is called summation, and is discussed in Chapter 9.

The approximation given above is valid only if both summation and self-absorption can be neglected.

1.2.4. Analysis of INAA gamma-ray spectra

The analysis of gamma-ray spectra as obtained in INAA can be considered to consist of spectrum reduction, standardization and spectrum interpretation.

The high energy resolution of the Ge detectors allows for the conversion of the spectrum to a list of photopeak energies and net areas. The energies identify the radionuclides, the net areas are proportional to the amounts of the elements present in the sample. This reduction of the spectrum is performed in two steps: First, the peaks in the spectrum are located. Second, the peaks are fitted to empirical shape functions to obtain their energies and net areas.

Standardization is the determination of the proportionality factors that relate the net peak areas in the spectrum to the amounts of the elements present in the sample. The standardization method best suited for multi-element analysis with INAA is the single comparator method, as will be explained in Chapter 5. In all single comparator methods, a k-factor[4] is defined which is a dimensionless compound physical parameter that can be thought of as the ratio of sensitivities for the element of interest and the comparator element. Each k-factor refers to a pair of peaks: one peak representing the comparator element and one representing the element of interest. The ratio of the two peak areas is used to calculate the concentration from.

The process of identifying the elements contributing to the spectrum and computing their concentrations is called the interpretation of the spectrum. The process is complicated by different radionuclides emitting photons with undistinguishable gamma-ray energies, and by different elements yielding the same radionuclides when activated.

1.3. Historical development of NAA

Georg von Hevesy and Hilde Levi introduced neutron activation analysis as a method for the quantitative determination of element concentrations as early as 1936[5]. The relatively weak neutron sources available at the time, however, limited the possibilities of the method. Element specificity was obtained through chemical separations and decay curve analysis. Twenty years later, nuclear research reactors became available as intense sources of activating radiation and the detection limits of activation analysis reached the mg/kg and μg/kg levels.

This development opened up an entirely new field of investigation: the properties of elements present at very low concentrations. The availability of the analysis technique stimulated research in various fields such as chemistry, solid state physics, biology and environmental science. Other trace element analysis techniques such as Atomic Absorption Spectrometry (AAS), Proton Induced X-ray Emission (PIXE) and recently Inductively Coupled Plasma Mass Spectrometry (ICP/MS) and Atomic Emission Spectroscopy (ICP/AES) were developed since.

In the early sixties, the development of neutron activation analysis was strongly accelerated when NaI(Tl) gamma-ray detectors and multichannel pulse-height

analyzers became available. Now, it was possible to obtain gamma-ray spectra with high efficiency and moderate energy resolution which allowed for the simultaneous determinination of the activities of different radionuclides and rendered some chemical separations superfluous.

Around 1970, germanium semiconductor detectors and programmable minicomputers were introduced. The energy resolution of the Ge detectors was much better than that of the NaI(Tl) detector and the computer was used to determine the net peak areas in the gamma-ray spectrum and calculate concentrations from these. Chemical separations were less necessary except when the lowest possible detection limit was required.

On several occasions, such as the Modern Trends in Activation Analysis Conference in Vienna, 1991, it was stated that NAA is the best analysis technique for solid samples[6]. It has the following strong points to offer:
- independence of chemical and physical state
- low detection limits for many elements, including the halogens for which ICP/MS is not very sensitive
- simplicity of sample preparation for solid samples: No dissolution and thus little risk of loss or contamination
- virtually no matrix effects

RNAA is important still because of its very low detection limits (down to the ppt level for some elements)[7], at the expense, however, of multi-element capability. It also requires more labour, time and facilities than INAA.

1.4. Developments at the Interfaculty Reactor Institute

Beginning in the sixties, developments in INAA have always been closely followed or even initiated at the Interfaculty Reactor Institute. By 1975, this had resulted in an automated system for INAA that could be used by laymen after a short training period[8]. The system was based on the use of zinc as a single comparator element. By 1980, irradiations could be performed at two irradiation facilities. One was especially suited for short irradiations (up to 30 seconds) and consecutive short measurements, the other for long irradiations (up to four hours). Several fully automated gamma-ray spectrometers with sample changers were available for the longer measurements. One of these spectrometers comprised a well-type detector. The spectrometers were controlled by a central PDP-9 computer using a CAMAC interface. All software needed was developed in-house, including administrative and bookkeeping software. The most important program, that performed the spectrum analysis, was ICPEAX[8].

Up to 1988, the system was not changed essentially. Attention was directed to the applications of the technique in the applied fields of biology, environmental studies and geology. More terminals and spectrometers were added, and the sample through-put increased to several thousands per year. The PDP-9 was replaced by a PDP-11 computer, but after a few years even the PDP-11 was no longer powerful enough to perform all its tasks.

The CAMAC interface was considered to be unnecessarily complicated. There were too many single points of failure in the system, resulting in loss of valuable counting time.

The mostly undocumented FORTRAN software did not allow for improvements or extensions. The ICPEAX program could only analyze one spectrum of a sample at a time. The combination of the results from different spectra pertaining to one sample required considerable knowledge from the analyst. Changes in the reactor core that would partly invalidate the nuclear catalogues of the single comparator method obtained by calibrations at IRI were foreseen. A new irradiation facility for very large samples (up to 50 kg) was planned. Analysis of the gamma-ray spectra obtained from these samples would require substantial additions to the software.

It was therefore decided to modernize the system, replacing both computer hard-ware and software completely. Between 1988 and 1991, the single PDP-11 computer was replaced by networked, interchangeable UNIX workstations. The single CAMAC interface was replaced by independent interfaces servicing one spectrometer each. The non-interactive ICPEAX program that performed the complete analysis of a single spectrum was replaced by separate interactive programs, each allowing the analyst to view the intermediate results. The possibilities of the analyst to influence the outcome of the analysis were minimized, but on the other hand the amount of information available to the analyst was maximized. The combination of analysis results from different spectra of the sample was automated.

1.5. Scope of the present study

This thesis describes the scientific aspects of the analysis software written for the new automated system for INAA at IRI. Its scope is limited to the computerized analysis of gamma-ray spectra as obtained with Ge detectors in INAA with a research reactor as a source of neutrons. The analysis of gamma-ray spectra is considered to consist of reduction, standardization and interpretation. The standardization com-prises the theoretical modelling of the processes occurring during activation and measurement, indicated in preceding paragraphs.

At IRI, only low Z samples with weights in the order of 100 mg are routinely analyzed, e.g. plastics, geological and biological materials. For these samples, self-

shielding is negligible. Furthermore, for photon energies above 100 keV, self-absorption can also be neglected. Therefore, only peaks in the 100 keV to 4 MeV range are interpreted, and both self-shielding during activation and self-absorption during measurement are considered to be negligible.

No attention is paid to activation and measurement procedures. Implementation specific information is provided only when necessary.

I.6. Aims of the present study

INAA has on many occasions proven to be a potentially accurate technique for trace element analysis because of the simplicity of the sample preparation and the physical basis of the technique. Intercomparisons however reveal large discrepancies between the results obtained by different laboratories[9]. Several possible causes for these discrepancies are examined and remedies looked for in this work.

One of the causes may be the treatment of spectral interferences (two elements contributing to the same peak in the gamma-ray spectrum). Most INAA protocols are based on activity and subsequent concentration calculations from pairs of characteristic peak areas (the "characteristic peak method"): One peak from the gamma-ray spectrum of the sample, one from the spectrum of the comparator. Interferences may go unnoticed because the presence or absence of other peaks in the spectrum is disregarded.

In the present study, an attempt is made to interpret *all* peaks in the spectra obtained from a sample at once. The principles of this "holistic" approach are the following:

The net peak areas in the reduced gamma-ray spectra are proportional to the element concentrations. Therefore, the interpretation of gamma-ray spectra mathematically is the solving or fitting of a system of linear equations. Each element concentration is an unknown, and each peak area yields an equation. Usually, many more equations than unknowns are available. The standard method to deal with such systems of equations is the linear least squares (LLS) method. Several requirements must be fulfilled before the LLS method for the interpretation of gamma-ray spectra can be attempted. First, the net peak areas in the spectra must be determined: the spectra must be reduced. Second, the proportionality factors relating the peak areas to the element concentrations must be known for all peaks to be expected in the spectra. Third, the measured peak areas and the expected peaks must be matched. This is not a trivial step because, in general, not all expected peaks will be detected in the measured spectrum, even if the corresponding element is present in the sample. Estimates for the upper limits of the areas of undetected peaks must be provided.

The attribution of a peak to an element is performed taking into account the presence or absence of other peaks to be expected from the same element. This is why the complete spectra to be expected from each element must be known prior to the interpretation of the measured spectra. In this respect, the "holistic" approach differs from the commonly applied approaches.

Part I: Reduction of gamma-ray spectra

The properties of the peak search filter used to find the photopeaks in the spectrum must be known to determine the detection limits of INAA as a whole. In Chapter 3, several peak search filters currently in use are discussed and compared. The properties of the filter that was selected were measured and modelled.

No attempts were made to find new techniques for the fitting of single peaks to the shape function. Nevertheless, an overview of the techniques used is given in Chapter 4.

A multiplet is a group of overlapping photopeaks in a gamma-ray spectrum. Another cause of intercomparison discrepancies may be the deconvolution of these multiplets. Most gamma-ray spectrum reduction software packages attempt to determine the positions and areas of all photopeaks constituting a multiplet, but prominent researchers in this field, like Aarnio, have given up hope[10]: "No auto-mated procedure is capable of doing complex analysis and giving correct answers". The deconvolution process may inherently lead to unstable results because it attempts to retrieve information that is physically lost. Not deconvoluting multiplets, on the other hand, will increase the number of spectral interferences and reduce the number of equations to be subjected to the LLS fit. In Chapter 4, an interactive procedure for the determination of the net area of a multiplet as a whole by integration is described.

Part II: Standardization

The proportionality factors relating the peak areas to the element concentrations depend on many experimental parameters. To compute the proportionality factors, the dependence on all these parameters must be known.

The rates of all activation reactions taking place during irradiation must be known. In the past, these rates were all measured relative to the activation rates of the single comparator element zinc at IRI. The resulting k_{Zn}-factors, however, only applied to specific irradiation facilities and spectrometers, and may be sensitive to changes in the reactor neutron energy distribution resulting from e.g. xenon poisoning and core modifications. Laboratories not being able to compare their sets of k-factors may also contribute to the intercomparison discrepancies. A solution was presented in 1975 in the form of the k_0 method[11]. This method offered versatility with respect to both irradiation facilities and detectors. Thus another aim of the present work was to

make the transition to the k_0 method. It was necessary to revise the k_0 method in order to make it more generally applicable, especially to gamma-ray spectrometry with highly efficient detectors. The changes and extensions are discussed in Chapter 6, 7 and 10.

In Chapter 8, a comparison between the recently published k_0 constants[12] and the previously determined constants at IRI is presented.

The k_0 method provides k-factors only for the most important peaks to be expected from each element. For the holistic analysis method, however, all peaks to be expected from all radionuclides resulting from neutron activation must be known. In case of detectors with moderate efficiencies, these can easily be obtained from literature. For highly efficient detectors, however, the relation between radionuclide activity and measured peak area is less simple due to coincidence summing.

Well-type detectors are the only highly efficient gamma-ray detectors without much counting geometry sensitivity. Still, they are rarely used for single comparator INAA because of the coincidence summing effects. The attempts to bridle these and make the use of well-type detectors feasible for single comparator INAA are presented in Chapter 9.

The dependence of the proportionality factors on activation, decay and measuring times must also be known. This dependence can be very complicated. A generally applicable computer algorithm, developed for this purpose, is presented in Chapter 10.

Part III: Interpretation of gamma-ray spectra

The methods used to match the measured and expected peaks and to solve or fit the resulting system of linear equations by LLS methods are described in Chapter 13. The results of an experimental comparison between the holistic interpretation method and the more commonly used "characteristic peak" interpretation method are presented in Chapter 13.

The unstability of the interpretation results based on multiplet deconvolution as compared to integration was experimentally tested. The results are presented in Chapter 14.

The hypothesis that the holistic approach more than compensates for the loss of information resulting from not deconvoluting multiplets was tested by an experimental comparison of the performance of the holistic analysis method, not deconvoluting multiplets included, and the performance of the ICPEAX analysis program. The results are presented in Chapter 15.

1.7. References

1. O.T. Høgdahl, Neutron Absorption in Pile Neutron Activation Analysis, Rept. MMPP-226-1, 1962
2. O.T. Høgdahl, Proc. Symp. Radiochemical Methods of Analysis, Salzburg 1964, IAEA, Vienna, 1965.
3. C.H. Westcott, J. Nucl. Energy, 2 (1955) 59
4. F. Girardi, G. Guzzi, J. Pauly, Anal.Chem., 37/9 (1965) 1085
5. G. Hevesy, Hilde Levi: "The action of neutrons on the rare earth elements", Det Kgl. Danske Vidanskabernes Selskab, Mathematish-fysiske Meddelelser 14, 5 (1936) 1-34.
6. V. Krivan. "The position of Activation Analysis among other Trace Element Analysis Methods today." Proc. 8th Int. Conf. on Modern Trends in Activation Analysis, J. Radioanal. Nucl Chem. (in press)
7. J.J.M. de Goeij, J.R. Woittiez, J. Radioanal.Nucl.Chem. 168 (1993) 429-437
8. M.de Bruin, P.J.M.Korthoven, Anal.Chem. 44 (1972) 2382-2385
9. R.M.Parr, *Intercomparison of Minor and Trace Elements in IAEA animal Bone*, IAEA Progress Report, Vienna, 1982.
10. P.A.Aarnio, M.T.Nikkinen, J.T.Routti, "Sampo 90, High Resolution Interactive Gamma Spectrum Aanlysis Including Automation with Macros", report TKK-F-A682, Helsinki University of Technology, 1991.
11. A.Simonits, F.De Corte, J.Hoste, J.Radioanal.Chem. 24 (1975) 31

Part I

Reduction of
Gamma-ray Spectra
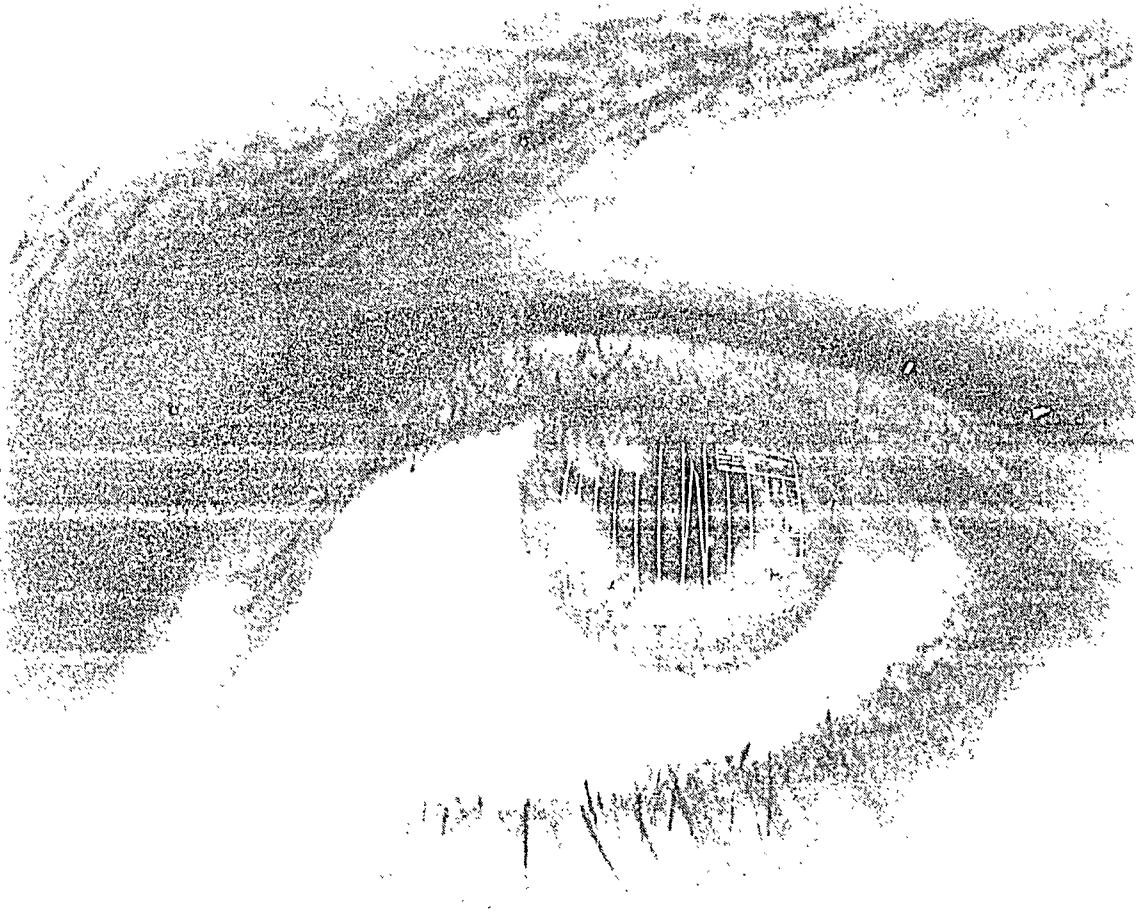
Chapter 2
Introduction to Spectrum Reduction

2.1. Introduction to gamma-ray spectrometry with Ge detectors

The aim of gamma-ray spectrometry in NAA is to measure the energies and intensities of the photons emitted by the radionuclides. To obtain this information from a gamma-ray spectrum, the response function of the spectrometer for these photons must be known.

The gamma-ray spectrometers used consist of a radiation detector, electronic signal processing units and a digital memory. In the detector, the energies deposited by individual photons are converted into electronic signals of proportional size. The response function of a detector, i.e. the pulse height distribution obtained when measuring mono-energetic photons, is determined by the different mechanisms involved in the interactions between photons and detector material. The contributions of photo-effect, Compton interaction and pair production to the response function are indicated in Fig.2.1. In practice, the response function is complicated further by secondary effects occurring in the spectrometer (summation and pile-up) and in the material surrounding the detector or in the sample itself (fluorescence, scattering and pair production followed by annihilation). For more information, the reader is referred to G.F.Knoll's book on radiation detection and measurement[1]. In this thesis, peaks resulting from full absorption of the photon, as well as escape peaks and sum peaks are called photopeaks.

Summation is the simultaneous detection of two or more photons, resulting in so-called sum peaks if both their energies are deposited completely. If the summation is the result of the detection of photons emitted in cascade by a single decaying nucleus, it is called coincidence or cascade summing, otherwise it is called random summing. More about coincidence summing can be found in Chapter 9.

The detector signals are amplified and shaped in suitable pulse amplifiers and digitized individually by an analogue to digital converter (ADC). The digitized information is collected in a memory as a pulse-height distribution.

The influence of several sources of noise in the spectrometer and stochastic processes in the detector crystal can be modelled as a convolution of the entire spectrum with a Gaussian function. As a result, photopeaks have a more or less Gaussian shape and may overlap.

Most of the radionuclides produced by neutron activation emit beta-radiation. This radiation generally does not reach the detector crystal because of its low

penetrating power. However, interactions within the sample may nevertheless contribute to the gamma-ray spectrum:

Beta+-Radiation is converted to gamma-radiation by annihilation. Two photons with energies of 511 keV are the result. One or both photons may subsequently contribute to the area of the 511 keV photopeak in the spectrum.

Beta- and beta+-Radiation are decelerated when passing through matter, leading to so-called Bremsstrahlung. Bremsstrahlung shows up as a continuum in the lower part of the gamma-ray spectrum. The higher the average Z of the material that stops the beta particle, the higher the average energy of the resulting photons. If the beta
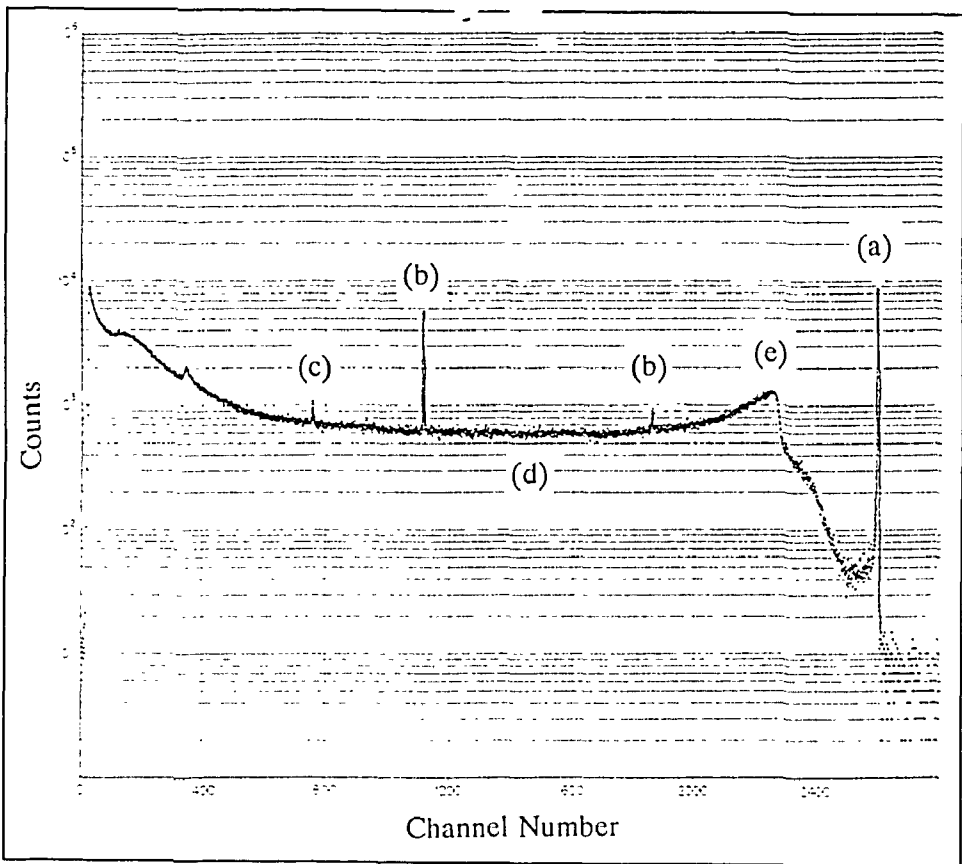
Fig.2.1. γ-Ray spectrum of ^{28}Al, showing (a) the full energy photopeak, (b) the two pair peaks, (c) the annihilation peak, (d) the Compton continuum and (e) the Compton edge

emission occurs simultaneously with the emission of photons by the decaying nucleus,

the Bremsstrahlung may be detected simultaneously with the photon. As a result, the photon may not contribute to the photopeak area.

The processing of the electronic signals takes time (in the order of 1 μs). During this so-called dead time, the spectrometer cannot register other pulses. In the IRI system, dead time is monitored using a pulser that generates an artificial peak in a part of the spectrum where no other peaks are expected. The number of counts missing from the pulser peak area is a measure of the dead time.

It should be noted that the word "background" is confusingly used for two different phenomena in gamma-ray spectrometry: Both the continuum in the gamma-ray spectrum and the gamma-ray spectrum obtained without a radioactive sample are denoted by this term. In this thesis, the first is called the continuum and the second the background.

2.2. Description of the problem

Ideally, a gamma-ray spectrum would be a histogram with non-zero channel contents only in the channels corresponding to photon energies. The position of such a peak would indicate the radionuclide and its area would be a measure of the number of disintegrated nuclei. In practice, the processes mentioned in the previous section deteriorate the measured spectrum. The process of restoring the ideal spectrum from the measured spectrum could be called "spectrum analysis", but this is commonly understood to also encompass the quantitative interpretation of the spectrum. The term "spectrum reduction" indicates that
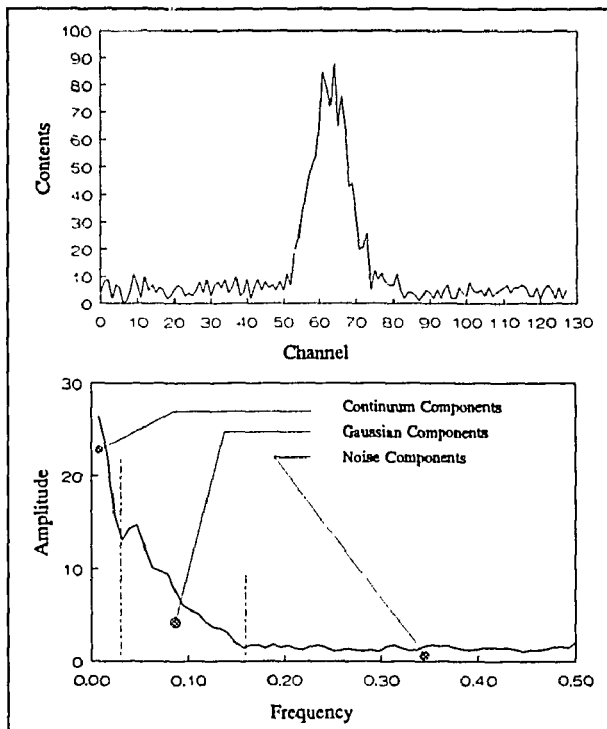
Fig.2.2: Section of γ-ray spectrum and its Fourier transform

the final result of the restoration process is a list of peak energies and areas which usually can be represented much more compact than the measured spectrum itself.

Some of the physical processes deteriorating the measured spectrum cause photopeaks to appear in the spectrum that do not correspond directly to an emitted photon energy (pair production, summation, annihilation). Other processes cause counts to appear in wide ranges of channels (the Compton effect, Bremsstrahlung). Finally, all spectrometer components contribute to the widening of the peaks in the measured spectrum. The resulting shape of the photopeaks is approximately Gaussian.

In terms of Fourier frequencies, it can be said that a gamma-ray spectrum is composed of frequency components in three zones of the Fourier spectrum: The first zone is dominated by the low frequencies present in the spectrum due to Compton interaction and Bremsstrahlung. These components represent channel contents slowly changing as a function of channel number. The second zone is dominated by the intermediate frequencies corresponding to the Gaussian photopeaks. The third zone contains high frequencies due to the fact that all channel contents in the spectrum vary according to the Poisson distribution. This Poisson noise is equally present in all Fourier frequencies, but only dominates in the high frequency zone (Fig.2.2).

In the past, when NaI(Tl) scintillation detectors where used for gamma-spectrometry, the first and the second zone where not clearly separated due to the poor energy resolution of these detectors. This forced the spectrum reduction process to deal with all effects at once, except for the Poisson noise that could be eliminated by smoothing.

The Ge semiconductor detector with its high energy resolution allows for the use of the domination of a frequency zone by the Gaussian photopeaks. Apart from the Poisson noise, the spectrum can be treated as some continuum without high-frequency components, upon which Gaussian photopeaks are superposed.

2.3. Mathematical representation of the problem

The influence of the spectrometer on the "ideal" spectrum can be modelled as a convolution with a so called Point Spread Function (PSF). If the original spectrum can be represented by

$$y(x) = \sum_i A_i \delta(x - p_i) \tag{2.1}$$

where
$y(x)$ = the channel content of channel x
A_i = the area of peak i
p_i = the position of peak i

$\delta(x)$ = the impulse function (Dirac function),

then the measured spectrum can be represented by

$$y(x) = continuum + \sum_i \int_{-\infty}^{\infty} A\delta(\tau - p_i) \, PSF(x-\tau) \, d\tau \tag{2.2}$$

If the Point Spread Function is defined as

$$PSF(x) = \frac{1}{\sigma\sqrt{2\pi}} e^{\frac{-x^2}{2\sigma^2}} \tag{2.3}$$

then the measured spectrum can be represented by

$$y(x) = continuum + \sum_i \frac{A_i}{\sigma\sqrt{2\pi}} e^{\frac{-(x-p_i)^2}{2\sigma^2}} \tag{2.4}$$

which is a superposition of Gaussians on the continuum.

2.4. Methods of solving the problem

The logical way to calculate the original A_i and p_i from the measured spectrum would be to find the inverse of the PSF and convolute the measured spectrum with it. This is theoretically possible. An effect known as "noise amplification", however, spoils the result. This will be clarified by an example:

The equations given above can also be used to describe the ink distribution at time t, if at time 0 a series of infinitely small spots of ink is placed in a one-dimensional solvent. At time t, due to diffusion, the spots will have taken a Gaussian shape, whith a width that is proportional to the elapsed time t. Physically, information about the original positions of the spots is lost. It will also become impossible to say whether such a Gaussian spot of ink is the result of diffusion of just one spot or maybe two that were originally close together in terms of the width of the Gaussian. The two situations at time 0 would yield virtually the same result at time t. This means that if an attempt is made to decide whether one or two spots were originally there, the result will be unstable: The smallest imperfection in the knowledge of the distribution at time t will have great influence on the outcome of the decision. This is called noise amplification. Not only this kind of decision making suffers from it, also the peak area and positions of multiplet components would suffer if they were determined by convolution with the inverse of the PSF.

On the other hand, the total amount of ink is constant in time, and can easily be determined for each blob of ink that is well separated from the others. The corresponding technique in spectrum analysis is called peak integration. The underlying continuum is determined and all counts exceeding this level are included in the net peak area.

Another possibility to find the p_i and A_i is to fit each channel in the measured spectrum to the PSF. This fitting is a standard technique and can yield results for the parameters of the PSF as well as for p_i and A_i. This technique is commonly used to reduce gamma-ray spectra. The PSF used then is somewhat more complicated than the simple Gaussian presented in this introduction, but essentially there is no difference.

The fitting of a photopeak to a PSF is a time consuming process. It is therefore worthwhile to first locate the photopeaks in the spectrum by other means. The detection limits of the peak search algorithm determine the detection limits of the technique as a whole in the end. Many peak search algorithms were presented in the course of time, and many were essentially identical without the authors realising it[2]. In Chapter 3, several algorithms will be discussed and the properties of one of them extensively measured.

In Chapter 4 a description is given of the IRI implementation of the least squares techniques used for the fitting of photopeaks. The interactive integration of multiplets is also described in this chapter.

Summarizing, it can be said that the contributions from the Compton effect and Bremsstrahlung can be removed from the spectrum on basis of their low Fourier frequencies. The peak widening is dealt with using peak search and fitting techniques, and the physical processes causing extra photopeaks to appear in the spectrum are not considered at all in the reduction process, but in the interpretation process, as described in Chapters 7, 9 and 12.

2.5. References

1. G.F.Knoll, *"Radiation detection and measurement"*, John Wiley & Sons, 1989.
2. P.S.Shoenfeld, J.R.DeVoe, Anal.Chem., <u>48</u> (1976), 403-411

Chapter 3
Statistical Properties of the Peak Search Algorithm as Related to Currie's Detection Limits

3.1. Introduction

The search for possible peaks is the first step in the reduction of gamma-ray spectra. Peaks which are not detected in this stage will not be introduced in the computation of concentrations or activities later on. It is therefore the peak search algorithm that primarily determines the detection limits of the NAA technique as a whole.

Curiously, the upper limit for the area of a peak not observed in the spectrum is generally determined by assuming that the peak search algorithm is "perfect" and will detect any peak of which the area is statistically significant as compared to the uncertainty of the area of the continuum under the peak, not by taking the properties of the peak search algorithm into account[1,2,3]. Also, the difference between the normal distribution and the Poisson distribution for low channel contents is rarely taken into account.

All commonly used peak search algorithms boil down to digital filters that transform the measured spectrum. In this chapter, several of these filters are discussed. The filters are all used in the same way: For each channel of the spectrum, the statistical significance of the filter output is calculated. The calculation of each new channel content will involve $2m+1$ original channel contents; m is called the filter width in this chapter. In the filtered spectrum, local minima (maxima in the case of a correlation filter) are looked for. If the minimum exceeds a threshold, a peak is considered to be detected. Low thresholds lead to a high probability of detecting peaks where only noise is present (The type 1 error), high thresholds reduce the probability of detecting a peak (The type 2 error). The statistical properties to be known of a peak search algorithm are the probabilities of making a type 1 error and of making a type 2 error, both as a function of continuum and peak width. The type 2 error probability also depends on the peak area. The type 1 error is of less importance, because fitting and interpretation methods in later stages of the handling of the data will intercept it, but its probability is nevertheless measured in the experiments described along with the type 2 error probability. Both probabilities are modelled as a function of continuum, peak area and peak width.

The channel widths of the ADC may not equal. The variation in channel widths is characterized by the so-called differential non-linearity of the ADC. The influence of this non-linearity on the performance of the peak search algorithm is also tested.

Currie's[1] critical level L_C, in terms of peak areas, is the peak area which is expected to just exceed the decision criterion (The decision criterion follows from the chosen probability α of making a type 1 error). The detection limit L_D is defined as the peak area with a probability β of being overlooked, given the decision criterion or the corresponding probability α. Both L_C and L_D can be calculated from the statistical properties of the peak search algorithm, as will be demonstrated.

3.2. Currently applied filters

When discussing peak search algorithms, a distinction is usually made between derivative methods, correlation methods and Fourier transform methods[4].

Derivative filters are all based on the idea that any part of a gamma-ray spectrum as wide as a peak can be modelled with a linear function, except for regions where a peak is present. In that case, the second derivative of channel content to channel number will show a significant minimum. Both the Savitzky-Golay[5] filter and the Mariscotti[6] filter are derivative.

Correlation methods are based on the idea that the peaks to be located all have more or less the same shape. The correlation between the part of the spectrum where a peak is present and a function representing the general shape of peaks should therefore be high. Black's filter[7] is an example of this approach.

Fourier methods[8] attempt to determine the smoothed second derivative of the channel contents subjecting the spectrum to a Fourier transform, filtering and transforming back.

All these methods, though arrived at by different pathways, result in filters which very much resemble each other, as will be shown below.

3.2.1. Cross correlation filters
At first sight, Black's idea is very appealing: When looking for a specific structure in noisy data, just establish to what extent the structure resembles the data at all possible positions. This can be done by computing the correlation between the structure looked for and the measured channel contents. The coefficients of the digital filter can be obtained directly from the Gaussian function representing the shape of the peaks.

However, there are several problems. Most important of all: the digital filter thus derived does not have a zero area (i.e. the sum of the filter coefficients is not 0) and therefore will not yield output 0 on a linear continuum without a peak. This can be solved by adding a constant to all coefficients such that the sum of the coefficients becomes 0. Black proposes to subtract the continuum from the spectrum first, never

mentioning the fact that the peak search problem is partly caused by not knowing what the continuum is.

In his paper, Black also mentions that his filter yields optimal results if the coefficients are *not* obtained from the Gaussian of the peaks, but from a Gaussian which is 2/3 narrower. He does not offer an explanation for this, but the reason for it will become clear in the following paragraphs.

The main advantage of Black's method as compared to some of the following examples is that a working relation between the width of the Gaussian in the filter and the Gaussian in the spectrum is provided.
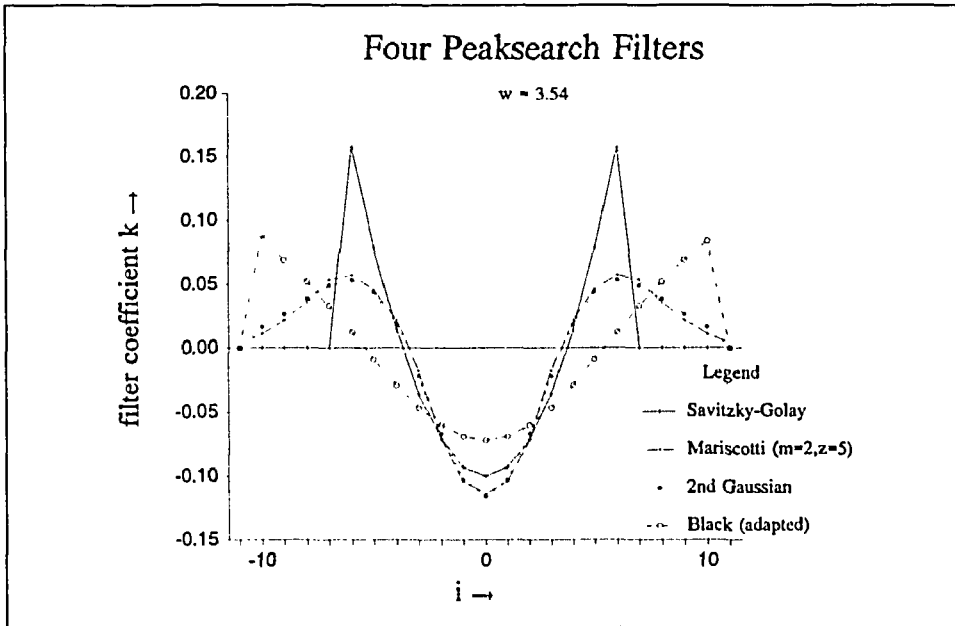
Fig.3.1: Four digital peaksearch filters, all optimized to look for peaks with a width of 3.54 channels. All four have zero area and unity norm.

Black's filter coefficients for a peak width w (i.e. the standard deviation of the Gaussian) of 3.54 channels, adapted to set the sum of the coefficients to 0, are shown upside down in Fig.3.1.

3.2.2. The Savitzky-Golay filter

It is possible to fit a polynomial function to measured channel contents using linear least squares (LSS) techniques. If the fit is performed without regard to the statistical uncertainty of the channel contents, the whole LSS procedure reduces to a convolution with a digital filter.

The Savitzky-Golay filter[5] fits a quadratic function to the channel contents in a limited region (the filter width), and replaces the content of the middle channel by the coefficient of the quadratic term found in the fit. The filtered spectrum finally obtained is the smoothed second derivative of the original spectrum, and should only significantly deviate from 0 in the peak positions.

The filter is symmetrical and has zero area, which means that its output will be 0 on a linear continuum.

A drawback of the Savitzky-Golay filter is the fact that the relation between the width of the peaks and the optimal filter width is unclear, which leads to errors. For example, in the ICPEAX program used at IRI in the past, the filter widths used were too narrow by a factor 2. The resulting probabilities of making type 1 as well as type 2 errors were thus raised unnecessarily. Moreover, the filter coefficients are determined completely by the filter width m which must be a whole number. The tuning of the filter to the peaks looked for will therefore be imprecise.

The filter coefficients for a peak width of 3.54 channels are shown in Fig.3.1. The optimal filter width of 13 channels was selected by comparison of the width of the negative part of the filter with those of the Mariscotti and the Routti-Prussin filters. In general, it can be said that the width of the negative part of the filter must be equal to twice the width w of the peak looked for.
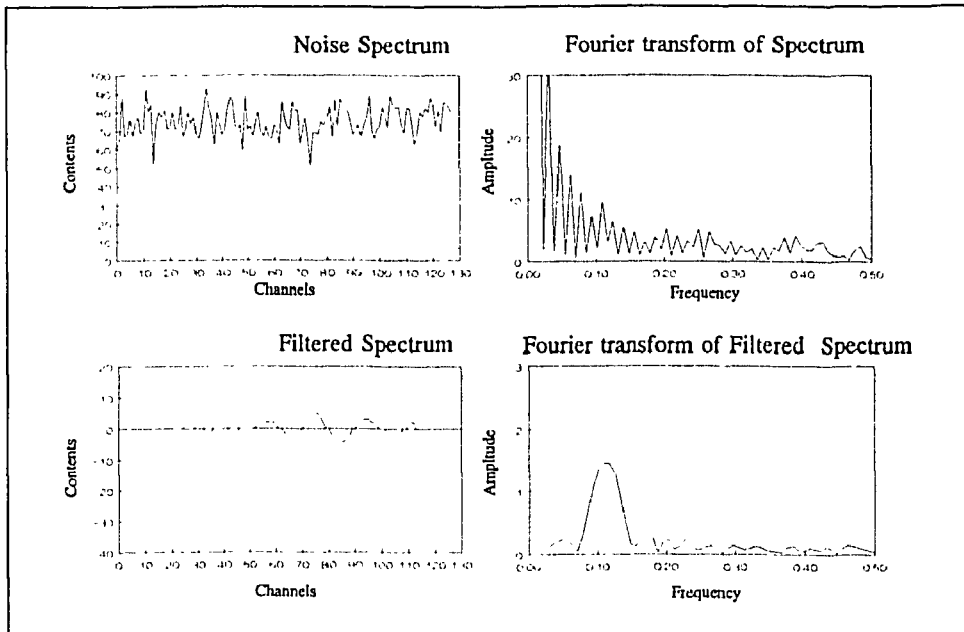
Fig.3.2: Noise spectrum before and after filtering by the Routti-Prussin filter.

3.2.3. The Mariscotti filter

The second difference in a channel can be calculated from the contents of the channel itself and its two neighbours using

$$S[i] = (c[i+1]-c[i]) - (c[i]-c[i-1]) = c[i-1] - 2c[i] + c[i+1] \qquad (3.1)$$

where

$S[i]$ = the second difference in channel i

$c[i]$ = content of channel i.

To introduce a smoothing effect, Mariscotti proposes to replace $S[i]$ by the average of $S[i]$ itself and the S of its $2m$ neighbours:

$$S[i,m] = \sum_{j=i-m}^{i+m} S[j] \qquad (3.2)$$

This averaging process is repeated z times. The filter coefficients $k_i(z,m)$ finally obtained are given by

$$k_i(z,m) = \sum_{j=i-m}^{i+m} k_j(z-1,m) \qquad (3.3)$$

and $k_i(0,m)$ =
$$0 \text{ if } |i| > 2,$$
$$1 \text{ if } |i| = 1 \text{ and}$$
$$-2 \text{ if } |i| = 0.$$

The relation between the optimal values for z, m and the peak width remains obscure, but Mariscotti proposes 5 as the optimum value for z for any peak width w, and $(w\sqrt{2} - 1)/2$ as the optimum for m.

Mariscottis filter is symmetric and has area 0. It can be shown that the filter coefficients are identical to the values of the second derivative of a Gaussian if z becomes very large.

The applicability of the filter is limited by the imprecise values that must be used for m because it has to be a whole number. Nevertheless, this filter is the most frequently used one in commercial spectrum analysis software.

The filter coefficients for a peak width of 3.54 channels are shown in Fig.3.1.

3.2.4. Continuum subtraction method

This method is based on the notion that peaks are what remains of a spectrum after subtraction of the continuum[9,10]. The technique is implemented by smoothing the spectrum as much as necessary to make the peaks disappear, and subtracting this smoothed spectrum from the original. The result contains high frequency components only, and can be subjected to a very simple peak search routine which discriminates

against statistical fluctuations. Even though the order of subtraction and smoothing is different, this method is a mathematical equivalent of the Mariscotti filter and therefore derivative.
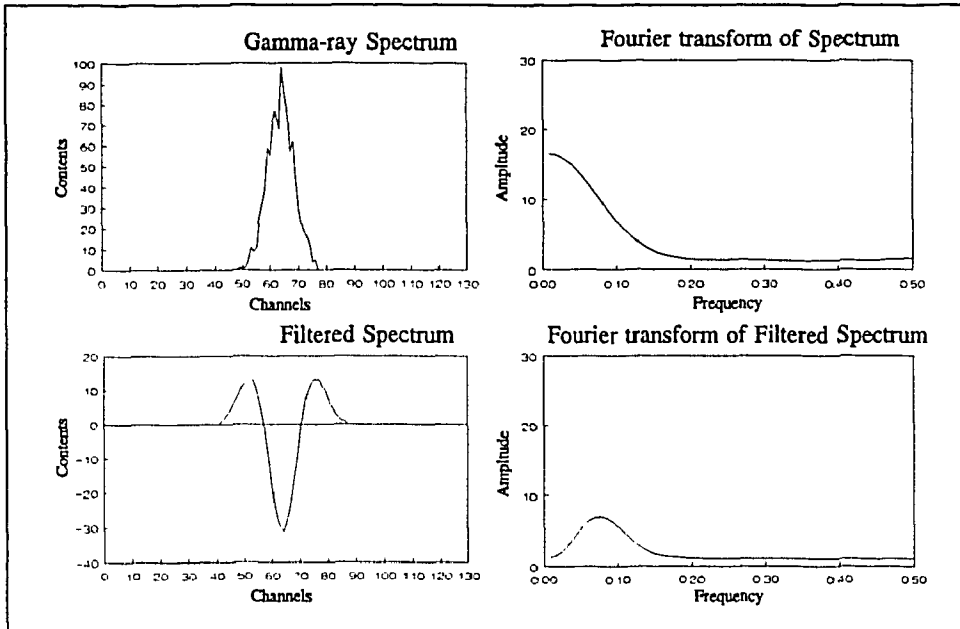
Fig.3.3: Spectrum containing only a gaussian peak before and after filtering with the Routti-Prussin filter

3.2.5. The Routti-Prussin filter

The filter coefficients of this filter[11] are obtained directly from the second derivative of a Gaussian function with the same width as the width of the peaks looked for. The developers of the filter state that the optimum width of the second derivative depends on the peak area to continuum ratio, and also on the presence of other peaks close to the peak of interest. According to them, in case of "infinite" continuum, very small peak area and optimized sensitivity, the width of the filter Gaussian should be 2.3 times wider than the Gaussian looked for. In order to detect the components of multiplets, the filter Gaussian should be narrower. They propose to use equal widths in practice. The relation between peak width and filter coefficients is thus specified, even though some authors failed to notice this relation in the past[12]. The filter is reported to be able to discriminate between the edges of the Compton continuum and photopeaks[11].

The filter coefficients for a peak width of 3.54 channels and equal filter Gaussian width are shown in Fig.3.1.

3.2.6. The Wiener filter

The Wiener filter[13] is a general smoothing filter, defined in terms of signal and noise. A translation of the derivation to the gamma-ray spectrum context is presented here. The measured spectrum is represented by

$$c(i) = f(i) + n(i) \qquad (3.4)$$

where

$c(i)$ = the channel content of channel i

$f(i)$ = the signal, i.e. the channel content as it would be in the absence of noise

$n(i)$ = the contribution of noise

The coefficients of a filter $k(i)$ are looked for, such that the spectrum after filtering will be the best mean-square estimate of $f(i)$. It can be proved[13] that the Fourier transform $K(\omega)$ of $k(i)$ is given by

$$K(\omega) = \frac{S_{fc}(\omega)}{S_{cc}(\omega)} \qquad (3.5)$$

where

$S_{fc}(\omega)$ = the Fourier transform of the cross-correlation between signal and channel content $R_{fc}(\tau)$

$S_{cc}(\omega)$ = the Fourier transform of the autocorrelation between the channel contents

This formula can be simplified. If noise and signal are considered to be orthogonal (i.e. the noise is not correlated with the signal), then

$$K(\omega) \approx \frac{S_{ff}(\omega)}{S_{ff}(\omega) + S_{nn}(\omega)} \qquad (3.6)$$

and if the noise is white (i.e. doesn't correlate with itself)

$$K(\omega) = \frac{S_{ff}(\omega)}{S_{ff}(\omega) + I} \qquad (3.7)$$

where

I = the intensity of the noise

If it is assumed that the power spectrum of the signal is very small as compared to the noise

$$K(\omega) = \frac{S_{ff}(\omega)}{I} \qquad (3.8)$$

so finally

$$k(i) = \frac{R_{ff}(i)}{I} \qquad (3.9)$$

The signal of interest is a Gaussian peak. The autocorrelation of a Gaussian is also a Gaussian, but $\sqrt{2}$ times as wide. The optimum Wiener filter coefficients for the smoothing of a noisy spectrum containing Gaussian peaks therefore represent a Gaussian $\sqrt{2}$ times as wide as the Gaussian peaks of interest.

To locate the peaks, the second derivative of the smoothed spectrum must be inspected for local minima. This second derivative can be obtained directly by using the second derivative of the Gaussian instead of the Gaussian itself to compute the filter coefficients from.

The Routti-Prussin filter thus is a Wiener filter, narrowed down to optimize the sensitivity for multiplet components, and can be obtained from general principles of signal analysis.

3.2.7. Comparison of filters

The Savitzky-Golay filter turns into the Routti-Prussin filter when it is perfected by multiplying the filter coefficients with the values of a Gaussian with the same width as the peaks looked for, reflecting the idea that channels which are located further away should have less bearing on the calculation of the current second derivative.

The Black filter turns into a good approximation of the Savitzky-Golay filter when it is narrowed down (apparently the 2/3 mentioned by Black is still too high a value), and can than be transformed into the Routti-Prussin filter in the same way as the Savitzky-Golay filter.

The Mariscotti filter by itself already closely approximates the Routti-Prussin filter, as can be seen in Fig.3.1.

The continuum subtraction method is mathematically identical to the use of the Mariscotti filter.

As compared to the Mariscotti filter, the advantages of the Routti-Prussin filter are several: The relation between peak width and filter coefficients is clear. The filter width m can be chosen independent from the width of the Gaussian used to calculate the coefficients, allowing for very precise tuning. Moreover, the filter has a firm foundation in the theory of signal analysis. This filter was therefore selected to be used in the system for INAA described in this thesis.

In Fig.3.2, A noise spectrum before and after filtering as well as the Fourier transforms are shown. Both continuum and noise suppression can be seen in both domains. In Fig.3.3, the same is shown for a spectrum containing only a Gaussian peak with low statistics. The Routti-Prussin filter can now be recognized as a differential filter suppressing those frequency zones where the Gaussian does not dominate in the Fourier domain. In the channel domain, the Gaussian peak is transformed into its second derivative.

3.3. Experimental

The properties of the Routti-Prussin filter were measured using simulated spectra. This filter is used in practice by computing the measured statistical significance $c[i]'$ of each channel in the filtered spectrum as the output of the filter divided by its uncertainty, as shown in

$$c[i]' = \frac{\sum_{j=i-m}^{i+m} k_j \, c[i-j]}{\sum_{j=i-m}^{i+m} k_j^2 c[i-j]} \tag{3.10}$$

where
k_i = filter coefficient i
m = filter width parameter
$c[i]$ = channel content of channel i
When the value of $c[i]'$ exceeds the threshold value t, a peak is considered to be detected.

Defining the expected output O of the filter for a Gaussian peak with area 1 by

$$O \equiv \sum_{i=-m}^{m} k_i \frac{1}{w\sqrt{2\pi}} e^{-\frac{i^2}{2w^2}} \tag{3.11}$$

where
w = standard deviation of peaks to locate
and defining the uncertainty U in this output by

$$U^2 \equiv \sum_{i=-m}^{m} k_i^2 \frac{1}{w\sqrt{2\pi}} e^{-\frac{i^2}{2w^2}} \tag{3.12}$$

and defining the norm $|F|$ of the filter by

$$|F|^2 \equiv \sum_{i=-m}^{m} k_i^2 \qquad (3.13)$$

the expected output divided by its uncertainty, which is defined as the statistical significance Z of the peak (as measured by the filter), is given by

$$Z = \frac{AO}{\sqrt{AU^2 + b|F|^2}} \qquad (3.14)$$

where
A = the area of the peak
b = continuum under the peak

For any combination of peak width w and continuum b, areas were computed to obtain Z values of 0 up to 5 with steps of 0.5. For the Z value of 0, 100 spectra were generated and subjected to the peak search algorithm to obtain a good estimate of the probability of making type 1 errors. For other Z values, 40 spectra were used to obtain the probability of detecting the peak. All spectra generated were 50 channels wide.

The continuum in the spectra was generated by first computing the total number of continuum counts in the spectrum, and subsequently placing each count in a channel selected randomly using a uniform probability distribution.

If a differential non-linearity d of the ADC was to be simulated, the channel widths were changed by adding a random value, taken from a normal distribution with mean 0 and standard deviation $d/\sqrt{2}$, to each channel width and subtracting half of the random value from the widths of the neighbouring channels. This resulted in the average channel width remaining 1, the standard deviation becoming d and nevertheless the total width of the channels remaining constant and no gaps or overlaps between channels arising. The resulting widths of neighbouring channels were strongly correlated. The probability of a count being added to a channel content was made to be proportional to the channel width.

Subsequently, the peaks were added using ten times the number of counts to be expected in the peak. Each count was subsequently added to the spectrum if a random number, drawn from a homogeneous distribution between 0 and 1, was smaller than 0.1. The channel where the count was to be placed was obtained by drawing random numbers from a normal distribution with width w and comparing these numbers to the channel numbers and widths. The peak position, i.e. the mean of this normal distribution was set to 25.5 in all cases.

The peak search algorithm used a threshold value t of -2 to decide whether a peak was detected. If so, the channel with the minimum content was reported as the
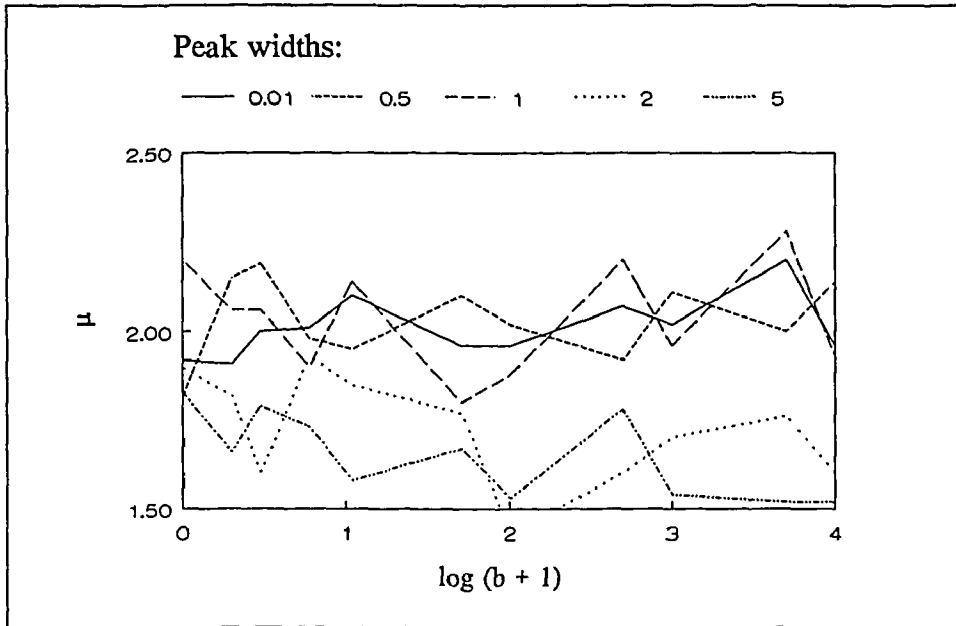
Fig.3.4: The measured values of μ as a function of peak width and background.

peak position. If three or more adjacent channels had the same minimum content, the middle channel was reported. If this channel was within the peak width w of the peak position, the generated peak was considered to be detected. This means that for a w value of 0.01 and 0.5 only one channel was regarded, but for w values of 1, 2 and 5 ranges of 3, 5 and 11 channels respectively were involved.

The error function

$$erf(x) = \frac{1}{\sigma\sqrt{2\pi}} \int_{-\infty}^{x} e^{\frac{-(\tau-\mu)^2}{2\sigma^2}} d\tau \qquad (3.15)$$

was used to model the probability of detecting a peak, given continuum and peak width, as a function of the statistical significance Z of the peak as measured using the filter.

The error function was fitted to the experimental data by least squares techniques, yielding values for μ and σ for each combination of continuum and peak width. The value of μ can be interpreted as the statistical significance Z of a peak with a 50 % probability of being detected. The value of σ defines the slope of the detection probability as a function of the statistical significance of the peak.

3.4. Results

3.4.1. The values of μ (no differential nonlinearity)

The values obtained for μ without differential nonlinearity as a function of continuum and peak width are shown in Fig.3.4. For narrow peaks, μ is equal to the threshold level of the peak search algorithm as was to be expected. It can be seen that μ does not depend on the continuum, but only on peak width. It was therefore considered justifiable to compute the unweighted mean value of μ and its external uncertainty for each value of w.

If a peak is allowed to be detected in more than one channel, the probability of detection is amplified. This amplification is described by

$$1 - \beta = \prod_{i=-w}^{w} (1 - (1 - r_i)\beta_{ri}\,\beta_0) \qquad (3.16)$$

where

β_0 = the probability of peak detection in the peak centre channel
β = the probability of peak detection in any channel within the peak width w
r_i = factor resulting from the correlation between filter outputs at the centre channel and at channels removed i or less channels from it.
β_{ri} = factor resulting from the decrease of the detection probability in channel i as channel i is further removed from the centre channel.

The correlation factor r_i is 0 for $i = 0$ and is defined for other i by

$$r_i^2 = \frac{\sum_{j=1}^{i} g_2^2(j, \sigma)}{i} \qquad (3.17)$$

where g_2 is the second derivative of the Gaussian function, normalized to get $g_2(0, \sigma) = 1$.

The relative probability decrease factor β_{ri} is defined by

$$\beta_{ri} = erf(t - g_2(i, \sigma))/\beta_0 \qquad (3.18)$$

where

t = the threshold of the peak search algorithm ($t < 0$)
and Z is given by

$$Z = t - erf^{-1}(\beta_0) \qquad (3.19)$$

The value of μ should, per definition, correspond to a detection probability β of 50%. From this value of β, the corresponding value of β_0 can be determined by iterative
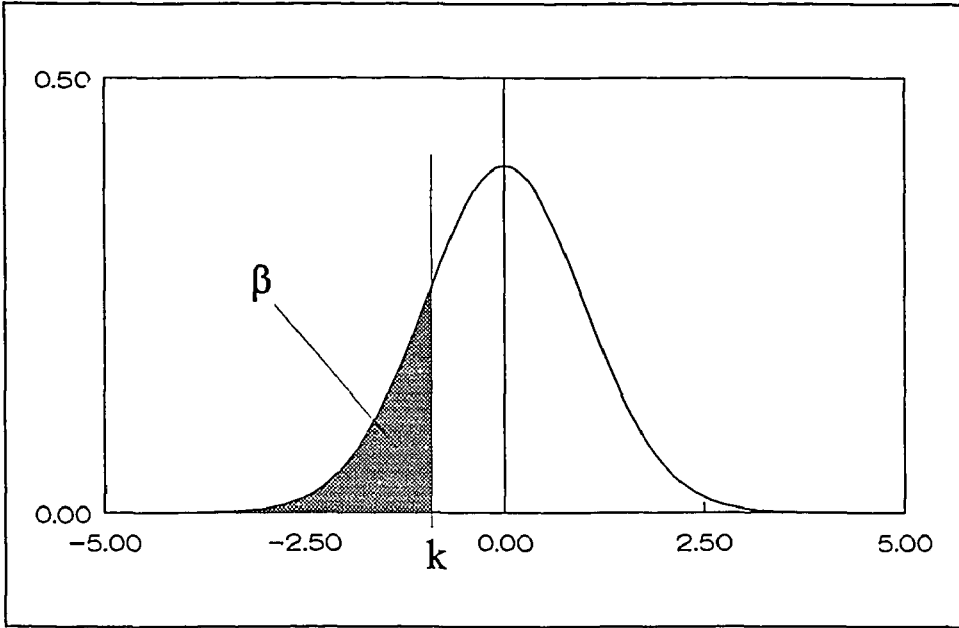
Fig.3.5: Relation between k-value and β_0.

procedures. The value of β_0 will be less than 50%. The corresponding value of μ will be closer to 0 than t. The difference k can be obtained from the value of β_0 using the normal distribution, as illustrated in Fig.3.5. The value of μ is given by

$$\mu = k - t \tag{3.20}$$

w	μ measured	μ calculated	σ calculated
0.01	1.97 ± 0.03	2.00	1.00
0.5	2.03 ± 0.03	2.00	1.00
1	2.03 ± 0.05	1.92	1.00
2	1.72 ± 0.05	1.77	1.01
5	1.66 ± 0.03	1.67	1.03
10	1.52 ± 0.05	1.53	1.00

Table 3.3: Measured and calculated values of μ

In Table 3.3, the μ values thus obtained are shown along with the measured values. Values for σ can also be obtained from this model by finding a second k value for a value of β of 97.5%. The difference between the two k values is twice the value of σ.
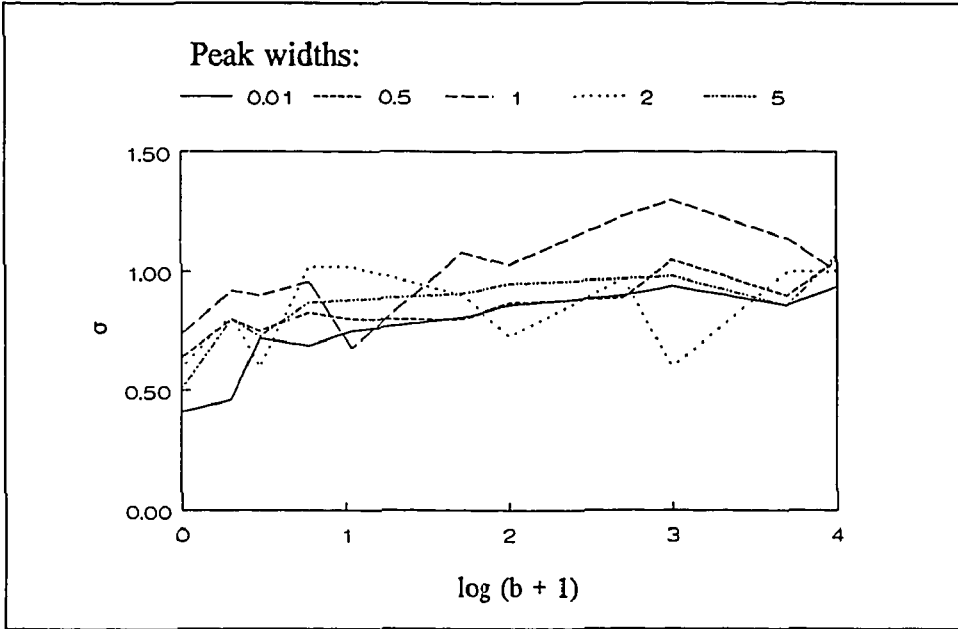
Fig.3.6: Values of σ as a function of background and peak width.

Values for σ thus obtained are also shown in Table 3.3.

3.4.2. The values of σ (no differential nonlinearity)

The values obtained for σ are shown in Fig.3.6. Surprisingly, it can be seen that σ does not depend as much on the peak width as μ does, but it does depend on the continuum. This must be the result of the fact that, for low channel contents, the Poisson distribution differs significantly from a normal distribution. For high continuum values ($b > 100$), σ approaches its expected value of 1, in agreement with the calculated values in Table 3.3.

Even though a dependence of σ on the peak width can be seen, it was deemed to be of practical importance only to find a relation between continuum and σ. To do this, mean values of σ were determined for each continuum value. An empirical relation was found given by

$$\sigma = 0.65 + 0.35(1 - (b+1)^{-0.25}) \tag{3.21}$$
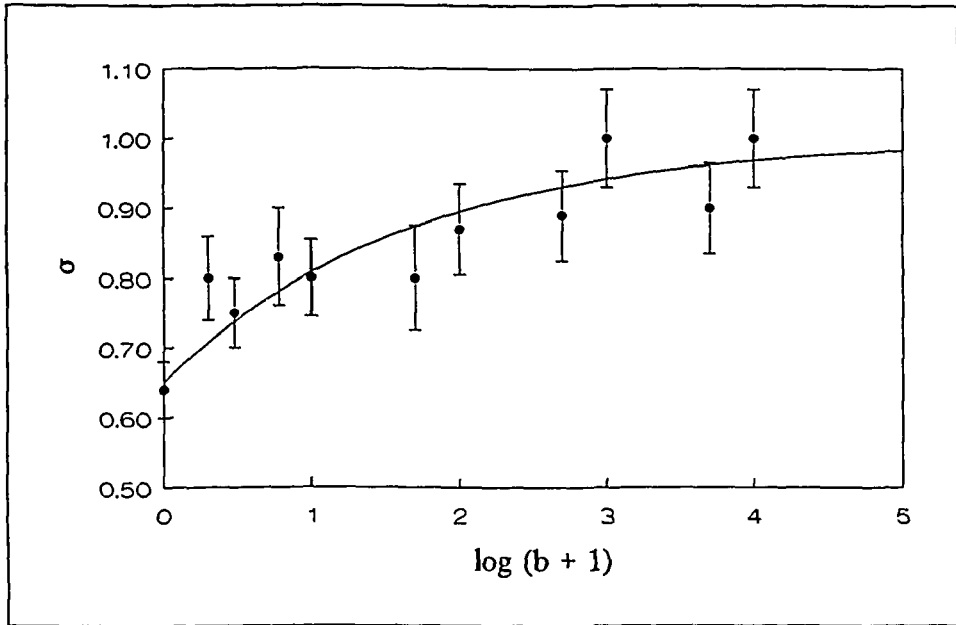
Fig.3.7: Emperical relation between σ and background.
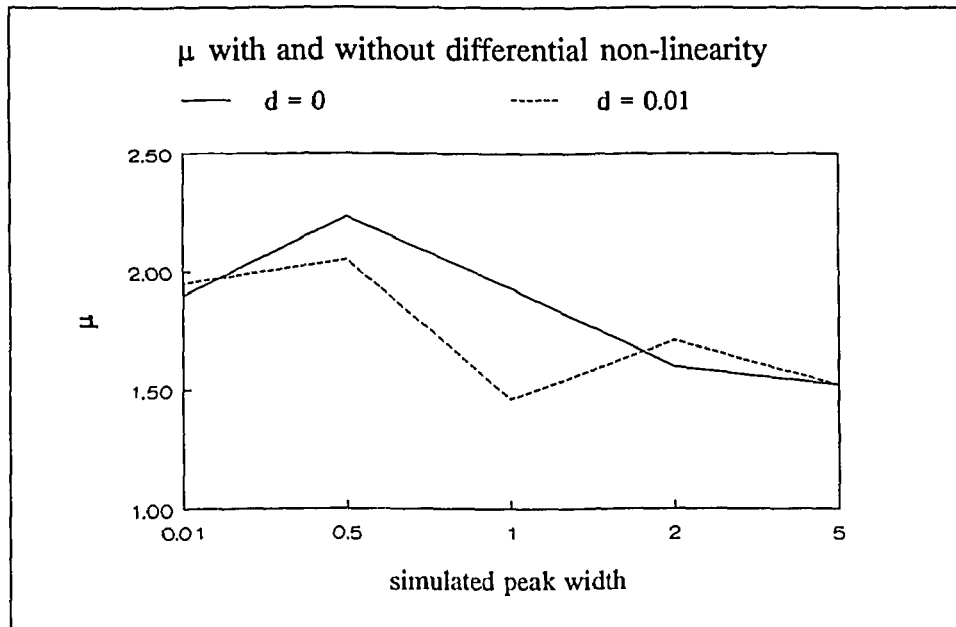
Fig.3.8: Values of μ obtained with and without differential non-linearity at a background level of 10^4 counts

The quality of this emperical relation can be assessed in Fig.3.7. The values of σ obtained as described in the preceding paragraph need to be corrected using Eq.(3.21) before they can be used to obtain detection limits.

3.4.3. The probability of making a type 1 error

This probability can be obtained from the values of μ and σ as reported in the preceding paragraphs. If $\mu = 2$ and $\sigma = 1$, for example, the probability of detecting a peak with area 0 and resulting statistical significance 0 is 2.5%. The very low values of σ at low continuums correspond to lower probabilities, the low values for μ at high peak widths to higher probabilities of making a type 1 error.

3.4.4. Differential non-linearity

As expected, the influence of differential non-linearity of the ADC increases with the continuum level. The results obtained with a continuum level of 10^4 counts for μ
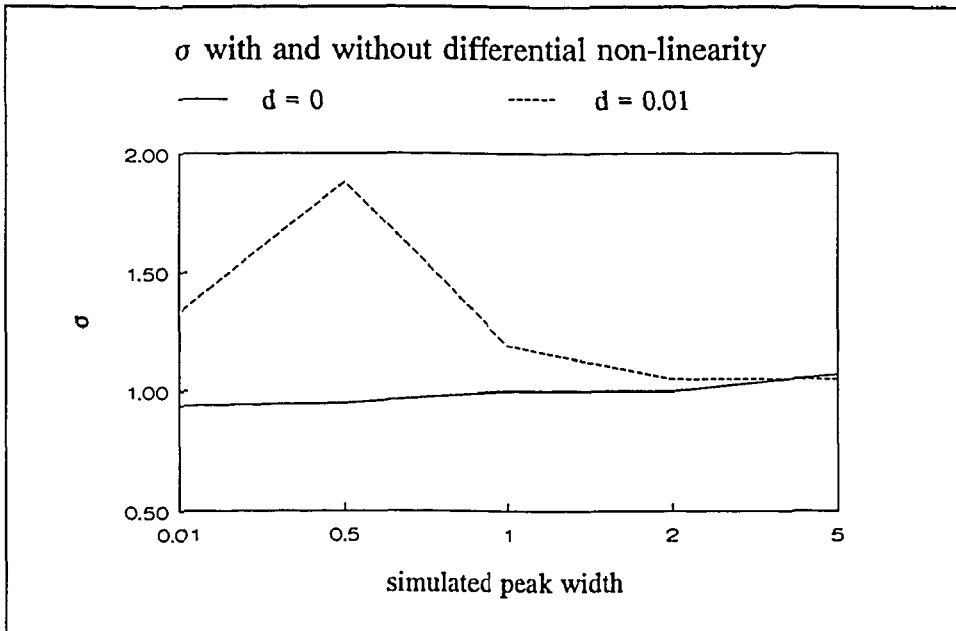
Fig.3.9: Values of σ obtained with and without differential non-linearity at a background level of 10^4 counts

and σ, resp., are shown in Fig.3.8 and Fig.3.9.

The results obtained for a peak width of 0.01 channel can be modelled by considering the non-linearity to be a source of noise of which the magnitude is the product of the non-linearity d and the continuum b. For a continuum of 10^4 counts

and a non-linearity $d = 0.01$, this noise adds up with the Poisson noise for a total of 140. At this peak width, the value of μ only depends on the threshold of the peak search algorithm, but the value of σ is proportional to the noise in the channel contents.

The non-linearity is not a source of "white" noise, because of the strong negative correlations introduced between neighbouring channels. In the Fourier spectrum, its contribution is maximal in the same region where the contribution of a Gaussian with width 1 is maximal. This means that at high peak widths, the influence of the non-linearity will be smoothed away by a peak search filter matched to the peak width, but at peak width 1 its influence will not be reduced at all. This explains the low value of μ at peak width 1, which is mainly due to the high probability of making a type 1 error of 20%, as well as the general trends shown in Fig.3.8 and Fig.3.9.

3.5. Discussion

From simple statistical considerations, one would expect the value of the error funtion parameters μ to be always equal to $-t$, t being the the threshold value of the peak search algorithm, and the value of σ to always be 1 in the absence of differential non-linearity of the ADC. In practice, neither is true. The value of μ is lowered by a "peak width boost", and the value of σ by differences between the Poisson and the normal distribution. Both effects are now under control for the Prussin-Routti filter. The formulas provided in this work can be used to accurately calculate Currie's critical level L_C and his detection limit L_D. It should be noted however that differential non-linearity of the ADC, i.e. differences between channel widths, deteriorates the detection limit. This property of the ADC is systematic for each channel and therefore very difficult to deal with. It enhances the sensitivity for some peaks, but deteriorates the sensitivity for others. The μ of the error function, corresponding to the critical level L_C, slightly suffers from it, but σ is strongly affected. The fact that the influence of differential non-linearity diminishes when the peak width increases is a strong argument in favour of 8192 (or more) channel ADCs as compared to 4096 channel ADCs. If the non-linearity would show periodic behaviour, the influence would be even worse than established here.

Currie's critical level L_C can be indentified as the peak area having a probability of 50% of being detected and thus corresponding to the μ value as defined in this work. This μ value can be converted to a peak area using Eq.(3.14). In his paper, Currie states that L_C must be 0 if the continuum is 0. In practice, this is only true if the peak search algorithm *a priori* knows the continuum level to be 0. If this is not the case, the algorithm has to decide what is more probable: Whether it is looking at a spurious counts stemming from a continuum level between 0 and 1, or at a count

stemming from a peak. This leads to non-zero critical levels in the case of the Prussin-Routti filter as well as for the other filters discussed in this work.

The detection limit L_D as defined by Currie is the peak area with a probability β of being overlooked, given the decision criterion or the corresponding probability α. Choosing both α and β to be 2.5%, the resulting threshold level t of the Prussin-Routti filter is -2 and the detection limit $\mu + 2\sigma$, μ and σ defined as in this work. The $\mu + 2\sigma$ level can also be converted to a peak area using Eq.(3.14). It should be noted that Z is not a linear function of the peak area, and it would therefore be erroneous to separately convert μ and σ, and calculate $\mu + 2\sigma$ in terms of areas afterwards.

In his paper, Currie criticizes those who think of detection limits as having only one reliability, because L_D depends on the two confidence levels α and β. In my opinion however, a statement like "this detection limit is the concentration level with a probablity of 97.5% of being detected" can be correct. The 97.5% covers both α and β.

3.6. Conclusions

The statistical behaviour of peak search algorithms based on digital filters is not as simple as one would expect. For the Prussin-Routti filter, differences between the Poisson and the normal distribution diminish the probability of finding a very small peak on a very low continuum, but amplify the probability of finding larger peaks on very low continuums. These effects are visible for continuum channel contents of less than 100 counts. When the peaks become wider than 1 channel, all detection probabilities are amplified because the peak can be detected in more than 1 channel.

These deviations from straightforward statistical behaviour can be dealt with by empirical formulas.

The influence of differential non-linearity is difficult to deal with for peak widths close to 1. For wide peaks ($w > 2$) it is negligible. This is a strong argument in favour of ADCs with as many channels as possible, as long as the increase of the number of channels isn't matched by an increase of the differential non-linearity of the ADC.

Currie's critical level L_C is not 0 when the continuum is 0 for the peak search algorithms considered in this chapter.

3.7. References

1. L.A.Currie, Anal.Chem.,40 (1968) 3, 586-593
2. F.T.Avignone III, Nucl.Instr.Meth.in Phys.Res. A245 (1986) 525-529
3. O.Helene, Nucl.Instr.Meth.in Phys.Res. A300 (1991) 132-136 eind

4. R.G.Helmer, M.H.Putnam, C.M.McCullagh, Nucl.Instr.Meth.in Phys.Res. A242 (1986) 427-436
5. A.Savitzky, M.J.E.Golay, Anal.Chem. 36 (1964) 1627-1639
6. M.A.Mariscotti, Nucl.Instr.Meth 50 (1967) 309-320
7. W.W.Black, Nucl.Instr.Meth. 71 (1969) 317-327
8. T.Inouye, T.Harper, N.C.Rasmussen, Nucl.Instr.Meth 67 (1969) 125
9. B. Grosswendt, Nucl.Instr.Meth., 93 (1971) 461-472
10. R.Gunnink and J.B.Niday, Computerized quantitative analysis by γ-ray spectrometry, UCRL-51061, vols 1-4(1972)
11. J.T. Routti, S.G.Prussin, Nucl.Instr.Meth. 76 (1969) 109
12. G.W.Phillips, K.W.Marlow, Nucl.Instr.Meth. 137 (1976) 525-536
13. L.A. Weinstein, V.D.Zubakow, "Extraction of Signals from Noise," Prentice-Hall Inc., Englewood Cliffs, N.J., 1962 in: A.Papoulis, "Signal Analysis", McGraw-Hill, 1986.

Chapter 4
The Fitting of Photopeaks

4.1. Introduction

One would expect the fitting of the photopeaks to be a straightforward process, once the locations of the peaks have been determined as described in Chapter 3. Regrettably, reality proves to be different. Back in the seventies, many attempts were made to make this process completely automatic. Only recently, Helmer[1] stated that "Since a completely automatic code may supply answers which are not the best possible, the capability for some form of user intervention is desirable" and this notion is expressed even more strongly by the creators of the famous SAMPO program[2]: "No automated procedure is capable of doing complex analysis and giving correct answers". Modern computers with their graphical displays and advanced user interfaces have made it possible to create spectrum analysis software that is interactive and yet can reduce a gamma-ray spectrum in a minimum of time. To assure the quality of the results however, the influence of the user on the final results of the reduction process must be limited; a situation must be created where the imperfect software and the imperfect user together yield optimal results.

In this chapter, an extensive description of the fitting techniques used in the IRI system for INAA is offered, user interaction included. This component of the IRI software package is called SPECFIT. The conversion of peak positions to peak energies, as well as the corrections for dead time, pile-up and background are also discussed in this chapter. Where appropriate, comparisons will be made with well known software packages such as HYPERMET[3], SAMPO 90[2], GAMANAL[4] and GAUSS VII[1].

The SPECFIT program does not attempt to obtain the information from the spectra that would be needed for research techniques other than INAA. Several criteria, estimates and approaches were selected with the routine INAA measurements at IRI in mind.

4.2. Peak shape

The variation in photon energies emitted by the decaying nuclei is very small as compared to the detector resolution, except for annihilation photons and X-ray photons. The natural line width of annihilation photons is determined by Doppler broadening, X-ray photons show a Lorentzian distribution. The statistical nature of

the charge collection process in the detector crystal, as well as electronic noise in the amplifiers, causes the resulting peaks in the spectrum to have a basically gaussian shape. Incomplete charge collection in the crystal results in the so-called "low energy tail". This is a part of the peak, at the low energy side, where the shape is no longer gaussian but simply exponential. Photons can be scattered by surrounding materials into the detector crystal, causing a discontinuity in the continuum under the peak known as the "Compton step". When a spectrum has been acquired at a high count-rate, the photons may be detected simultaneously with others. This results in sum peaks caused by random summing. Also, the detection of a second photon at a point in time where the amplifier has not yet returned to its steady state results in a "high energy tail". This tail can also be described by a simple exponential function.

The shape function reflecting all these considerations is given by the following set of equations:

$$z = \frac{i - p}{\sigma} \tag{4.1}$$

the continuum, the Compton step included, is given by

$$B(i) = a(p-i) + b + S \int_{-\infty}^{i} \frac{1}{\sigma\sqrt{2\pi}} e^{\frac{-(t-p)}{2\sigma^2}} dt \tag{4.2}$$

and the photopeak itself by:
if $1 < z < r$ (the gaussian region):

$$c(i) = \frac{A}{\sigma\sqrt{2\pi}} . e^{-z^2/2} + B(i) \tag{4.3}$$

if $z < 1$ (the left tail region):

$$c(i) = \frac{A}{\sigma\sqrt{2\pi}} e^{\frac{(l + 2p/\sigma).l}{2}} e^{\frac{li}{\sigma}} + B(i) \tag{4.4}$$

and if $z > r$ (the right tail region):

$$c(i) = \frac{A}{\sigma\sqrt{2\pi}} e^{\frac{r(r + 2p/\sigma)}{2}} e^{\frac{-ri}{\sigma}} + B(i) \tag{4.5}$$

where
σ = the standard σ parameters of the gaussian function
A = the area of the gaussian (which is not the total area of the peak)
p = the position of the peak

l = the low-energy tail parameter
r = the high-energy tail parameter
S = the Compton step parameter

Most authors on the subject agree that this is a good shape function to use for the fitting of photopeaks. Only HYPERMET includes a second low energy tail and excludes the high energy tail. Both SAMPO and HYPERMET use parabolic continuums instead of linear ones, but SAMPO uses linear continuums when the region to fit is small. The parameters that must be represented as a function of channel number in the shape calibration thus are the peak width σ, the low energy tail parameter l, the high energy tail parameter r and the Compton step parameter S.

It should be noted that the function given here can be represented in different ways. The Gaussian for example could be represented using the peak height instead of the peak area as a parameter. So could the continuum be represented by $ai+b$ instead of $a(p\text{-}i)+b$. These notations however introduce high correlations between the parameters in the fitting procedure. As a result, the propagation of the uncertainties in the fitted parameters will become more complicated due to the covariations. Also, resulting near-singularity of the matrices to invert in the LLS procedure may lead to the inability of the algorithms to find a satisfactory fit.

4.3. Overlapping peaks and multiplets

If two or more peaks are positioned very close together in the spectrum, the fitting of the one cannot be performed independent of the fitting of the others. It is common practice in all programs mentioned in this chapter to define multiplets as groups of peaks that are not fully separated. The criteria used to decide about this are usually not all that subtle. SAMPO for example considers peaks to be well separated if the distance between the peak positions is larger than 6 FWHM (1 FWHM = 2.55 σ). This is correct only as long as neither of the peaks is intense enough to contribute significantly to the channel contents of the other.

It is also common practice to fit all peaks in a multiplet simultaneously. However, the computer time needed for a fit increases with the square of the number of parameters involved in the fitting. If the fitting does not yield the statistically optimal result, expressed in the reduced χ^2 of the fit, the value of χ_r^2 must be propagated to the areas of the peaks as determined in the fit. When a multiplet is fitted, the χ_r^2 will apply to all components of the multiplet, even when some of the components were fitted very well. These components will be reported with too high an uncertainty in the area. The component that caused the trouble however will be reported with too small an error.

For these reasons, SPECFIT attempts to minimize the number of multiplets by carefully deciding whether it is really necessary to fit groups of peaks simultaneously. It therefore discerns three levels of seperateness:

1) A peak is considered part of a multiplet if the distance to others peaks is less than 3σ. The peaks composing a multiplet are fitted simultaneously.

2) A peak overlaps with another peak if it significantly contributes to the channel contents of the region to fit of the other peak. This relation between the peaks need not be mutual: If one of the two is very intense for example, it will probably overlap with the other, less intense peak, but the other will not overlap with the intense peak. If the overlap is mutual, the two peaks are treated as a multiplet.

3) Peaks which are no part of a multiplet and do not suffer from overlapping other peaks are fitted independently.

4.4. An overview of the procedure

The reduction of a gamma-ray spectra usually starts with the determination of the parameters describing the peak shape, i.e. σ, l, r and S, as a function of channel number from a calibration spectrum. (Only HYPERMET and GAUSS VII refrain from doing this; HYPERMET determines the calibration curves from the unknown spectrum itself, GAUSS VII takes the parameters from user input.) The calibration spectrum must have well defined peaks, separated from each other. The results of the shape calibration serve two purposes: It has been shown that the fitting of overlapping peaks or of peaks with low statistics yields much better results if the shape parameters are already known before the fitting starts. Also, it saves computer time. A single set of shape calibration curves can be used for the reduction of many spectra acquired using the same detector.

If the peaks in the calibration spectrum have known energies, the spectrum can be used to determine the relation between peak energy and channel number, resulting in an "energy calibration".

Once the calibration curves are available, the reduction of an unknown spectrum can begin. This is done in three steps: First, the peaks in the spectrum are located. Second, the peak areas and positions are determined. Third, the positions are converted to energies. The procedure for the reduction of an unknwon spectrum very much resembles the procedure of the shape calibration. In case of unkown spectrum reduction, shape parameters are taken from the calibration curves, and multiplets and peaks with low statistics are fitted.

4.5. Shape calibration using a calibration spectrum

A suitable spectrum with well separated, intense peaks is used for the shape calibration. The approximate positions of the peaks may be known beforehand or be determined using a peak search algorithm. In the latter case, an estimate of the average peak width in the spectrum must be available. This estimate need not be very accurate: Intense peaks are easily located, even when using peak search filters tuned to incorrect values of the peak width. If a previous shape calibration of the same spectrometer is available, SPECFIT uses the peak width in the centre channel of the spectrum for this purpose. If not, it proposes to use 1.5 as its value. (This is a suitable value for spectra with approximately 0.5 keV/channel.) The user of the program can see and set the value used.
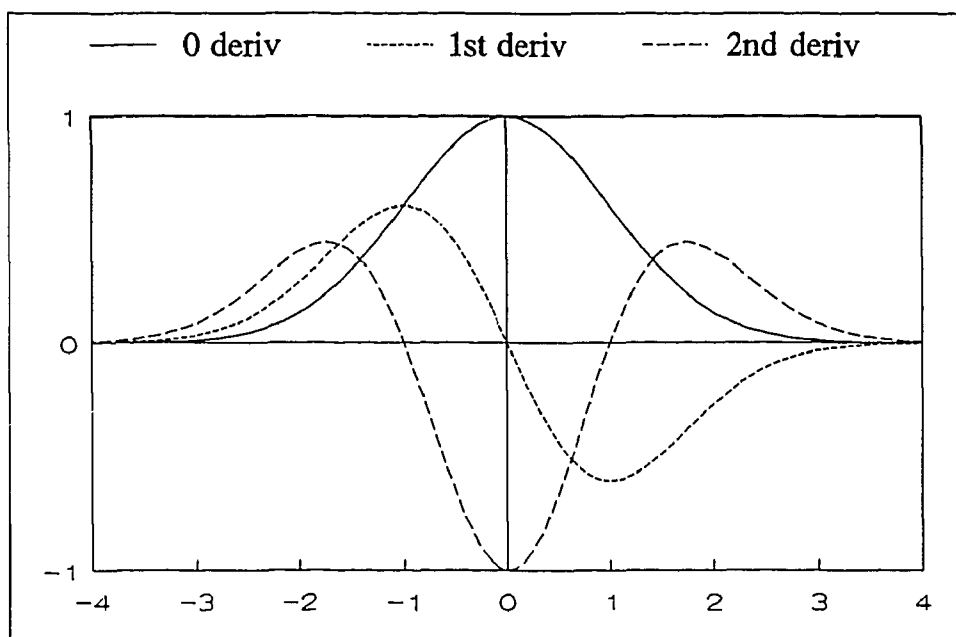
Fig.4.1: Gaussian function and its first and second derivate.

Once the locations of the peaks are known, the parameters describing the shape of each peak must be estimated before attempting to fit the peak. This not only saves computer time, but the outcome of iterative fitting procedures is much more reliable if good estimates of all peak parameters are made first. Information about the procedures used for parameter estimation is missing from the literature about the other programs. The SPECFIT program uses filtered spectra instead of raw channel contents to estimate the parameters from. For the computation of these spectra filters are used that are based on a gaussian function, its first and its second derivate. These

functions are shown in Fig.4.1. The σ of these filters is the same as the estimated σ used for the peak search filter.

4.5.1. Estimation of peak position

The peak position is estimated using the smoothed first derivate of the spectrum. As can be seen in Fig.4.1, the first derivate of the peak is 0 at its position. A very precise estimate of the point where this first derivate crosses the x-axis is obtained by linear interpolation between channel contents. The estimate of the peak position obtained in this way is usually accurate to within 0.05 channels.

4.5.2. Estimation of peak width

The peak width is estimated using the smoothed second derivate of the spectrum. As can be seen in Fig.4.1, the distance between the points where the second derivate crosses the x-axis is 2 σ. These points are also determined using linear interpolation between channel contents. The σ thus estimated is too high however, because of the broadening effect of the smoothing. The true σ of the peak is computed using

$$\sigma_p^2 = \sigma_e^2 - \sigma_s^2 \tag{4.6}$$

where

σ_p = the true σ of the peak
σ_e = the σ obtained as described above
σ_s = the σ used for the computation of the smoothed second derivate.

If the result for σ_p is negative, which sometimes occurs when estimating peaks with very low statistics, its value is set to σ_s.

4.5.3. Estimation of tail parameters

The value of these parameters is more or less the same for all peaks measured with any spectrometer in the IRI system. The left tail parameter l is therefore estimated to be -2.0, the right tail parameter r to be 2.0 (which is a suitable value for higher count rates).

4.5.4. Estimation of peak area

For this estimation, the smoothed version of the spectrum is used. A parabola is fitted to the three channels with the highest content at or near the estimated peak position. Once the parabola has been found, the height of the curve at the peak position is computed. The height at p-σ and p+σ is obtained by linear interpolation. Because the spectrum has been smoothed, the σ_e defined in the previous paragraph is used for this. From these three values, the peak area can be estimated independent of the continuum.

4.5.5. Estimation of Compton step

The parameter S is estimated to be 0, which in most cases is whithin the 68% confidence interval obtained for this parameter during the fitting.

4.5.6. Estimation of continuum parameters

For this estimation, the smoothed version of the spectrum is used. The channel contents at $p-2\sigma_c$ and $p+2\sigma_c$ are obtained by linear interpolation. From these two channel contents and the value of the peak position p, the continuum parameters a and b can be determined.

4.5.7. Determination of region of spectrum to fit

The region of the spectrum to be fitted is independently determined for each peak as the region where the peak contributes significantly to the channel contents, using the smoothed second derivate of the spectrum. SPECFIT resembles GAUSS VII in this respect. SAMPO uses the smoothed version of the spectrum and, starting at the peak position, searches in both directions for the first channels where the contents start increasing significantly. This method is sensitive to steep continuums and was therefore not used in SPECFIT.

The region selected is checked to see if there are more channels in the region than free parameters in the fit to be performed later on. If not, it is expanded. If necessary, the region is finally expanded to contain at least 6σ channels.

4.5.8. Selection of peaks to use

Those peaks which are not well separated from the others (i.e. peaks wich are part of a multiplet or suffer from overlapping other peaks), as well as peaks with statistical significance smaller than 20, are excluded from the shape calibration.

4.5.9. The fitting procedure

The theoretical peak shapes are fitted to the original channel contents essentially by common Non-Linear Least Squares techniques. The weights of the individual channel contents are obtained from the square root of the channel content, in accordance with the Poisson distribution, but the minimum error is set to 3 to correct for the different nature of the Poisson distribution as compared to the normal distribution for low channel contents. All parameters of the shape function are allowed to vary, but none of them is allowed to change by more than 50 % in a single iteration. Some peak parameters are forced furthermore to remain within reasonable limits by a check at the end of each iteration. The peak area is forced to remain positive, the peak position is not allowed to change by more than 0.5 σ. The tail parameters are forced to keep their sign. All these checks stabilize the outcome of the fitting procedure.

4.5.10. Shape calibration curves

The peak parameters σ, r, l, and S as determined by the fitting procedure can all be represented as functions of channel number. Linear functions are commonly used for r, l and S. The curve for σ is less simple; the relation

$$\sigma = \sqrt{ax + b} \qquad\qquad (4.7)$$
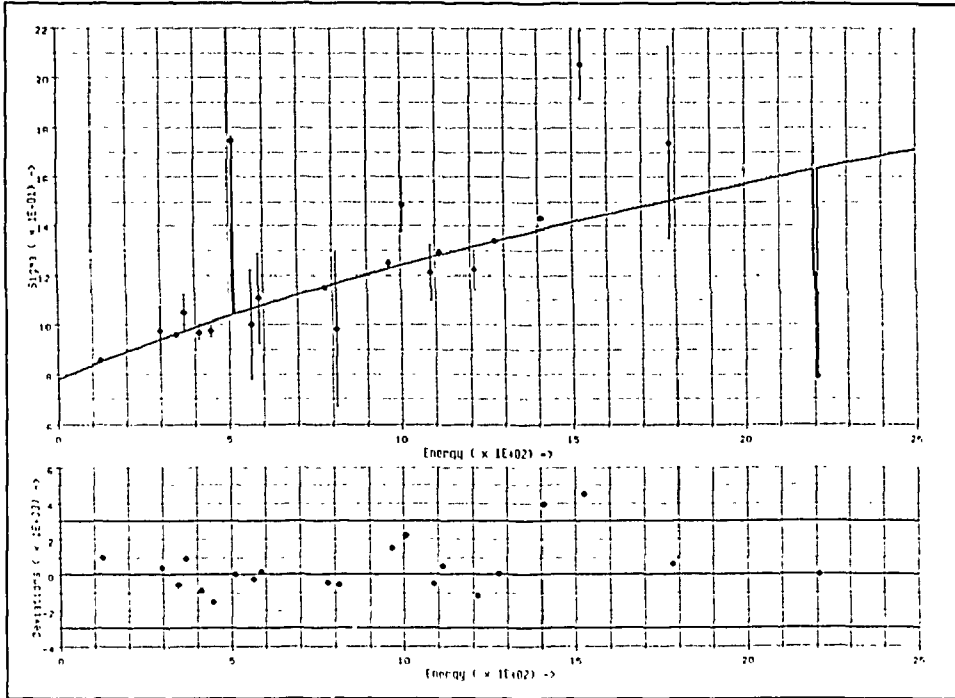
Fig.4.2: Shape calibration curve for the peak width σ. The exceptions made for the annihilation peak and the pulser peak can be seen. The bottom part of the graph shows the standardized deviations between measured peak widths and the curve.

can be used for all ordinary photopeaks. The annihilation peak at 511 keV however is much wider than neighbouring peaks. In the IRI system, a second exception must be made for the pulser peak, which is much narrower than its neighbours.

SPECFIT solves the problem indicated by using the functional representation given above for the σ calibration to fit the experimental values of σ to a curve. Iteratively, all points are excluded from the fit to see which point has the largest effect on the χ_r^2 of this fit. Once the "worst" point has been found, it is excluded completely. This process is repeated until the χ_r^2 is smaller than 2. Now, all points are used again to find out which two are separated the most from the curve: One in the positive direction, the other in the negative direction. The first one must be the

annihilation peak, the second one the pulser peak. A typical example of the resulting curve can be seen in Fig.4.2.

The other shape parameters are fitted to a linear curve. The parameters of the pulser and annihilation peak are excluded from the fit again and stored separately.

4.5.11. User interaction.

The user performing the shape calibration can see the calibration curves as determined by the program. If the pulser peak or the annihilation peaks was incorrectly identified, he can exclude peaks from the shape calibration process by pointing them out using a graphical display and a mouse.

4.6. Energy calibration

The energy calibration consists of a quadratic curve fitted to the relation between peak position and corresponding peak energy, using the uncertainties in peak position to obtain a χ_r^2 indicating the quality of the calibration.

4.7. Reduction of an unknown spectrum

4.7.1. Peak search

The peak search is performed as for the calibration spectrum, but the width of the peak search filter is adjusted every 100 channels to the width of the peaks in the spectrum, as known from the shape calibration.

4.7.2. Estimation of parameters

The parameters σ, r,t and S, which were all determined in the shape calibration, are taken directly from these calibrations. Peak area and position are estimated as described in the preceding paragraphs. After estimation of all parameters, it is decided which peaks overlap or constitute a multiplet.

4.7.3. The fitting procedure

The fitting procedure deals with two lists of multiplets: The list of estimated peaks or multiplets to be fitted and the list of already fitted peaks or multiplets. First, it searches the list of multiplets to be fitted for the multiplet with the highest total area and removes it from this list. Second, it searches both lists for any multiplet overlapping the multiplet now to be fitted. If such a multiplet is found, its contribution to the channel contents now to be fitted is subtracted from them. Finally, the

multiplet parameters are fitted to the remaining channel contents. This procedure is repeated until no peaks are left in the list of estimates.

Again, the fit is performed by common non-linear least squares methods as described in par.4.5.9. In this case however, not all peak parameters are varied in the fitting. For highly significant multiplets consisting of a single peak, only the compton step S and the left tail parameter l are kept constant. For less significant multiplets, the peak width σ and the right tail parameter are kept constant as well.

As compared to the other software packages, this fitting procedure is very different from the others in one respect: It does not attempt to enhance the quality of a fit by introducing extra peaks in a multiplet. This results in more problematic fits to be handled by the user, but it stabilizes the results of other peaks enormously. The number of peaks as located by the peak search algorithm thus is equal to the number of peak positions and areas reported in the end.

4.7.4. Total area computation

The total area of the peak as computed must include the extra area outside the gaussian function but inside the tails. Only when the computation is performed like this can the results of manual fits as described in par.4.7.7 be compatible with the results of the automatic fitting procedure. Moreover, not including the area under the tails would introduce an uncontrolled source of variation in the results of the latter procedure.

4.7.5. The "range" concept

When the time comes to interprete the reduced gamma-ray spectrum, the uncertainties in the peak positions are of no use when comparing experimental peak energies and catalogued gamma-ray energies. Not only the amplifier may have shifted between energy calibration and measurement, but also unrecognized doublets and the like may cause discrepancies between experimental and theoretical peak energies. This is usually solved by setting the uncertainty in the peak positions to 0.5 keV or 1 keV, as in GAUSS VII.

SPECFIT determines a range for each peak that can be used as the uncertainty in the peak position for interpretation purposes. This range is defined as the number of channels where the peak introduces significant non-linearities in the spectrum. In this range, other, smaller peaks may have gone unnoticed. The range of a very intense peak thus is larger than the range of a peak with low statistics.

4.7.6. Recognition of problematic fits

Highly sophisticated algorithms have been devised to decide about the "goodness-of-fit". The simplest method is to check the χ^2 obtained from the fitting procedure. If the value of χ_r^2 exceeds the 95% confidence level, the fit can be classified as "bad". A

more sophisticated method is to test for auto-correlation between the residuals of the fit[5].

SPECFIT tests the χ_r^2 only. If the value of χ_r^2 exceeds 2.0, the fit is flagged as "bad". An exception is made for peaks of which the uncertainty in the area would remain better than 1 % after multiplication with the square root of χ_r^2. This seemingly illogical exception stops very intense peaks, of which the shape always significantly differs from the theoretical shape, from being marked as "bad".

4.7.7. User interaction
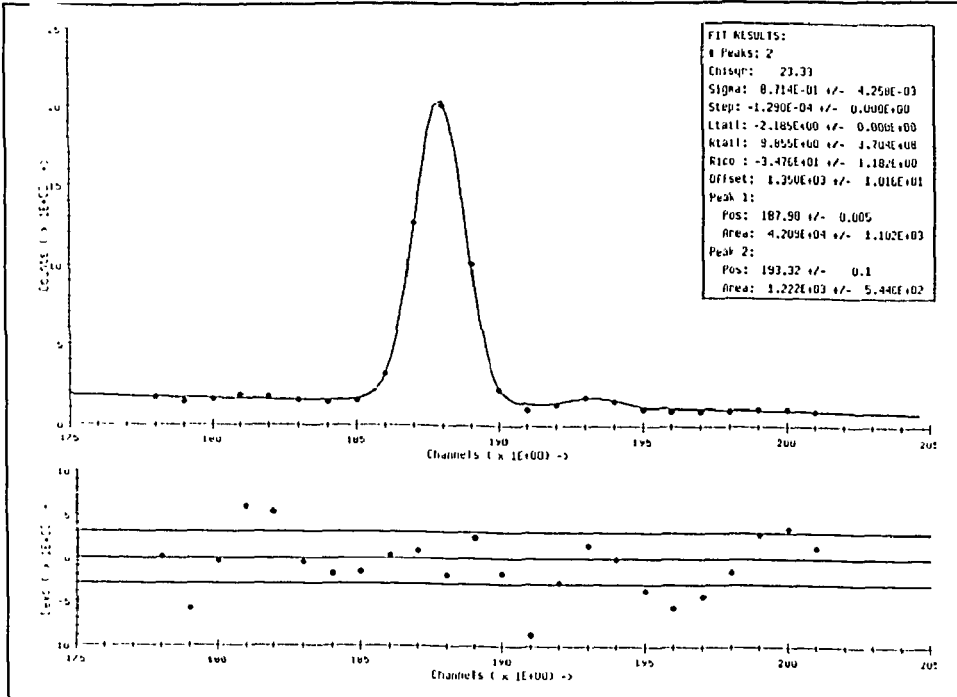
Fig.4.3: Photopeak fit as displayed by the SPECFIT program. The bottom part of the graph shows the standardized deviations between measured and fitted channel contents.

The user of the SPECFIT program can obtain graphical displays of the spectrum as a whole and of each individual fit. The program will also point out where the "bad" fits are in the spectrum. The quality of each fit can be assessed by looking at screens as shown in Fig.4.3. The top part of the picture displays the actual channel contents as well as the theoretical, fitted curve, the bottom part displays the residuals of the fit, i.e. the standardized differences between theoretical and actual channel contents. SAMPO uses similar displays to present its fits.

If the user decides that the fit is bad indeed, he can ask for a different presenta-
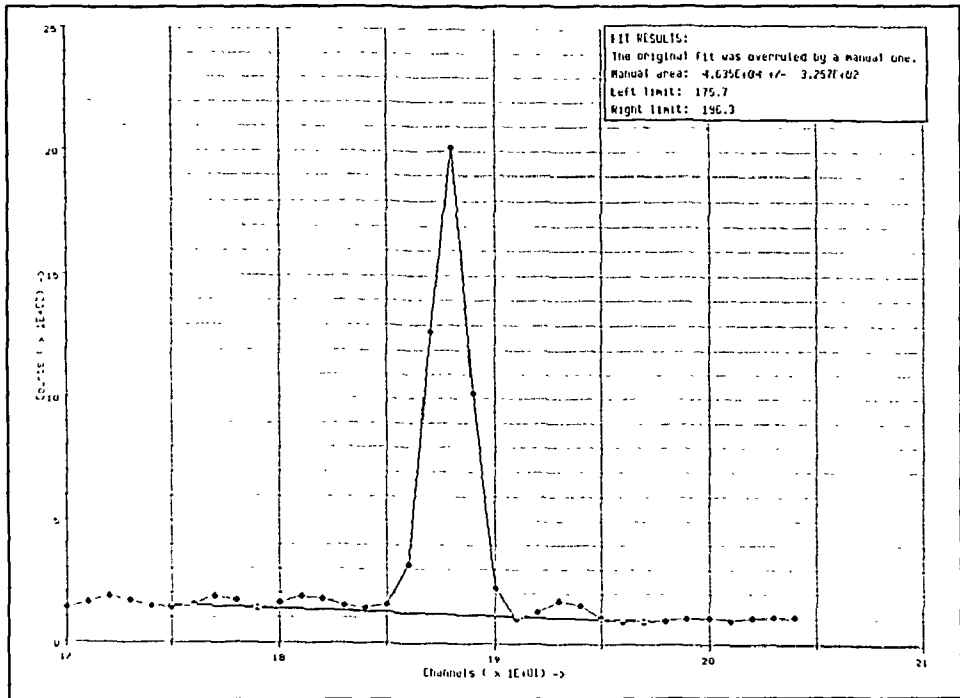
Fig.4.4: Manual fit as performed using the SPECFIT program. The user selected channels 1750 and 1980 as background channels.

tion of the peak and make a manual fit as shown in Fig.4.4. No other program encountered in literature or commercial brochures offers this possibility, even though it is a commonly recognized fact that the human eye can perform this task better than any computer program, as mentioned in the introduction to this chapter.

The user can also decide that the peak displayed is not a photopeak at all, but e.g. a Compton edge. In this case, he can set the uncertainty in the peak area to a huge value.

Again, the procedures available to the user cannot alter the number of peaks as determined by the peak search algorithm.

4.8. Conversion to energy, correction for dead time, pile-up and background.

Using the energy calibration curve created previously, the conversion of peak positions and ranges to peak energies is straightforward. The dead time of the spectrometer is determined from the pulser peak area: Since the pulser frequency is known for each spectrometer, the missing counts fraction can be computed from the

50

pulser peak area and the counting time, and subsequently be used for the dead time correction of all other peaks. This procedure also corrects for pile-up and random summing.

The counting rates and peak positions obtained separately when no sample was present in the spectrometer are used to correct for background.

4.9. References

1. R.G.Helmer, M.H.Putnam, C.M. McCullagh, Nucl.Instr.Meth in Phys.Res. A242 (1986) 427-436
2. P.A.Aarnio, M.T.Nikkinen, J.T.Routti, "Sampo 90, High Resolution Interactive Gamma Spectrum Aanlysis Including Automation with Macros", report TKK-F-A682, Helsinki University of Technology, 1991.
3. G.W.Philips, K.W.Marlow, Nucl.Instr.Meth. 137 (1976) 525-536
4. R.Gunnink, J.B.Niday, "Computerized quantitative analysis by γ-ray spectroscopy (program GAMANAL), UCRL-51061, vols 1-2 (1972).
5. P.A.Aarnio, M.J.Koskelo, P.Zombori, Nucl.Instr.Meth. 184 (1981) 487-492

Part II

Standardization
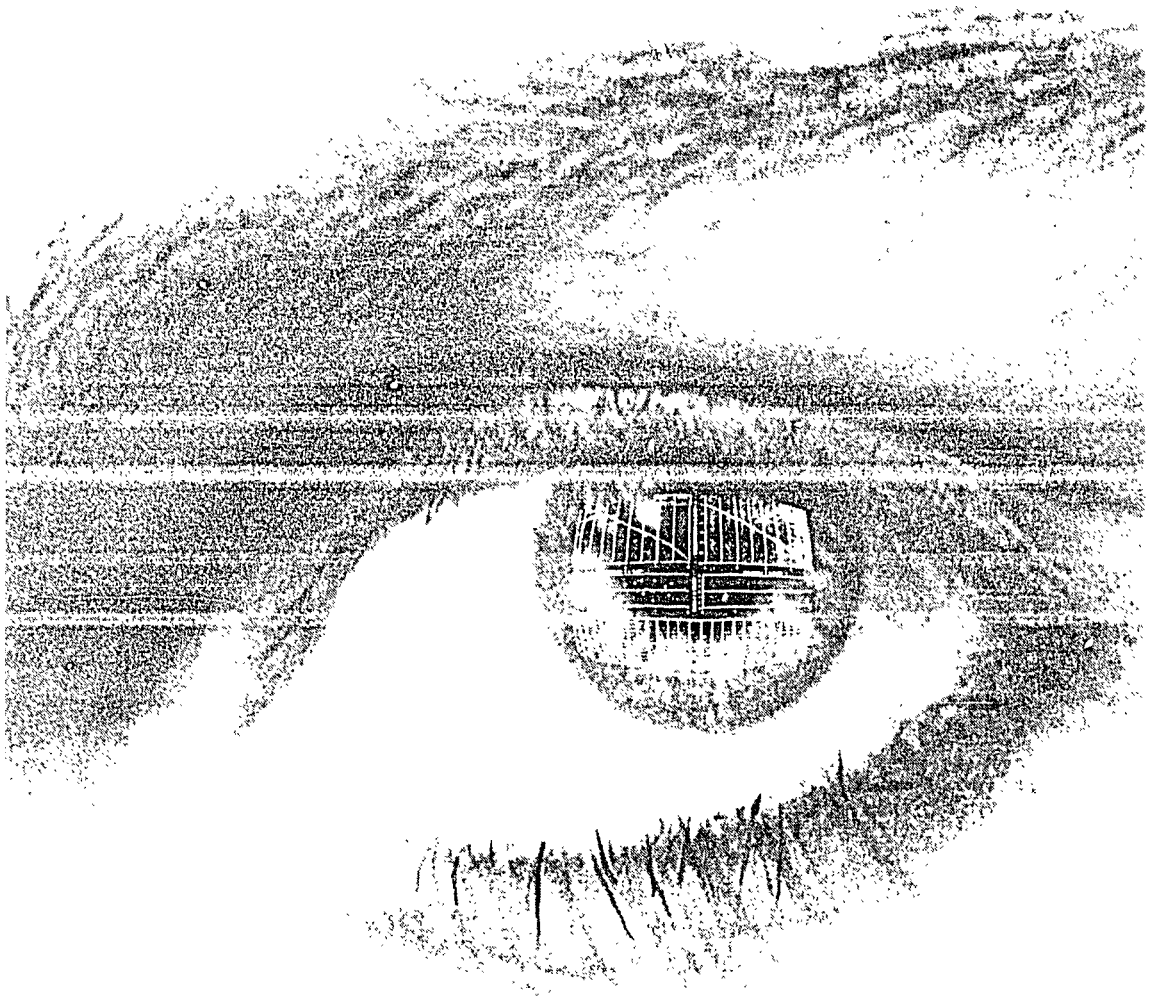
Chapter 5
Introduction to Standardization

5.1. Methods of standardization

In NAA, the proportionality factors F relating the amount of the elements present in the sample to the area of the photopeak observed in the gamma-ray spectrum are given by

$$F = \frac{A}{w} = \frac{\theta N_{Av} \sigma_{eff} \gamma}{M} \Phi \epsilon \, SDC \qquad (5.1)$$

where
A = photopeak area
w = amount of element [g]
θ = isotopic abundance
N_{Av} = Avogadro's number [mol^{-1}]
M = atomic mass [g.mol^{-1}]
σ_{eff} = effective neutron capture cross section [m^2]
Φ = effective neutron flux [m^{-2}s^{-1}]
γ = absolute gamma-ray abundance
ϵ = absolute photopeak efficiency of the detector
S = saturation correction [s]
D = decay correction
C = counting correction
The saturation correction S is given by

$$S = \frac{(1 - e^{-\lambda t_{ir}})}{\lambda} \qquad (5.2)$$

where
λ = decay constant of the activated nuclide
t_{ir} = irradiation time,
the decay correction D is given by

$$D = e^{-\lambda t_d} \qquad (5.3)$$

where
t_d = decay time,
and the counting correction C is given by

$$C = (1 - e^{-\lambda t_c})$$
<div style="text-align:right">(5.4)</div>

where

t_c = counting time.

The process of correlating the readings of any instrument with a standard is usually called "calibration", whereas "standardization" is the process of making something conform to a standard[1]. However, in INAA, where many calibration processes are involved, the determination of the aforementioned proportionality factor is called standardization. A distinction is made between absolute and relative methods for standardization.

In the absolute standardization method, the physical parameters determining the proportionality factors, e.g. σ, θ, γ, M are taken from literature. For many (n,γ)-reactions of interest, these parameters are not precisely known. Because they were determined by independent methods, their imprecisions will add up when calculating amounts of elements, leading to large systematic errors of more than 100 % in some cases.

In the relative standardization method, the unknown sample is irradiated together with a calibration sample containing a known amount of the element of interest. The calibration sample or standard is measured under the same conditions as the sample. The ratio of the net areas of the photopeaks corresponding to the element of interest in the two measured spectra is used to calculate the concentration when interpreting the spectra. In this procedure, all parameters except the half life of the radionuclide of interest cancel out and therefore are of no consequence. This standardization method is still being used in those cases where the highest accuracy is required, e.g. when certifying reference materials, but it is not suited for multi-element analysis. It is impossible to put individual standards for all 70 detectable elements that might be present in the sample in the same place as the sample during irradiation. It is also virtually impossible to produce a multi-element standard containing known amounts of all these elements with sufficient accuracy, homogeneity and stability. Sometimes, certified reference materials are used as multi-element standards. This is a dangerous practice, because reference materials are not primary standards - certified concentrations often are imprecise, sometimes even inaccurate.

Single comparator standardization methods make multi-element analysis with INAA feasible. Assuming stability in time of all relevant experimental conditions, standards for all elements are co-irradiated each in turn with the chosen single comparator element. Once the sensitivity for all elements relative to the comparator element is known, this comparator element can be used in routine measurements instead of separate standards for each element.

5.2. Single comparator methods

The original single comparator method used for multi-element analysis with INAA was based on the ratio of the proportionality factors of the analyte and of the comparator element after correction for saturation, decay, counting and sample weights, as expressed in the definition of the k-factor[2]:

$$k = \frac{M_c \gamma_a \epsilon_a \theta_a \sigma_{eff,a}}{M_a \gamma_c \epsilon_c \theta_c \sigma_{eff,c}} \qquad (5.5)$$

where the subscripts a and c denote analyte and comparator, respectively.
Concentrations were calculated from the k-factors and specific counting rates by

$$\rho = \frac{A_{sp,a}}{A_{sp,c}} \frac{1}{k} \qquad (5.6)$$

where

ρ = concentration [g/g]
A_{sp} = specific counting rate [in $s^{-1}g^{-1}$], given by

$$A_{sp} = \frac{A}{SDCw} \qquad (5.7)$$

These k-factors, obtained from direct measurements, are usually much more precise than the k-factors obtained from literature data in the absolute standardization method. On the other hand, the measured k-factors are valid only for a specific detector, counting geometry and irradiation facility, and remain valid only as long as the neutron flux parameters of the irradiation facility remain stable. At IRI, the k-factors were made versatile with respect to some detectors and counting geometries by removal of the photopeak efficiencies from the definition of the k-factor[3]. These efficiencies were obtained from efficiency curves measured for each detector and counting geometry. For well-type detectors, the old k-factors remained in use.

At the Institute for Nuclear Sciences in Ghent, Belgium, attempts were made to define k-factors that would be independent of neutron flux parameters as well as of spectrometer characteristics. Originally, De Corte[4] proposed to use the Høgdahl convention to relate the effective neutron cross section to the neutron flux parameters[5]. The Høgdahl convention was temporarily abandoned in favour of the Stoughton Halperin convention in the paper that presented the k_0-factor, but later on became the convention of choice again[6]. In the definition of the k_0-factor, the effective neutron cross section has been replaced:

$$\sigma_{eff} = \sigma_0 \left(1 + \frac{Q_0}{f} \right) \qquad (5.8)$$

where:

σ_0 = thermal neutron capture cross section [m^2]

f = thermal/epithermal flux ratio

Q_0 = resonance integral/thermal neutron cross section ratio

This equation describes how the effective cross section can be divided in the thermal part σ_0, and a part accounting for the activation by epithermal neutrons. The parameter f describes the presence of the epithermal neutrons, the parameter Q_0 describes the probability of these neutrons activating the nucleus.

The σ_0 part remains in the definition of the k_0-factor, the $(1 + Q_0/f)$ factor is removed from it. What remains is

$$k_0 \equiv k \, \frac{f + Q_{0,c}}{f + Q_{0,a}} = \frac{M_c \theta_a \sigma_{0,a} \gamma_a}{M_a \theta_c \sigma_{0,c} \gamma_s} \tag{5.9}$$

Ideally, the energy distribution of the epithermal neutrons can be described by a $1/E$ relation. In practice, deviations from the $1/E$ distribution can be modelled using a $1/E^{1+\alpha}$ relation. In the k_0 method, the Høgdahl convention was adapted to the non-ideal epithermal neutron spectrum shape by the introduction of the average resonance energy E_r, as a nuclide property, and α, as a neutron flux parameter. The neutron flux parameters f and α no longer cancel out in concentration calculations and must be measured in each irradiation facility, preferably even for each irradiation and sample[7]. At least three isotopes must be activated and measured to determine these parameters. Essentially, the k_0-method is therefore not a single comparator but a triple comparator method. The nuclide parameters k_0, E_r and Q_0 need be determined only once for each (n,γ) activation reaction. As compared to the original single comparator method, the k_0 method has gained versatility, but its parameters cannot be measured as directly as the original k-factor and the results will therefore be less precise. According to De Corte[8], the most important k_0 factors now have been determined with relative precisions better than 3 %.

In Chapter 6, an alternative for the Høgdahl convention is presented. This chapter can be regarded as a critique of the protocols the k_0-method prescribes for determination of its parameters. Similar criticism has been uttered elsewhere[9,10].

The k_0-method encompasses more than just the definition of the k_0-factor and a compilation of carefully determined values of these factors: It is concerned with coincidence corrections too. This part of the method has a much wider scope than the k_0 factors because it applies to gamma-ray spectrometry in general. In Chapter 7 of this work it is demonstrated that the gamma-ray abundance will have to be removed from the k_0 factor in order to deal with sum peaks introduced in the gamma-ray spectrum by coincidence summing. What remains is a factor k_1:

$$k_1 = \frac{M_c \theta_a \sigma_{0,a}}{M_a \theta_c \sigma_{0,c}} \tag{5.10}$$

The published k_0 catalogue[7] is not yet complete enough: it contains much less activation reactions than the catalogue determined at IRI. Especially many of the reactions involving short lived radionuclides are still missing. The k_0 catalogue could be supplemented by the constants measured at IRI, if these could be converted to values useful to all co-workers in this field. Chapter 8 offers a description of this procedure.

In Chapter 9 methods are presented to deal with the severe coincidence effects as observed in gamma-ray spectra obtained with well-type detectors, and take advantage of the versatility of the k_1-factor.

Most concentration calculations in activation analysis, including those in the k_0-method, are based on Eq.(5.1). This formula is an approximation which can only be used in the simplest cases where the radionuclide to be measured is produced directly and burn-up of all isotopes involved is negligible. To overcome this problem, De Corte specifies different activation formulas for different modes of activation of the radionuclide to be measured in the end. To correct for burn-up, De Corte but also others[11] use the effective neutron cross section on its own. Complex activation is much easier to deal with using cross-section values instead of k_1 values as well. This is obvious when the many complex, specific equations in De Corte's thesis[5] (p36-40) are compared to the generally applicable algorithm presented in Chapter 10 of this work.

5.3. References

1. F.G. Fowler, H.W. Fowler, "*The Oxford Handy Dictionary*", Oxford University Press, Lonodn, 1989.
2. F. Girardi, G. Guzzi, J. Pauly, Anal.Chem., 37/9 (1965) 1085
3. M. de Bruin, P. Korthoven, Anal.Chem., 44/14 (1972) 2382
4. A. Simonits, F. De Corte, J. Hoste, J. Radioanal.Chem., 24 (1975) 31
5. F. De Corte, A. Speecke, J. Hoste, J. Radioanal.Chem., 3 (1969) 205
6. F. De Corte, "The k_0-Standardization Method - A move to the optimization of neutron activation analysis", (1987) thesis, INW, Ghent.
7. P. Bode, M. Blaauw, I. Obrusnik, J.Radioanal.Nucl.Chem. 157 (1992) 310-312
8. F. de Corte, A. Simonits, A. de Wispelaere, A. Elek, J.Radioanal.Nucl.Chem. 133 (1989) 3-41
9. S. Yusuf, R.F. Fleming, Proc. Modern Trends in Activation Analysis 1991, J.Radioanal.Nucl.Chem., (in press)
10. N.B. Kim, K.S. Park, J.Korean Nucl.Soc., 18 (1986), 85-91
11. M. Verheijke, *Instrumental Neutron Avtivation Analysis Developed for Silicon Integrated Circuit Technology*, Ph.D. thesis, Philips Eindhoven, 1992.

Chapter 6

An Alternative Convention Describing the (n,γ)-Reaction Rate Suited for Use in the k_0-Method of INAA

6.1. Introduction

The relation between activation rates and energy distribution of the neutrons must be determined in order to find k-factors that do not depend on the shape of the neutron flux distribution. For the special case of a reactor neutron spectrum in combination with the majority of the (n,γ)-reactions, Høgdahl[1,2] introduced a conven-
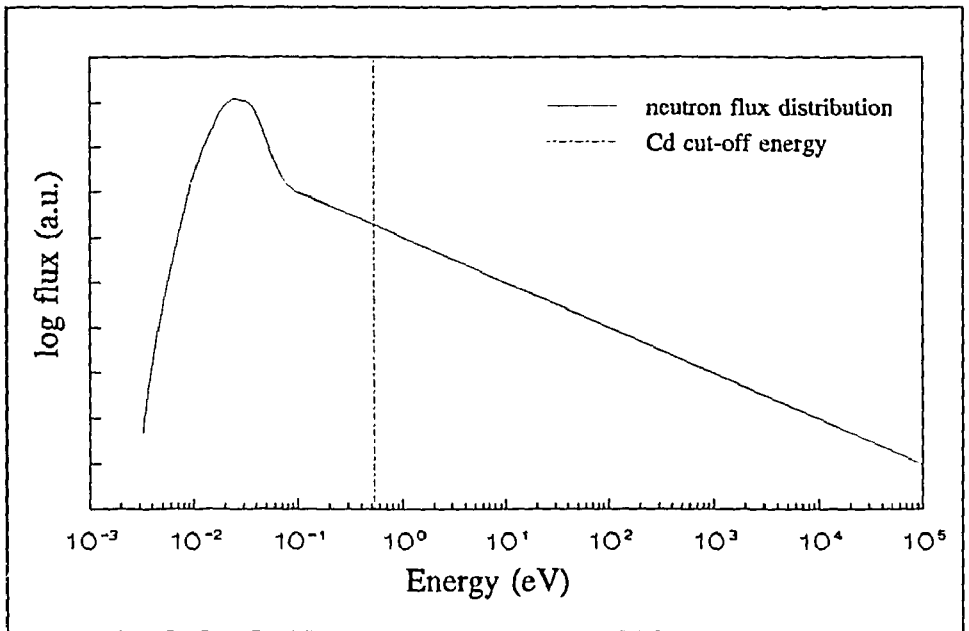
Fig.6.1: Neutron flux division according to the Høgdahl convention.

tion describing the activation rate as a function of two parameters for the (n,γ)-reaction (the thermal neutron capture cross section σ_0 and the resonance integral I_0) and two parameters for the neutron spectrum (the subcadmium en epicadmium fluxes Φ_s and Φ_e). The Høgdahl convention prescribes the determination of the parameters by irradiations with and without cadmium cover in a single irradiation facility. Cadmium was selected for this purpose because its neutron cross section as a function of neutron energy resembles a step function, with the step at 0.55 eV. This energy is a

reasonable approximation of the neutron energy 0.35 eV, above which the thermal neutron flux can be neglected as compared to the epithermal neutron flux (De Corte[3]).

Simonits[4] et al. used the Høgdahl convention when they introduced the k_0-method for INAA. A third parameter was introduced for both the spectrum (the deviation from the ideal $1/E$ epithermal neutron distribution α) and the nuclide (the effective resonance energy E_r).

The k_0-method was devised in order to avoid the extensive calibrations that where previously needed each time a new irradiation facility was used for INAA. It is not a theory describing a physical phenomenon, but a protocol for calibration procedures.

The accuracy of any calibration protocol may deteriorate if calibration measurements are not performed under the same experimental conditions as the actual measurements. This is the case when Cd-cover irradiations are used to calibrate parameters to be used for irradiations without Cd-cover. The resulting values will only be valid for those (n,γ)-reactions behaving exactly as described by the Høgdahl convention. Furthermore, the Cd-cover used may be a significant source of error itself.
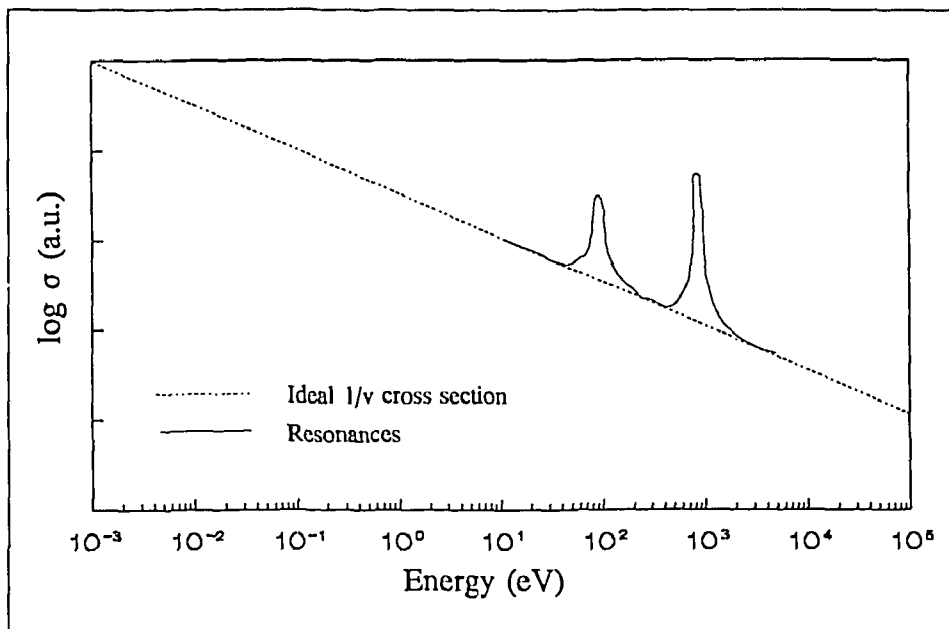
Fig.6.2: Neutron cross-section division according to the alternative convention.

In order to solve these problems, an alternative for the adapted Høgdahl convention for use in the k_0-method is presented here. Instead of dividing the neutrons in two groups (Fig.6.1), the neutron capture cross section of the nuclide is

divided in two parts (Fig.6.2). Neutrons with energies in the MeV range are neglected in both conventions. The resulting convention is mathematically simpler and physically mor meaningfull than the adapted Høgdahl convention, as will be shown.

6.1.1. Theory

In order to facilitate comparison between the two conventions, and clarify the dimensions of some of the variables involved, the relevant formulas used in the k_0-method will be reviewed in slightly adapted notations.

During reactor neutron irradiation of a nuclide, the (n,γ)-reaction rate (in s^{-1}) per nucleus is given by:

$$R = \int_0^{\infty} \sigma(v)\,\Phi(v)\,dv \qquad (6.1)$$

where

$\sigma(v)$ = (n,γ) cross-section [in m^2] at neutron velocity v,
v = neutron velocity [in m/s],
$\Phi(v)$ = neutron flux per unit of velocity [in m^{-3}] at neutron velocity v.

6.1.2. The adapted Høgdahl convention

According to the Høgdahl convention, Eq.(6.1) is split into

$$R = \int_0^{v_{Cd}} \sigma(v)\,\Phi(v)\,dv + \int_{v_{Cd}}^{\infty} \sigma(v)\,\Phi(v)\,dv \qquad (6.2)$$

where

v_{Cd} = velocity of a neutron corresponding with the Cd cut-off energy (0.55 eV).

For most (n,γ)-reactions the following description can be applied for velocities below v_{Cd}:

$$\sigma(v) = \sigma_0 \frac{v_0}{v} \qquad (6.3)$$

where

v_0 = the Maxwellian neutron velocity [in m/s], conventionally set to 2200 m/s.
σ_0 = $\sigma(v_0)$ [in m^2].

Substitution of Eq.(6.3) in the left-hand integral of Eq.(6.2) yields

$$\int_0^{v_{cd}} \sigma(v)\Phi(v)dv = \int_0^{v_{cd}} \frac{\sigma_0 v_0 \Phi(v)}{v}dv = \sigma_0 v_0 \int_0^{v_{cd}} n(v)dv \qquad (6.4)$$

where

$n(v)$ = the density of neutrons [in s.m^{-4}] at velocity v.

Definition of the conventional sub-cadmium neutron flux Φ_s by

$$\Phi_s \equiv v_0 \int_0^{v_{cd}} n(v)dv \qquad (6.5)$$

and substitution of Φ_s in Eq.(6.4) yields:

$$\int_0^{v_{cd}} \sigma(v)\Phi(v)dv = \sigma_0 \Phi_s \qquad (6.6)$$

For reactions with non-1/v behaviour in the sub-cadmium region, this equation becomes dependent on the Maxwellian neutron temperature T of the thermal neutrons.

The right-hand integral in Eq.(6.2) can be written as

$$\int_{v_{cd}}^{\infty} \sigma(v)\Phi(v)dv = \int_{E_{cd}}^{\infty} \sigma(E)\Phi(E)dE \qquad (6.7)$$

where

E = neutron energy [in eV], and

$\Phi(E)$ = flux at energy E [in m^{-2}s^{-1}eV^{-1}].

For energies higher than 0.35 eV the neutron flux can be described by

$$\Phi(E) = \frac{\Phi(E_{ref})}{(E/E_{ref})^{1+\alpha}} \qquad (6.8)$$

where

E_{ref} = an arbitrarily chosen energy. (usually 1 eV).

Defining the resonance integral I_0 by

$$I_0(\alpha) \equiv \int_{E_{cd}}^{\infty} \sigma(E)\frac{E_{ref}{}^{\alpha}}{E^{1+\alpha}}dE \qquad (6.9)$$

and the conventional epicadmium neutron flux Φ_e [in s^{-1}m^{-2}] by

$$\Phi_e \equiv \Phi(E_{ref})E_{ref} \tag{6.10}$$

and using Eq.(6.8) yields

$$\int_{E_{Cd}}^{\infty} \sigma(E)\Phi(E)dE = I_0(\alpha)\Phi_e \tag{6.11}$$

Defining the "pure" resonance integral $I_0'(\alpha)$ by

$$I_0'(\alpha) \equiv \int_{E_{Cd}}^{\infty} \{\sigma(E) - \frac{\sigma_0 v_0}{v}\} \frac{E_{ref}^{\alpha}}{E^{1+\alpha}}dE \tag{6.12}$$

and the effective resonance energy $E_r(\alpha)$ by

$$\{\frac{E_r(\alpha)}{E_{ref}}\}^{-\alpha} \equiv \frac{I_0'(\alpha)}{I_0'(0)} \tag{6.13}$$

and approximating $E_r(\alpha)$ by

$$E_r(\alpha) = E_r \tag{6.14}$$

the relation between $I_0(\alpha)$ and $I_0(0)$ is given by

$$I_0(\alpha) = E_{ref}^{\alpha} \{\frac{I_0(0) - 0.429\sigma_0}{E_r^{\alpha}} + \frac{0.429\sigma_0}{(2\alpha+1)E_{Cd}^{\alpha}}\} \tag{6.15}$$

where
$0.429 = 2(E_0/E_{Cd})^{1/2}$, using $E_0 = 0.0253$ eV and $E_{Cd} = 0.55$ eV.
The value of E_r does not depend on the choice of E_{ref}, since E_{ref} can be eliminated completely from Eq.(6.12) using Eq.(6.11).
     Ultimately, Eq.(6.1) is transformed to

$$R = \sigma_0\Phi_s + I_0(\alpha)\Phi_e \tag{6.16}$$

The parameters σ_0, I_0 and E_r are to be determined for each nuclide by calibration measurements, making use of Cd cover, and should not depend on the irradiation facility used for these measurements.

6.1.3. The alternative convention
     In the alternate approach, Eq.(6.1) is divided into

$$R = \int_0^\infty \frac{\sigma_0 v_0}{v} \Phi(v)dv + \int_0^\infty [\sigma(v) - \frac{\sigma_0 v_0}{v}] \Phi(v)dv \qquad (6.17)$$

This means that not the neutron spectrum, but the cross-section is divided into two parts. The first part is the underlying $\sigma_0 v_0/v$-part, the second part consists of the superposed resonances only.

Definition of the total conventional neutron flux Φ_t by

$$\Phi_t \equiv v_0 \int_0^\infty n(v)dv \qquad (6.18)$$

and substitution of Φ_t in the left-hand integral in Eq.(6.16) yields

$$\int_0^\infty \frac{\sigma_0 v_0}{v} \Phi(v)dv = \sigma_0 \Phi_t \qquad (6.19)$$

If the integrand in the right-hand integral in Eq.(6.16) is 0 up to 0.35 eV, the description of the epithermal neutron flux (Eq.(6.8)) can be used instead of $\Phi(v)$. This is the case for the (n,γ)-reactions considered here, which have $1/v$ behaviour below 0.35 eV. Definition of an alternate "pure" resonance integral $I_0''(\alpha)$ by

$$I''_0(\alpha) \equiv \int_0^\infty [\sigma(E) - \frac{\sigma_0 v_0}{v}] \frac{E_{ref}^{\alpha}}{E^{1+\alpha}} dE \qquad (6.20)$$

and substitution of the description of the epithermal neutron flux Eq.(6.8) in the right-hand integral in Eq.(6.16) yields:

$$\int_0^\infty [\sigma(v) - \frac{\sigma_0 v_0}{v}] \Phi(v)dv = I''_0(\alpha) \Phi_e \qquad (6.21)$$

$I_0''(\alpha)$ is identical to $I_0'(\alpha)$ for (n,γ)-reactions with $1/v$ behaviour between 0.35 eV and 0.55 eV. For those reactions, the relation between $I_0''(\alpha)$ and $I_0''(0)$ is also approximated by Eq.(6.12) and Eq.(6.13).
Ultimately, Eq.(6.1) is transformed to

$$R = \sigma_0 \Phi_t + I''_0(\alpha) \Phi_e \qquad (6.22)$$

which formally resembles Eq.(6.15) from the k_0-concept. The parameters σ_0, I_0'' and E_r are to be determined for each nuclide by calibration measurements using different irradiation facilities.

64

6.1.4. Suitability of the alternative convention for use in the k_0-method

The key expression in the k_0-concept, describing the influence of the spectrum parameters on the ratio of the activation rates is

$$\frac{Q_{0,a}(\alpha) + f}{Q_{0,c}(\alpha) + f} \tag{6.23}$$

where the subscripts a and c denote analyte and comparator,

$$Q_0(\alpha) \equiv I_0(\alpha)/\sigma_0 \tag{6.24}$$

and

$$f \equiv \frac{\Phi_s}{\Phi_e} \tag{6.25}$$

To be consistent with the other parameters, f must be measured using irradiations under Cd-cover. At least two isotopes should be used to obtain a value for α as well.

Defining

$$Q_0'(\alpha) \equiv I_0''(\alpha)/\sigma_0 \tag{6.26}$$

and

$$f' \equiv \frac{\Phi_t}{\Phi_e} \tag{6.27}$$

the following is mathematically true:

$$Q_{0,a}'(\alpha) + f' = Q_{0,c}(\alpha) + f \tag{6.28}$$

To measure f' and α, a combination of suitable isotopes is to be used without Cd-cover.

Thus the alternative convention hardly introduces any changes in the k_0-formalism at this level, and is suitable for use in it.

6.2. Discussion

6.2.1. Mathematical simplicity and applicability

In the adapted Høgdahl convention, the (n,γ)-reaction rate is described by Eq.(6.15); the relation between $I_0(\alpha)$ and the commonly tabulated $I_0(0)$ is given by Eq.(6.14). In the alternative convention, the (n,γ)-reaction rate is described by

Eq.(6.20) and the relation between $I_o''(\alpha)$ and $I_o''(0)$ is given by Eq.(6.13). The latter equation is much simpler because of the absence of the Cd cut-off energy.

For those nuclides with 1/v behaviour below 0.55 eV, $I_o''(0)$ can be calculated from $I_0(0)$ with

$$I''_0(0) = I_0(0) - 0.429\sigma_0 \qquad (6.29)$$

For these nuclides the alternative convention is mathematically equivalent, albeit simpler, than the adapted Høgdahl convention. The alternative convention, however, handles all (n,γ)-reactions with 1/v behaviour below 0.35 eV. The adapted Høgdahl convention can handle only those with 1/v behaviour below 0.55 eV. Even for nuclides without 1/v behaviour below 0.35 eV, the alternative convention should improve the accuracy of the k_0-method.

6.2.2. The role of Cd

The intended use of this adapted Høgdahl convention, i.e. the approximate description of activation rates under different irradiation conditions as used for common INAA, is not reflected by the formulas, which still implie the use of irradiations under Cd cover for calibration purposes. The resulting values of determined parameters may not even be valid for use in the k_0-method, because of the differences between calibration and normal experimental setup. It is not only possible to determine the parameters by other means[5,6]; it should be highly recommended, especially for (n,γ)-reactions without $\sigma(v) \sim 1/v$ behaviour below 0.55 eV. These reaction rates cannot be described by the Høgdahl convention and therefore calibration protocols should resemble measurement protocols as much as possible. Besides, the formulas have become unnecessarily complicated by the introduction of α and E_r.

It is important to note that the value of the commonly tabulated resonance integral at $\alpha = 0$, $I_0(0)$, is determined per definition by measurements using Cd-cover. The same goes for f. If the I_0 and E_r values were established by irradiating with different neutron energy distributions *as used for common INAA irradiations*, the results would be of more practical importance for those (n,γ)-reactions with non-1/v behaviour below 0.55 eV. Unknown relations between f, α and the neutron temperature T would be incorporated partly in the experimental $I_0(0)$ value.

In general, the relation between n, the number of (n,γ)-reactions whose parameters must be determined and p, the number of irradiation facilities with different but unknown neutron energy distributions needed to accomplish this, can be derived as follows: Each facility and each (n,γ)-reaction introduce three unknowns in the system of equations to be solved. Each combination of an isotope and a facility yields one equation. The number of unknowns equals the number of equations when

$$np = 3n + 3p \qquad (6.30)$$

from this, it follows that

$$p = 3n/(n-3) \qquad (6.31)$$

This means that at least four (n,γ)-reaction are needed to obtain a solvable system of equations. The accuracy of the results will depend on the degree to which the neutron spectra in the irradiation facilities differ.

On the other hand, knowing the parameters for some suitable reactions, as is the case for[2, 3] ^{94}Zr -> ^{95}Zr, ^{96}Zr -> ^{97}Zr, and ^{197}Au -> ^{198}Au, the parameters for an unknown reaction can be determined by irradiating the isotope together with these comparators with three different neutron energy distributions.

The fact that irradiations under Cd-cover should not be used for the determination of any of the parameters to be used in the k_0-method is reflected by the alternative convention. The newly derived formulas refer to the Cd cut-off energy only to relate the value of $I_0''(0)$ to the commonly tabulated values for $I_0(0)$ for those (n,γ)-reactions with 1/v behaviour below 0.55 eV.

6.3. Conclusions

The alternative convention describing the (n,γ)-reaction rate presented in this study is better suited for use in the k_0-method than the adapted Høgdahl convention previously used by De Corte et al[2, 3].

The formulas ultimately needed to describe the (n,γ)-reaction rate and the dependence between the resonance integral and the spectrum parameter α are simpler.

The alternative convention is less stringent as to the lower limit of non-_1/v_ behaviour of the cross-section (0.35 eV as compared to 0.55 eV), and should yield better results for nuclides which do not satisfy this condition.

Moreover, it reflects the fact that that no irradiations under Cd-cover are used for the the kind of INAA the k_0-method was devised for, and that no irradiations under Cd-cover should be used to determine the parameters defined in the k_0-formalism.

6.4. References

1. O.T. Høgdahl, Neutron Absorption in Pile Neutron Activation Analysis, Rept. MMPP-226-1, 1962

2. O.T. Høgdahl, Proc. Symp. Radiochemical Methods of Analysis, Salzburg 1964, IAEA, Vienna, 1965.
3. F. de Corte, The k_0 Standardization Method - a Move to the Optimization of NAA, thesis, Rijksuniversiteit Ghent, Ghent, Belgium, 1987.
4. A.Simonits, F.de Corte, J.Hoste, J. Radioanal. Chem., <u>105</u> (1975) 31
5. P.Z. Hien, T.K. Mai, T.X. Quang, N.T. Thuy, J. Radioanal. Chem. 105 (6) (1986) 351
6. Y. Zhou, H. Shan, W. Zhang, He Huaxe Yu Fangshe Huaxe, 4 (4) (1982) 216

Chapter 7

Introduction of the k_1-Concept for the Interpretation of "Artificial" Peaks in k_0-Based INAA

7.1. Introduction

In gamma-ray spectrometry with Ge detectors, "artificial" photopeaks may appear in the measured spectrum that do not directly correspond to the energy of a photon emitted by a decaying nucleus, i.e. escape peaks due to pair production in the detector, contributions to the annihilation peak due to pair production in the materials surrounding the detector, and sum peaks due to coincidence summing.

The k_0-method[1] was conceived in 1975, when Ge-detectors had typical efficiencies of 20% (relative to a 3"x3" NaI(Tl) crystal), and well-type detectors were exceptional. Ge detectors with relative efficiencies of 100% and higher are on the market now, and highly efficient well-type detectors are also used for INAA. These detectors introduce sum peaks in the gamma-ray spectra. Also, many radionuclides emit photons with high energies, which introduce escape peaks in the spectra and contribute to the annihilation peak at 511 keV.

· As opposed to escape peaks, sum peaks are rarely used to calculate concentrations from. They may interfere, however, with full energy photopeaks that are more important. ^{82}Br for example has 17 peaks with gamma-ray abundances in excess of 0.1%[2]. When counting in a well-type detector, 10 sum peaks are introduced with comparable intensities, two of which may interfere with the peaks of ^{60}Co. It should be noted that an interference like this may introduce serious errors in the determination of cobalt, while the coincidence losses from the full energy photopeaks of ^{82}Br may be much less significant.

The annihilation peak at 511 keV is the only peak that can be used to determine copper from the medium lived ^{64}Cu radionuclide. This determination can only be carried out if all other contributions to the peak are known. Contributions due to pair production in the sample will depend on the sample matrix.

Furthermore, the holistic interpretation of both natural and artificial peaks will improve the precision of the interpretation results.

The k_0-method cannot deal with these "artificial" peaks. Many users of the k_0-method will have made their own extensions to the method to overcome this problem. In this chapter we propose an alternative k_1-constant for sum peaks and additional efficiency curves for escape peaks as the standard way to solve the problem.

7.2. The inability of the k_0-method to deal with "artificial" peaks

In the k_0-method, concentrations are calculated from

$$\rho = \frac{A_{sp,a}k_{0,c}}{A_{sp,c}k_{0,a}} \frac{\epsilon_{f,c}c_c}{\epsilon_{f,a}c_a} \frac{f+Q_{0,c}(\alpha)}{f+Q_{0,a}(\alpha)} \qquad (7.1)$$

where the subscripts a and c denote analyte and comparator, resp.,

ρ = concentration [g/g]
A_{sp} = specific counting rate [in $s^{-1}kg^{-1}$]
ϵ_f = photopeak efficiency of the detector
c = coincidence correction factor
f = ratio of thermal to epithermal flux
$Q_0(\alpha)$ = ratio of resonance-integral to thermal neutron cross-section

The definition of the k_0-constant as shown in Eq.(6.3) includes γ, the emission probability of the photons corresponding to the photopeak involved. For some photopeaks observed in gamma-ray spectra, however, this value does not exist. These peaks, here denoted as "artificial", are divided in two classes:

1) "artificial" peaks of the first kind are defined as photopeaks which correspond only to the detection of two or more photons: sum peaks resulting from true coincidence (cascade summing). For these peaks, γ and the k_0-constant do not exist and no coincidence correction factor can correct for that, because it is a multiplication factor and can only correct k_0-constants of "natural" peaks - which correspond to the complete detection of a single photon - for coincidence gains or losses. This problem dates back to Debertin[3], who originally defined the coincidence correction factor.

2) "artificial" peaks of the second kind are defined as peaks which do correspond to the detection of a single photon, but not directly to its energy: escape peaks and contributions to the annihilation peak stemming from pair production in materials surrounding the detector.

7.3. "Artificial" peaks of the first kind: Definition of the k_1-constant

Sum peaks caused by true coincidence result from the simultaneous emission of two or more photons by a single decaying nucleus, followed by complete registration of two or more of them in one peak. No k_0-constant can be defined for these peaks, if no single γ exists for them. To solve this problem, it will be necessary to define an alternative for the k_0. The newly defined k_1-constant should apply to all peaks, irrespective of their nature. The solution appears naturally when Eq.(7.1) is rearranged as follows:

$$\rho = \frac{A_{sp,a}(k_{0,c}/\gamma_c)}{A_{sp,c}(k_{0,a}/\gamma_a)} \frac{\gamma_c \epsilon_{f,c} c_c}{\gamma_a \epsilon_{f,a} c_a} \frac{f + Q_{0,c}(\alpha)}{f + Q_{0,a}(\alpha)} \tag{7.2}$$

For natural photopeaks, the probability P of obtaining a count in the photopeak when the nucleus decays is given by

$$P = \gamma \epsilon c \tag{7.3}$$

Whereas γ does not exist for a sum peak, P does. The k_1-constant is therefore defined as

$$k_1 = \frac{M_c \theta_a \sigma_{0,a}}{M_a \theta_c \sigma_{0,c}} = \frac{\gamma_c}{\gamma_a} k_0 \tag{7.4}$$

and Eq.(7.1) changes to

$$\rho = \frac{A_{sp,a} k_{1,c}}{A_{sp,c} k_{1,a}} \frac{P_c}{P_a} \frac{f + Q_{0,c}(\alpha)}{f + Q_{0,a}(\alpha)} \tag{7.5}$$

The introduction of the k_1-constant amounts to the separation of the k_0-constant into a part related to activation (the k_1) and a part related to spectrometry (the gamma-ray abundance). There is no separate k_1-constant for each peak of a radionuclide. The gamma-ray abundance must be used together with decay scheme information and detector efficiencies to calculate P.

7.4. "Artificial" peaks of the second kind: Extension of the description of detector efficiency

In Eq.(7.1), the photopeak efficiency ϵ_f is to be used for full energy photopeaks only. To handle "artificial" peaks of the second kind, additional efficiencies have to be defined so they can be substituted for ϵ_f in Eq.(7.1):
- The single escape efficiency ϵ_{s1} of a gamma-ray spectrometer at a given energy is the probability that a photon with that energy is transduced and registered as if it was a completely registered photon with 511 keV less energy.
- The double escape efficiency ϵ_{s2} of a gamma-ray spectrometer at a given energy is the probability that a photon with that energy is transduced and registered as if it was a completely registered photon with 1022 keV less energy.
- The annihilation contribution efficiency ϵ_{s11} of a gamma-ray spectrometer at a given energy higher than 1022 keV is the probability that a photon with that energy is transduced and registered as if it were a completely registered photon of 511 keV.
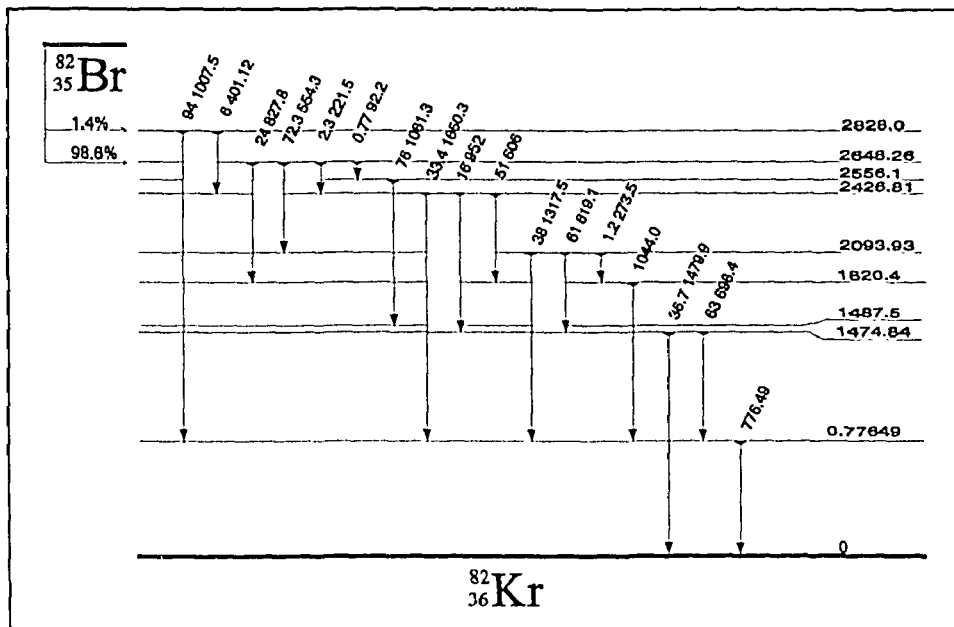
Fig.7.1: Simplified decay scheme of ^{82}Br.

Many useful mathematical descriptions of the relation between photopeak efficiency and photon energy are known. Likewise, ϵ_{s1} and ϵ_{s2} can be related to photon energy[4]. In each case, only a few efficiencies need be measured to enable calculation of the rest. ϵ_{s11} is difficult to measure and will depend on the sample composition. Possibly, it will be necessary to measure the P-values for the annihilation peak for the relevant radionuclides in varying sample compositions.

Using Eq.(7.1) and the substitutions defined above, all peaks measured under circumstances where coincidence effects can be neglected can be interpreted or corrected for. Only minor changes to existing k_0-software are necessary to implement this.

7.5. The k_1-method in practice

7.5.1. Determination of the k_1-constant

The k_1-constant cannot be measured directly, as is possible for the k_0. It must be derived from the k_0-constant, to maintain the advantages stemming from the careful determination of the k_0-constant. Moreover, the information contained in the different k_0-constants for different peaks of a single radionuclide, possibly in disagreement with the published gamma-ray abundances, must not be lost.

This can be accomplished by calculating the k_1-constant from the k_0-constant of the most characteristic peak of the radionuclide and its gamma-ray abundance. The latter value can be taken from literature. The gamma-ray abundance of any other peak can be calculated now from this k_1-constant (that applies to the activation reaction only) and its own k_0-constant (that consists of the k_1-constant and the gamma-ray abundance of the peak in question). Errors in the gamma-ray abundance taken from literature will only propagate to the results of the coincidence calculations, because the gamma-ray abundances will be recombined with the corresponding k_1-constants in the concentration calculations.

When coincidence corrections are required, decay scheme information must be used to calculate the P values. This information should be represented in such a way that no inconsistencies arise, as might happen when both a decay scheme as shown in Fig. 1 and a list of gamma-ray abundances based on k_0-constants would be used.

It is possible to supply the decay scheme information in such a way that it can be used by computers to perform the coincidence calculations. The decay scheme of ^{82}Br is represented both in Fig.7.1 and Text box 1.1. The latter representation does not allow for inconsistencies and also directly shows the experimental, "natural" gamma-ray abundances for those who choose to neglect the coincidence corrections.

7.5.2. The use of the k_1-constant

The k_1-constant can only be applied in conjunction with a list of gamma-ray abundances and decay scheme information. When no correction for coincidence effects is necessary, these abundances will recombine with the k_1-constant to yield the original k_0. In this case, the decay scheme information can be neglected. When coincidence corrections are necessary, the decay scheme information must be used to calculate P values corrected for coincidence or, in the case of sum peaks, P values that consist entirely of coincidence effects. This can be done after the efficiency curves of the detector have been measured. An alternative approach would be the direct measuring of P values. This may be necessary for well-type detectors and for radionuclides of which the decay schemes are not very well known. It will also be practical for the contributions to the 511 keV photopeak mentioned before.

7.6. Discussion

The k_1-method presented above offers several additional advantages as compared to the k_0-method. Primarily, it permits the interpretation of "artificial" peaks or correction for interference by "artificial" peaks.

The solution offered here for the interpretation of escape peaks, however, could have been added to the k_0-method as it is. In those cases where only escape peaks

```
The decay scheme of ⁸²Br

    E          I                  ICC         ILP          FLP          ILE

  1007.50  1.32E+00                        0820360014  0820360005   2828.00
   401.1   0.08E+00                        0820360014  0820360009   2828.00
   827.8   2.37E+01                        0820360013  0820360005   2648.26
   554.3   7.06E+01            1.01E-02    0820360013  0820360007   2648.26
   221.5   2.16E+00            5.26E-02    0820360013  0820360009   2648.26
    92.2   0.32E+00            1.32E+00    0820360013  0820360012   2648.26
  1779.6   1.10E-01                        0820360012  0820360002   2556.10
  1081.3   0.58E+00                        0820360012  0820360003   2556.10
   735.6   7.18E-02                        0820360012  0820360005   2556.10
  1650.3   0.79E+00                        0820360009  0820360002   2426.90
   952.0   0.38E+00                        0820360009  0820360003   2426.90
   606.3   1.20E+00                        0820360009  0820360005   2426.90
  1317.5   2.71E+01                        0820360007  0820360002   2093.93
   619.1   4.34E+01                        0820360007  0820360003   2093.93
   273.5   0.84E+00            2.04E-02    0820360007  0820360005   2093.93
  1044.0   2.71E+01                        0820360005  0820360002   1820.50
  1474.9   1.63E+01                        0820360003  0820360001   1474.90
   698.4   2.80E+01                        0820360003  0820360002   1474.90
   776.5   8.31E+01                        0820360002  0820360001    776.50


E:    energy of emitted photon
I:    gamma-ray abundancy (%)
ICC:  internal conversion coëfficiënt
ILP:  initial level pointer, containing atomic number and mass number
      of the radionuclide and an energy level number
FLP:  final level pointer
ILE:  initial level energy
```

Text box 1.1: The decay scheme of ⁸²Br in a γ-ray abundancy oriented representation.

(and no sum peaks) are relevant, this will be the most practical solution.

The separation of the k_0-constant into an activation- and a spectrometry-related part allows for the direct measurement of the spectrometric part in those cases where theoretical attempts to obtain the P values yield unsatisfactory results. In practice, this means that the k_1-method is applicable to NAA performed with well-type detectors, wheras the k_0-method is not.

It might seem as if the k_1-method, as compared to the k_0-method, is useful only when "artificial" peaks are involved. In some cases, however, where the contribution to a photopeak from summing effects is much larger than the contribution resulting
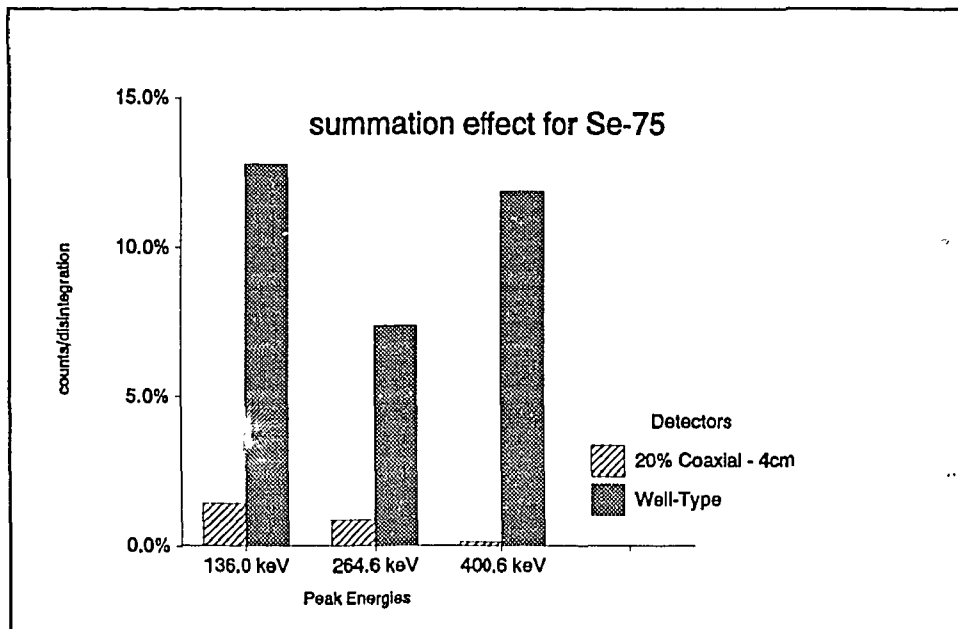
Fig.7.2: The severity of summation effects for ^{75}Se. The P-values were obtained at 4 cm distance from the endcap of a 20% coaxial detector, and in a well-type with an absolute efficiency of 5% at 1332 keV.

from the direct transition, the k_1-method is less sensitive to error propagation. In Fig.7.2, P values for the 136, 265 and 401 keV peaks of ^{75}Se as measured on a 20% coaxial and a well-type detector are shown. It will be clear from the experimental data that the intensity of the 401 keV line as measured on a well-type detector has more to do with the gamma-ray abundances of the 265 keV and the 136 keV peak than with that of the 401 keV peak. An experimental error, made in the determination of the k_0-constant of the latter should therefore not be allowed to propagate to the calculated concentration when interpreting this peak. This will not happen when the k_1-method is used.

It should be noted that self-absorption of gamma- or X-rays in the sample will change the P values of all peaks influenced by coincidence with these photons. Neither the k_0-method, nor the k_1-method as yet provide the means to correct for this effect. Furthermore, angular correlations between photons emitted in cascade are not accounted for in either of the two methods. Many radionuclides show significant angular correlations, some of them even show angular correlations influenced by the chemical state of the radionuclide. This implicates that both the k_0- and the k_1-method can only be used in conjunction with counting geometries where the coinci-

dence corrections are small, or in counting geometries where the solid angle approximates 4π, i.e. well-type detectors.

7.7. Conclusions

The k_0-method as yet provides no means to interprete or correct for "artificial" photopeaks in the gamma-ray spectrum.

Escape peaks and contributions to the annihilation peak can be dealt with defining an additional efficiency curve for each, in conjunction with k_0-values.

Sum peaks can be dealt with by defining a k_1-constant, the value of which is obtained from the k_0-value, and a detection probability P replacing the $\gamma\epsilon c$ product. The k_0-constant is thus seperated into an irradiation- and a spectrometric specific part. The k_1-constant is as reliable as the k_0-constant, because of their careful experimental calibration. No difference in calculated concentrations between the methods exists principally, except for the concentrations calculated from sum peaks or corrected for interference by sum peaks.

Moreover, improved accuracies can be expected when using the k_1-method in those cases where the contributions of summing effects to a photopeak are much larger than the "natural" contribution. Interpretation of both "natural" and "artificial" peaks using the k_1-method will result in more precise results.

7.8. References

1. A. Simonits, F. de Corte. J. Hoste, J. Radioanal. Chem., 105 (6) (1975) 31
2. E. Browne, R.B. Firestone, Table of Radioactive Isotopes, John Wiley & Sons, New York, 1986.
3. K.Debertin, U.Schötzig, Nucl.Instr.Meth. 158 (1979) 471-477
4. Heydorn, K., Advance Prediction of Single - and Double Escape Peak Areas in Gamma Ray Spectrometry., Trans. Am. Nucl. Soc. 60 (1989), 3.

Chapter 8
Comparison of the k_0- and the k_{Zn}-catalogues

8.1. Introduction

The k_0- and the k_{Zn}-method resemble each other very much. In the k_{Zn}-method, zinc is used as comparator instead of gold, but that is of little importance. The k_{Zn}-catalogue, however, contains many more (n,γ)-reactions than the k_0-catalogue at this moment. Also, the k_{Zn}-catalogue contains threshold and fission reactions. Before making the transition to the k_0-method, it was therefore attempted to compare the catalogues and possibly merge them later on.

8.2. Comparison of catalogues

8.2.1. Old-style IRI catalogues for coaxial detectors

The k_0-constant is defined for all gamma-transitions ocurring in every radionuclide produced by a (n,γ)-activation reaction by

$$k_0 = \frac{M_c \theta_a \sigma_{0,a} \gamma_a}{M_a \theta_c \sigma_{0,c} \gamma_c} \tag{8.1}$$

where a and c denote analyte and comporator, resp., and
M = atomic mass [g.mol^{-1}]
σ_0 = thermal neutron cross section [m^2]
θ = isotopic abundance
γ = absolute gamma-ray abundance
but the k_{Zn}-constant for (n,γ)-reactions is divided in two parts. The first part applies to the reaction the radionuclide is produced by

$$k_{Zn,1} = C \frac{M_c \theta_a \sigma_{eff,a}}{M_a \theta_c \sigma_{eff,c} \gamma_c} \tag{8.2}$$

where σ_{eff} is the effective neutron capture corss section, and the second part applies to a specific peak of the radionuclide

$$k_{Zn,2} = \frac{\gamma_a}{C} \tag{8.3}$$

The normalization constant C was chosen such that the sum of the $k_{Zn,2}$ of the peaks of each radionuclide was 1000. Characteristic or "main" peaks were flagged as such. Because the k_{Zn}-constant contains the effective neutron capture cross section, it could also be used for threshold reactions.

Fig.8.1: Section of IRI catalogue concerning ^{46}Sc

Some radionuclides can be produced by different reaction mechanisms. In that case, the $k_{Zn,1}$ was specified for each production pathway. Different $k_{Zn,1}$ constants were also specified for different irradiation facilities. In Fig.8.1, a section of this catalogue concerning ^{46}Sc is shown.

To interpret a gamma-ray spectrum, measured on a coaxial detector, this catalogue was used in conjunction with a relative photopeak efficiency curve. No attention was paid to coincidence effects. The detector mainly used for calibration purposes actually did not suffer from these effects to a significant degree.

8.2.2. Old-style IRI catalogues for well-type detectors

The catalogue described in the previous paragraph was already in use when the first well-type detector was purchased. As was soon discovered, a completely different catalogue was needed to deal with the coincidence effects encountered when using this detector. A practical solution was found by setting the photopeak efficiency to unity for all energies, and by adapting the $k_{Zn,2}$ constants in a separate copy of the catalogue for this detector. In the definition of the $k_{Zn,1}$-constant, the γ_c parameter was replaced by the P_c parameter (the P parameter is the probability of obtaining a

count in the photopeak per disintegration of the radionuclide). Likewise, the γ_a parameter was replaced by the P_a parameter in the definition of the $k_{Zn,2}$-constant. The normalization constant C was still chosen such that the sum of the $k_{Zn,2}$-values was 1000 for each radionuclide. This resulted in the $k_{Zn,1}$ constants being different for coaxial detectors on the one hand and the well-type detector on the other. These were also determined by separate calibration measurements.

Later on, two more well-types were purchased. Separate catalogues were set up for each of them. The k_{Zn}-constants were measured for each radionuclide of interest.

8.2.3. Conversion to k_1-catalogues

The separate k_{Zn}-catalogues had to be merged to a unified catalogue to allow for the comparison of k_0- and the k_{Zn}-constants. This unified catalogue also had to be used in the new system for INAA, and it had to be much more manageable that the old, separate catalogues. All this had to be done without any loss of calibration information.

As a first step, it was decided to consider the gamma-ray abundances of the "main" peaks of each radionuclide as found in the Table of Radioactive Isotopes[1] to be correct. This made it possible to remove the normalization constants C from both parts of the k_{Zn}-constant in the catalogue for the coaxial detectors. The abundance of the comparator peak was removed from $k_{Zn,1}$, and the known absolute efficiency curves of the coaxial detectors were used to convert the gamma-ray abundances to P values for each coaxial detector. The resulting definitions are

$$k'_{Zn,1} = \frac{M_c \theta_a \sigma_{eff,a}}{M_a \theta_c \sigma_{eff,c}} \tag{8.4}$$

and

$$k'_{Zn,2} = P_a \tag{8.5}$$

The catalogue now consisted of an irradiation-dependent part, containing the $k'_{Zn,1}$ constants, with different versions for different irradiation facilities, and a detector-dependent part, containing the P values, with a version for each coaxial detector.

Knowing the $k'_{Zn,1}$-constants for each reaction and each irradiation facility, the normalization constants C could also be removed from the catalogues for the well-type detectors, resulting in P values for all peaks in these catalogues. The spectrometer dependent parts of the catalogue now were equivalent.

It should be noted that long-lived radionuclides were calibrated carefully only on the well-type detectors. The $k'_{Zn,1}$-constants for the corresponding activation reactions

might therefore be unreliable. The product of the $k'_{zn,1}$ and the $k'_{zn,2}$ constants, which is used for the interpretation of the spectra, was still as reliable as it was before.

By now, the k_{zn}-catalogues had been transformed almost completely to k_1-catalogues. The only step remaining is the conversion of the effective neutron capture cross sections of the (n,γ)-reactions to thermal neutron capture cross sections. This step has not been performed yet. The catalogues are currently in use in the IRI system as described here.

8.2.4. Comparison of k_{zn}- and k_0-catalogues

The $k'_{zn,1}$-constants contain effective neutron capture cross sections. These cross sections exist for all activation reactions. The thermal neutron cross section σ_0, however, only exists for (n,γ)- and fission reactions. It was therefore decided to convert the k_0-constants to $k'_{zn,1}$-constants.

F-19 → F-20	Al-27 → Al-28	S-36 → S-37	V-51 → V-52
Cu-65 → Cu-66	Br-79 → Br-80	Rb-87 → Rb-88	Nb-92 → Nb-93m
Pd-108 → Pd-109m	Ag-107 → Ag-108	Ag-109 → Ag-110	I-127 → I-128
Gd-160 → Gd-161	Na-23 → Na-24	Mg-26 → Mg-27	Al-27 → Mg-27
U-238 → U-239	Sc-45 → Sc-46	Ti-46 → Sc-46	T-50 → Ti-51
Cr-50 → Cr-51	Mn-55 → Mn-56	Zn-68 → Zn-69m	Ga-71 → Ga-72
As-75 → As-76	Se-72 → Se-75	Br-79 → Br-80	Sr-84 → Sr-85m
Nb-93 → Nb-94m	Ru-96 → Ru-97	Ru-102 → Ru-103	Ru-104 → Ru-105
In-113 → In-114m	Sb-121 → Sb-122	Sb-123 → Sb-124	Te-128 → Te-129m
Te-130 → Te-131m	Cs-133 → Cs-134m	Ba-138 → Ba-139	La-139 → La-140
Ce-138 → Ce-139	Ho-165 → Ho-166	Yb-174 → Yb-175	Lu-176 → Lu-177m
Hf-174 → Hf-175	Hf-179 → Hf-180m	Re-187 → Re-188m	Pt-196 → Pt-197
Au-197 → Au-198	Hg-196 → Hg-197	Hg-196 → Hg-197m	Hg-202 → Hg-203
Th-232 → Th-233			

Table 8.1: Reactions of which the IRI effective cross-sections agree with the values published by De Corte et al. to within 5%.

For (n,γ)-reactions, the relation between the effective cross section σ_{eff} and the thermal cross section σ_0 is given by

$$\sigma_{eff} = \sigma_0(1 + Q_0(\alpha)/f) \tag{8.6}$$

where $Q_0(\alpha)/f$ describes the contribution to the activation rate by epithermal neutrons. For threshold reactions, the relation is given by

$$\sigma_{eff} = \sigma_f \, (\Phi_f / \Phi_t) \qquad (8.7)$$

where

σ_f = fast neutron cross section [m^2],

Φ_f = fast flux [m^{-2}s^{-1}]

Φ_t = thermal flux [m^{-2}s^{-1}]

For the (n,γ)-reactions, the $k'_{Zn,l}$-constants could therefore be calculated from the published k_0-constants, the known flux parameters of one of the IRI irradiation facilities[2], and the parameters published by De Corte. Many discrepancies were revealed. More information was needed to help decide which of the two constants was correct in any specific case. The isotopic abundances and atomic masses were therefore stripped from both the k_l- and the $k'_{Zn,l}$-constants, the thermal cross section of zinc as published along with the k_0-constants by De Corte et al.[3] was assumed to be correct and all $k'_{Zn,l}$- and k_0-constants were converted to effective neutron cross sections.

This also allowed for the comparison of the k_{Zn}-constants for threshold reactions and (n,γ)-reactions not yet listed in the k_0-catalogue with literature data. In these cases, the tables by Glascock[4] and Erdtmann[5] were used as a supplement. Missing values for the effective resonance energy for (n,γ)-reactions were simply set to unity, and effective cross sections were calculated from the literature data using Eq.(8.6) and Eq.(8.7).

Some radionuclides are produced from a single target nuclide by different activation reactions. An example is shown in Fig.8.2. In cases like this, it was noted that De Corte et al. mainly specify the combined thermal cross section (σ_{m+g} in the example) in case of short lined metastable radionuclides, but sometimes explicitly specify them separately. This has not always been noted by Glascock when he copied the k_0-catalogue into his tables, i.e. for ^{103}Rh and ^{187}Re, leading to
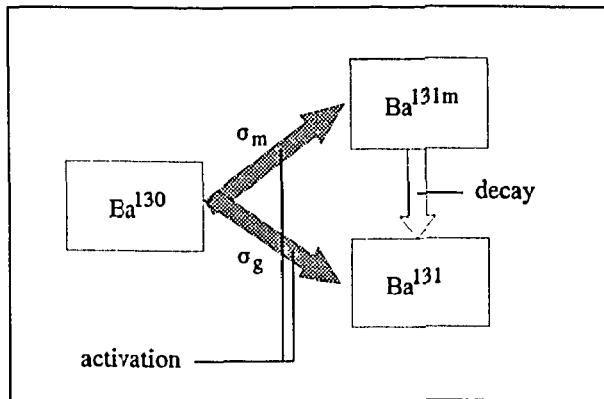
Fig.8.2: Indirect and direct production of Ba^{131}

inconsistencies in his tables. In the IRI catalogues, these cross sections are always specified separately. If neither De Corte et al., nor Glascock specified separate cross sections, the cross section for the activation of the metastable radionuclide was taken from Erdtmann's tables.

8.3. Results

Agreement between the catalogues was found to within 5% for the 54 reactions listed in Table 8.1.

A second comparison was made by dividing the k_0-values in two groups: Primary k_0-values as determined by De Corte et al. and secundary k_0-values from other
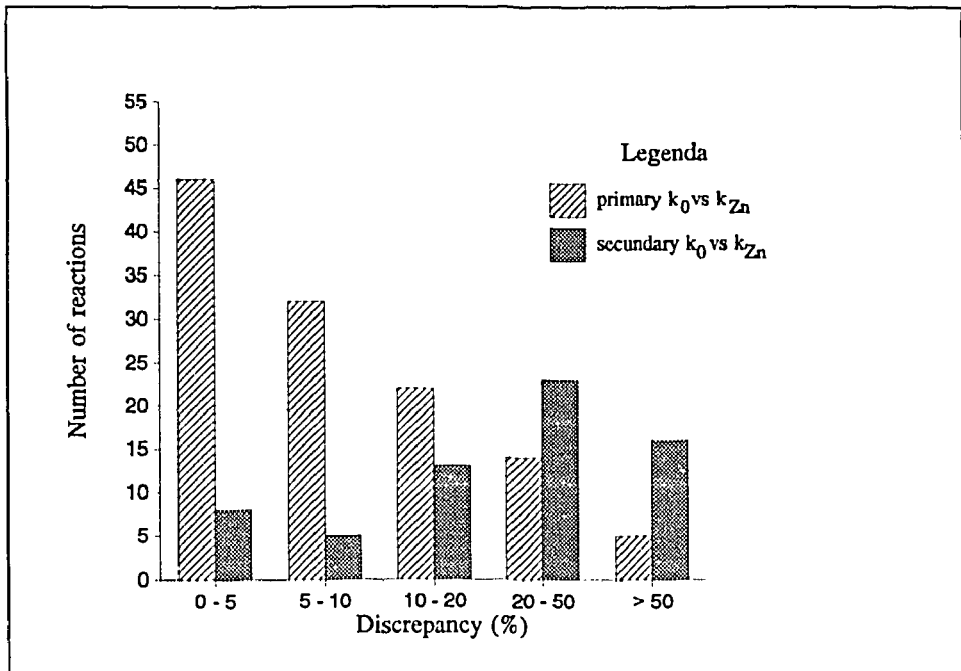
Fig.8.3: Comparison of differences between effective cross-sections from the k_{Zn} catalogue and the k_0 catalogues

sources. The primary k_0-catalogue should probably be preferred to the IRI catalogue in case of disagreement, because the k_0-constants in this catalogue were determined by at least two institutes. In Fig.8.3, it can be seen that the agreement between the k_{Zn} cross sections and the primary k_0-values is much better than between the k_{Zn} cross sections and the secundary k_0-values. This indicates that, in those cases where no

primary k_0-constant has been determined yet, the k_{Zn}-values should be preferred to the secundary values.

There are two published k_0-constants that are believed to be erroneous. The isotopic abundance of ^{36}S is subject to severe (up to 15%) natural variation[6]. The published uncertainty in the k_0-constant for the $^{36}S->^{37}S$ reaction is only 1.8%. This is clearly a mistake. The published k_0-constant for the $^{114}Cd -> ^{115}Cd$ reaction corresponds to a σ_0 of 0.23 b. The IRI value corresponds to a σ_0 of 0.3 b, and is in perfect agreement with the value listed by Erdtmann. De Corte et al. determined their value using isotopically enriched cadmium. Self-shielding at IRI cannot explain the difference: It could only enlarge the difference. It is believed that the isotopic abundances of the enriched cadmium used by De Corte et al. may have been incorrect.

8.4. Conclusions

The comparison of the catalogues shows that the k_{Zn}-catalogue contains information that could not be replaced by literature data so far. On the other hand, the primary k_0-catalogue is probably more accurate than the k_{Zn}-catalogue. It was therefore decided to use the k_{Zn}-catalogue as a supplement to the k_0-catalogue, and perform new calibration measurements for those reactions that show large discrepancies between the k_0- and the k_{Zn}-catalogues.

8.5. References

1. E.Browne, R.B.Firestone, "Table of Radioactive Isotopes", John Wiley and Sons, 1986
2. I.Obrusnik, M.Blaauw, P.Bode, J.Radioanal.Nucl.Chem. 152 (1991) 2 507-518
3. F.De Corte, A.Simonits, A.De Wispelaere, A.Elek, J.Radioanal.Nucl.Chem. 133 (1989) 3-41
4. M.D.Glascock, "Tables for Neutron Activation Analysis", Univ. of Missouri (1988)
5. G.Erdtmann, "Neutron Activation Tables", Weinheim, New York, (1976)
6. R.F. Fleming, R.M.Lindstrom, Trans.Am.Nucl.Soc. 41 (1982) 19

Chapter 9

The Use of Sources Emitting Coincident Gamma-rays for Determination of Absolute Efficiency Curves of Highly Efficient Ge Detectors

9.1. Introduction

To reduce the counting time needed to measure activity at a required precision, detector efficiency can be increased by decreasing the distance between sample and detector in the counting geometry, or by increasing the volume of the detector crystal. The deterioration of the precision that occurs due to imprecise sample positioning at close sample-detector geometries[1] can be strongly reduced by using well-type detectors.

Whenever the detector efficiency increases, so will the magnitude of the coincidence summing effects, rendering activity calculations from photopeak areas much more complex than in the classical situation. These effects are in principle well understood and can be computed using the formulas given by Andreev[2] and rewritten by McCallum and Coote[3]. The probability P of obtaining a count in a photopeak per disintegration must be computed for each radionuclide and each peak using these formulas, in order to calculate activities later on. Precise knowledge of both the absolute photopeak efficiency and the absolute total efficiency of the detector as a function of photon energy is required. These curves can be difficult to obtain in a simple way, because the coincidence summing interferes with their experimental determination. Without them, the detector can only be calibrated by determining the gamma-ray spectrum of each radionuclide of interest experimentally.

Efficiency curves can be determined by several methods, ranging from purely theoretical to purely experimental. Several authors have found good agreement between experiment and theoretical calculations using efficiency curves calculated from the properties of the Ge and the dimensions of the detector, e.g. McCallum and Coote[3], Gunnink[4]. In general however, the dimension specifications of the detector will often be absent or inaccurate.

De Corte[5] developed an intermediate method. The efficiency curves are measured in the so-called reference geometry, where coincidence summing effects are negligible, using calibrated sources. For other counting geometries, the curves are computed from the measured curves by the SOLANG program which makes use of the detector dimensions. Inaccuracies in these dimensions will thus propagate to the efficiency curves only marginally. This method cannot be used however for detectors without a reference geometry, like well-type detectors or moderately efficient detectors placed in very confined spaces.

Already in 1973, Andreev[6] demonstrated the possibility of measuring the photopeak efficiency curve in close-geometry conditions using a single nuclide (^{152}Eu) with a complicated decay scheme, correcting for the coincidence summing effects. The same approach was suggested independently by de Bruin et al[7]. Semkow et al.[8] developed a method similar to Andreev's, using formulas in matrix notation. The total efficiency curve had to be measured separately in both Andreev's and Semkow's approaches. All three methods were intended to allow for the use of radionuclides emitting coincident gamma-rays for the determination of the photopeak efficiency curve in spite of the coincidence effects: In the classical situation, the shape of the curve can be determined much more accurately using these radionuclides than using multiple radionuclides not emitting coincident gamma-rays.

All methods involving experiments outlined above have some drawbacks in common. They all involve the use of calibrated radioactive sources. For the measurement of total efficiency curves, only sources can be used that contain a single radionuclide with at most two gamma-ray lines[8]. The measurement can also be complicated by the ADC-threshold, which hides a part of the spectrum from view.

In this paper, a novel method is presented to determine the absolute photopeak efficiency, total efficiency and source activity all at once. It can be regarded as a combination of Semkow's method and the much older methods developed to determine the absolute source activity using the information provided by sum peaks[9]. It was based on the idea that, if efficiency curves are to be used for coincidence correction calculations, they should be obtained from coincidence effects. The method was tested using a coaxial detector without significant coincidence effects, a coaxial detector with a close sample-detector geometry and a well-type detector. ^{82}Br was measured on these detectors to determine the efficiency curves. Subsequently, the photopeak areas to be expected of ^{152}Eu were computed from the efficiency curves and verified experimentally.

9.2. Theory

9.2.1. Coincidence summing

A radionuclide with a decay scheme as shown in Fig.9.1 will have six photopeaks in a gamma-ray spectrum. The gamma-ray abundancess a_{ij} can be calculated from the branching ratios X_{ij} and the internal-conversion coefficients α_{ij} (for clarity's sake, the level feeding fractions are set to 0 for all levels except level 3 in this example). The branching ratios X_{ij} are defined such that

$$\sum_j X_{ij} = 1 \tag{9.1}$$
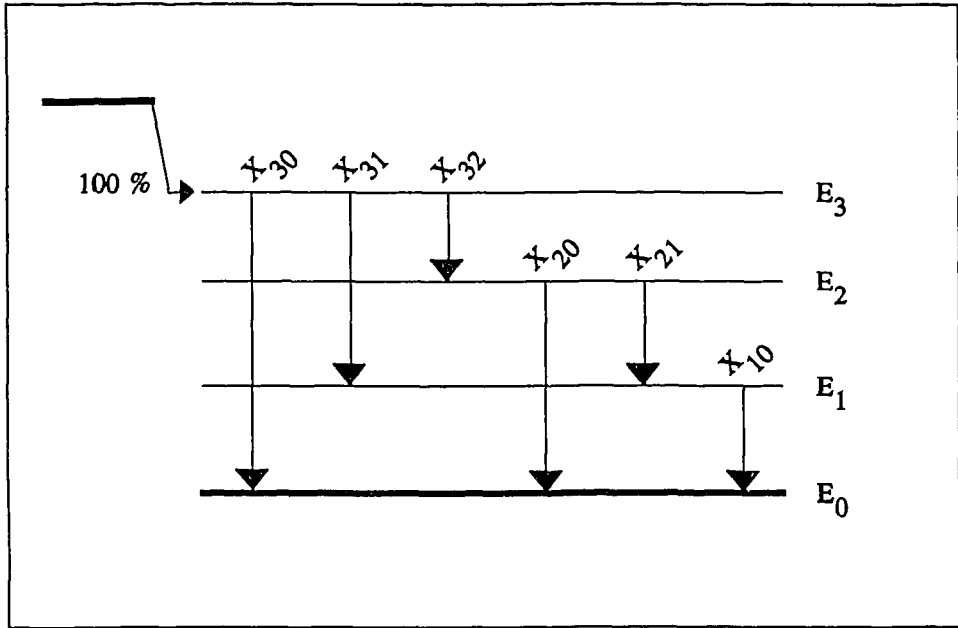
Fig.9.1: Example decay scheme defining some of the parameters to be used in coincidence calculations

Examples are given in Eq.(9.2) and Eq.(9.3).

$$a_{10} = (X_{31} + X_{32}X_{21})X_{10} \; \frac{1}{1 + \alpha_{10}} \tag{9.2}$$

$$a_{30} = X_{30} \; \frac{1}{1 + \alpha_{30}} \tag{9.3}$$

In the absence of coincidence summing, the probability per disintegration of obtaining a count in a photopeak P_{ij} for any decay scheme is given by

$$P_{ij} = a_{ij}\epsilon_{pij} \tag{9.4}$$

where ϵ_{pij} is the photopeak efficiency of the detector for photon energy $E_\gamma = E_i - E_j$. In the presence of coincidence summing, this basic probability has to be corrected for the probability of detecting other photons, emitted simultaneously by the decaying nucleus. If this happens, even if the other photon deposits only part of its energy in the detector, the count will be lost from the photopeak ("summing out"). On the other hand, the simultaneous detection of photons with energies that add up to the energy of interest will lead to extra counts in the photopeak ("summing in").

Examples of resulting probabilities are given for P_{10} (summing out) and P_{30} (summing in) in Eq.(9.6) and Eq.(9.5), respectively. Coincidence with X-rays is neglected.

$$P_{10} = X_{10}\frac{1}{1+\alpha_{10}}\epsilon_{p10}\ X_{31}(1 - \frac{1}{1+\alpha_{31}}\epsilon_{t31}) +$$

$$X_{10}\frac{1}{1+\alpha_{10}}\epsilon_{p10}\ X_{32}(1 - \frac{1}{1+\alpha_{32}}\epsilon_{t32})\ X_{21}(1 - \frac{1}{1+\alpha_{21}}\epsilon_{t21})$$

$$(9.5)$$

$$P_{30} = X_{30}\frac{1}{1+\alpha_{30}}\epsilon_{p30} +$$

$$X_{31}\frac{1}{1+\alpha_{31}}\epsilon_{p31}\ X_{10}\frac{1}{1+\alpha_{10}}\epsilon_{p10} +$$

$$X_{32}\frac{1}{1+\alpha_{32}}\epsilon_{p32}\ X_{20}\frac{1}{1+\alpha_{20}}\epsilon_{p20} +$$

$$X_{32}\frac{1}{1+\alpha_{32}}\epsilon_{p32}\ X_{21}\frac{1}{1+\alpha_{21}}\epsilon_{p21}\ X_{10}\frac{1}{1+\alpha_{p10}}\epsilon_{p10}$$

$$(9.6)$$

where ϵ_{tij} is the total detection efficiency for a photon with energy $E = E_i - E_j$. The formulas are complicated further by angular correlations between the photons emitted in cascade. These effects are neglected in this work. When the radionuclide represented by the decay scheme in Fig.9.1 is measured, six photopeak areas can be measured. Knowing the values of all parameters except the ϵ_{pij}, the six equations representing the probabilities of detecting a photon in each photopeak can be solved for the photopeak efficiencies ϵ_{pij}.

Andreev[6] indicates a method of solving the equations directly, Semkow et al.[8] developed an iterative, Newton-Raphson-like method for solving them. Both Andreev and Semkow consider decay schemes where all the possible transitions in fact occur. The method presented in this paper considers decay schemes where some transitions do not. If the branching ratios X_{30}, X_{32} and X_{20} in the decay scheme in Fig.9.1 are all zero, six photopeaks can nevertheless be measured. The probabilities P_{30}, P_{32} and P_{20} now refer to so-called sum peaks, and no longer depend on the corresponding photopeak efficiencies ϵ_{30}, ϵ_{32} and ϵ_{20}, but only on the photopeak efficiencies for the energies adding up to them. There now are more equations (6) than unknowns (3). In this case, the system of equations must be fitted by least squares methods, which closely resemble Semkow's iterative method.

The peak-to-total ratio of detector efficiencies can be appoximated by a linear curve on a log-log scale. This means that only two parameters need be used to cover all total efficiencies. These two parameters can also be determined from the six equations mentioned above. Finally, the number of disintegrations of the source can

be regarded as an unknown. Six unknowns are yet again to be determined from six equations. In general, this approach can be applied if

$$N_{obs} - N_{em} > 3 \qquad (9.7)$$

where N_{obs} and N_{em} are the numbers of observed photopeaks and of emitted photon energies, respectively.
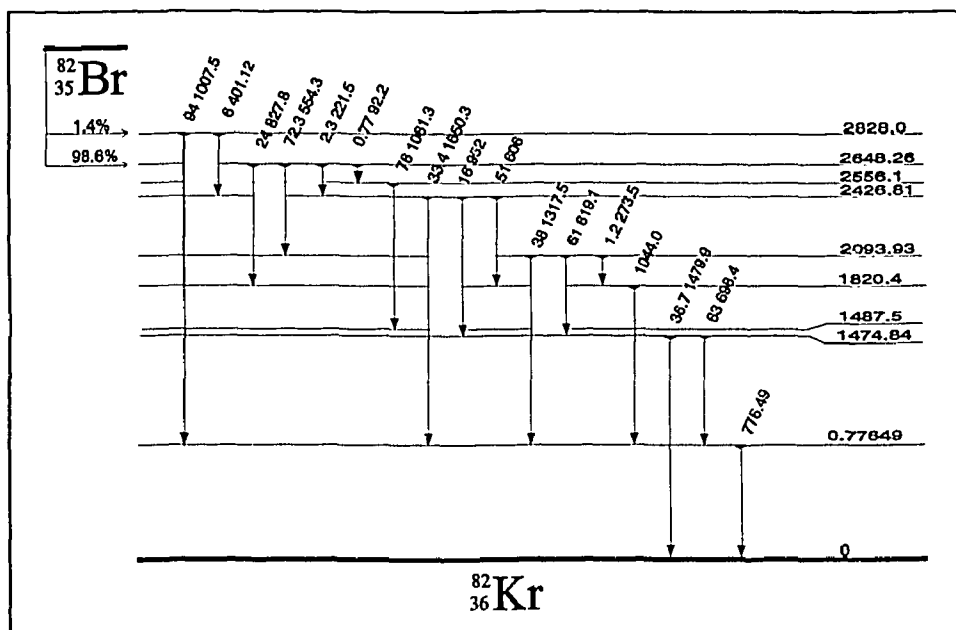
Fig.9.2: Simplified decay scheme of ^{82}Br.

In the case of ^{82}Br, of which the simplified decay scheme is shown in Fig.9.2, only 19 different photon energies are emitted, whereas over 40 photopeaks can easily be observed with an efficient detector. This means that over 40 equations can be solved for 19 photopeak efficiencies, two peak-to-total parameters and the number of disintegrations. This can be done by least squares methods as described in the next paragraph.

9.2.2. Determination of the efficiency curves and source activity from a measured spectrum

In principle, the photopeak efficiencies, the peak-to-total relation and the number of disintegrations can be obtained by non-linear least squares methods, where the χ_r^2-value of the measured photopeak areas as compared to the computed areas is minimized, χ_r^2 being defined by

$$X_r^2 = \frac{\sum_i \frac{(A_{mi} - A_{ci})^2}{\sigma_i^2}}{N_{obs} - (N_{em} + 3)} \qquad (9.8)$$

where A_c and A_m are the computed and measured peak areas, respectively, and σ is the uncertainty of the measured peak area.

As is always the case when using these methods, a reasonable estimation of the values of the parameters is a prerequisite. If a calibrated source is used, an estimation of the number of disintegrations during the measurement is readily available. If the source was prepared by irradiation, activation computations will yield an estimate of the number of disintegrations. From this number, the measured areas of "true" photopeaks and the gamma-ray abundancess, the photopeak efficiencies can be estimated. An estimate of the peak-to-total parameters can be taken from a separate measurement of any Ge detector, or by setting the peak-to-total ratio to unity for all photon energies at the beginning of the computation.

The fitting algorithm needs the partial derivatives of all photopeak areas to all parameters to be determined. An easy way to get reasonable values for these derivatives was to slightly vary each of the parameters in turn and observe the changes in the computed photopeak areas. This determination of derivatives must be repeated after each iteration because of the non-linearity of the formulas describing the coincidence effects.

A computer program was written to perform all these tasks. The database of decay scheme information for all gamma-ray emitters was obtained on tape from E.Browne. When testing, it was found that is was necessary to be able to exclude subsets of parameters from the fitting procedure in some cases. When dealing with a well-type detector for example, with photopeak efficiencies of 0.4 or more in the 100-150 keV region, the first estimates of the photopeak efficiencies may be off by a factor of 4. In this case, the program fitted each photopeak efficiency in turn, until no significant improvement of the χ_r^2 -value could be obtained. Only afterwards, the total efficiency parameters and sometimes the number of disintegrations were included in the fit.

To prevent convergence problems, the values of the parameters were checked for physical meaningfulness in each iteration. Photopeak efficiencies were kept from changing by more than 50% in a single iteration, and were also kept positive and less than unity. The total efficiencies were kept larger than the photopeak efficiencies, but again less than unity.

A fourth-order polynomial was fitted through the photopeak efficiencies as a function of photopeak energy on a log-log scale. This polynomial and the peak-to-

with 0.4 mm zirconium metal to absorb low-energy gamma-rays. Sources were placed in glass test tubes on the bottom of the cryostat well.

Counting times were chosen long enough to get a number of counts in the order of a million in the 776 keV photopeak of ^{82}Br. The ^{152}Eu-source was counted only long enough on each detector to get uncertainties in the main photopeak areas of less than 1%, because they were to be compared with theoretical results, and no more precision is needed in practice.

To monitor dead time and pile-up, 25 Hz pulsers were used to generate a peak in the high energy part of the spectra, where background is negligible. The photopeak areas were determined using in-house analysis software, based on the same principles as the SAMPO package. The areas were corrected for dead time, random summing and pile-up by the pulser method. The ^{82}Br spectra also showed ^{24}Na photopeaks, which did not interfere with the photopeaks of interest. The ^{152}Eu photopeak areas were corrected manually for the small ^{154}Eu contributions, based on previous measurements of the ^{154}Eu spectrum on each detector. These corrections were statistically significant only for the 121.8 keV, the 244.7 keV and the 1508.3 keV photopeaks.

9.3.3. Data processing

The efficiency curves and source activity were obtained from the ^{82}Br spectra for each detector as described in Section 2. In the case of the CO1 detector, the source activity was reported by the fitting algorithms with a precision of 1.5 %. In the case of the CO2 detector, the precison was infinite, and in the case of the WELL detector, the precision surprisingly was reported to be only 15 %. These precisions correspond to the precision with which the minimum of the χ_r^2-curve as a function of source activity can be determined.

To investigate the source activity sensitivity of the method, the source activity from the results of the CO1 detector was considered to be "correct". Efficiency curves were constructed for each detector using the "correct" activity multiplied by 0.75, 0.95, 1.00, 1.05 and 1.25. The numbers of disintegrations were computed from the activity, decay and measuring times. After the determination of each set of efficiency curves, the ^{152}Eu spectrum was computed from the decay scheme using the curves, and compared to the measured ^{152}Eu spectrum. In this comparison, an "efficiency" multiplication factor for the theoretical Eu photopeak areas was computed to get the best match in the least squares sense and compensate for the activity multiplication factor used.
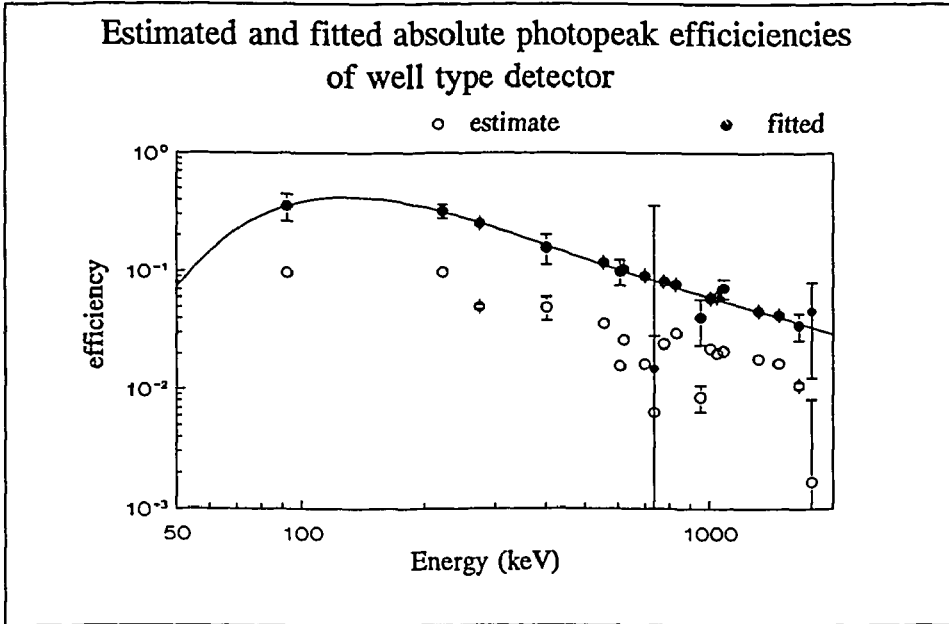
Fig.9.3: Estimated and fitted absolute photopeak efficiencies for the WELL detector. A fourth-order polynomial was fitted through the fitted peak efficiencies. As can be seen, most first estimates are off by a factor of 4.

9.4. Results and discussion

9.4.1. Demonstration of the feasibility of the method

A photopeak efficiency curve as obtained from the ^{82}Br spectrum measured on the WELL detector, with activity multiplication factor 1, is shown in Fig.9.3. A fourth-order polynomial was fitted through the fitted photopeak efficiencies, yielding a χ_r^2-value of 0.62. This can be regarded as a measure of the "smoothness" of the curve, indicating that it is even slightly smoother than could be expected from the uncertainties in the efficiencies as reported by the fitting algorithms.

The minimum χ_r^2-value of the match between the measured and the computed ^{82}Br photopeak areas was 1.13. The individual values for each photopeak can be seen in Table 9.9. In this table, the relative precision of the measured photopeak areas, the ratio between measured and computed areas and the z value of this ratio, computed from

$$z = (A_m - A_c)/\sigma \qquad (9.9)$$

For ^{152}Eu, the χ_r^2-value of the match between the measured photopeak areas and the areas computed from the efficiency curves was 1.96. The individual values for

E (keV)	prec (%)	ratio	z	E (keV)	prec (%)	ratio	z
92.20	2.4	1.00	0.1	1265.50	8.0	0.85	1.9
221.50	1.0	1.00	0.2	1317.50	1.0	1.00	-0.4
273.50	4.0	1.01	-0.2	1330.80	1.0	1.00	-0.5
401.10	22.0	0.97	0.2	1382.80	45.0	1.93	-2.1
554.30	1.0	1.00	0.0	1395.60	1.3	1.00	-0.1
606.30	5.0	0.93	1.4	1474.90	1.0	1.01	-0.7
619.10	1.0	1.00	-0.1	1567.10	21.0	0.91	0.4
698.40	1.0	1.00	-0.1	1604.30	1.1	1.02	-1.5
776.50	1.0	0.99	0.7	1650.30	6.0	0.99	0.3
790.60	27.0	1.13	-0.5	1783.90	14.0	1.04	-0.3
827.80	1.0	0.99	1.4	1820.50	1.2	0.98	1.4
868.70	20.0	1.12	-0.6	1871.80	1.0	1.00	-0.1
919.90	23.0	0.82	0.8	1949.90	4.0	1.04	-0.9
951.90	25.0	0.87	0.5	2029.20	1.1	1.00	0.1
998.00	3.0	1.01	-0.4	2042.00	26.0	0.89	0.4
1007.40	4.0	1.00	-0.1	2051.40	11.0	0.97	0.3
1044.00	1.0	1.01	-1.3	2094.00	1.0	1.00	0.3
1050.00	13.0	0.90	0.8	2426.80	16.0	1.10	-0.7
1081.20	7.0	0.99	0.1	2556.10	20.0	1.00	0.0
1173.40	1.0	1.00	-0.3	2648.30	1.3	1.00	0.1
1252.70	1.4	1.00	0.1	2827.90	18.0	0.93	0.4

Table 9.9: Match between computed and measured [82]Br peak areas. See text for explanation.

each photopeak can be seen in Table 9.9. One notices some large z values in this table, i.e. for the photopeaks with the energies 244.7, 719.33, 841.2, 1292.78 and 1529.78 keV. The photopeak at 1529.78 keV is part of a doublet that may have been resolved incorrectly. The 244.69 keV discrepancy was also reported by Debertin[11] and may indicate that some property of the decay scheme of [152]Eu remains as yet unknown. Also, the correction for the contribution of [154]Eu may have been erroneous. A general explanation for the discrepancies may be the coincidence with [152]Sm X-rays penetrating the Zr absorber.

9.4.2. Source activity sensitivity of the three detectors

9.4.2.1. The CO2 detector

As expected, the χ_r^2 curve of the comparison of measured and calculated [82]Br photopeak areas of the CO2 detector as shown in Fig.9.4 shows no sensitivity for the activity multiplication factor, because this detector shows no significant coincidence effects. For the same reason it proved to be impossible to determine either the peak-to-total parameters or the source activity from the [82]Br spectrum of this detector. The

E (keV)	prec (%)	ratio	z	E (keV)	prec (%)	ratio	z
121.78	0.5	1.00	0.3	867.38	2.0	0.96	-2.0
147.96	25.0	0.64	-1.5	919.39	10.0	1.15	1.5
244.69	1.0	0.97	-3.2	926.31	20.0	0.99	-0.1
251.61	50.0	1.25	0.5	930.59	10.0	0.96	-0.4
271.13	40.0	0.65	-0.9	964.11	1.0	0.99	-1.2
295.93	5.0	0.89	-2.2	989.16	5.0	0.95	-1.0
324.81	25.0	0.95	-0.2	1005.26	20.0	0.82	-0.9
329.42	15.0	1.08	0.5	1022.00	100.0	1.26	0.3
344.29	0.5	1.00	0.3	1022.88	100.0	0.81	-0.2
366.47	3.0	1.00	0.1	1041.17	100.0	1.21	0.2
367.80	10.0	0.89	-1.1	1085.89	1.0	1.01	0.6
411.12	2.0	1.01	0.5	1089.71	5.0	0.92	-1.6
417.71	10.0	0.86	-1.4	1109.19	100.0	0.70	-0.3
443.89	2.0	0.98	-1.0	1112.07	1.0	0.98	-1.7
443.98	10.0	0.98	-0.2	1123.21	1.0	1.02	2.5
488.61	10.0	1.02	0.2	1171.00	20.0	1.13	0.6
503.41	25.0	0.79	-0.8	1212.93	5.0	0.96	-0.8
511.00	50.0	1.20	0.4	1233.85	1.0	1.03	2.8
564.01	10.0	0.82	-1.8	1249.95	7.0	0.94	-0.9
565.67	10.0	0.93	-0.7	1292.78	20.0	1.60	3.0
565.76	20.0	0.93	-0.4	1299.16	5.0	1.03	0.5
586.30	10.0	1.02	0.2	1334.50	100.0	0.02	-1.0
656.48	25.0	0.69	-1.2	1408.00	1.0	1.00	0.5
678.59	20.0	1.29	1.4	1434.00	5.0	1.01	0.2
688.67	5.0	1.02	0.4	1457.62	5.0	1.03	0.7
712.09	10.0	0.84	-1.6	1528.12	20.0	0.93	-0.3
719 33	20.0	0.25	-3.8	1529.78	2.0	1.09	4.5
755.41	5.0	1.01	0.3	1579.40	5.0	1.04	0.7
759.60	100.0	0.00	-1.0	1605.63	100.0	1.14	0.1
764.90	25.0	0.77	-0.9	1608.44	100.0	1.58	0.6
778.92	1.0	0.99	-1.2	1643.45	5.0	1.04	0.8
810.45	5.0	1.05	1.0	1649.90	10.0	1.00	0.0
841.20	20.0	0.31	-3.5	1769.07	100.0	0.66	-0.3
846.00	100.0	0.00	-1.0				

Table 9.9: Match between computed and measured [152]Eu peak areas. See text for explanation.

photopeak efficiencies are just scaled by the fitting algorithm to compensate for the activity multiplication factor, without the coincidence effects indicating that something is going wrong. This scaling is reflected by the efficiency multiplication factor for the CO2 detector being proportional to the reciprocal of the activity multiplication factor, as shown in Fig.9.5. The CO2 detector is an example of the classical situation, where photopeak efficiencies can be determined directly from the measured photopeak areas and the gamma-ray abundances, and the source activity must be known to get the right absolute efficiencies.
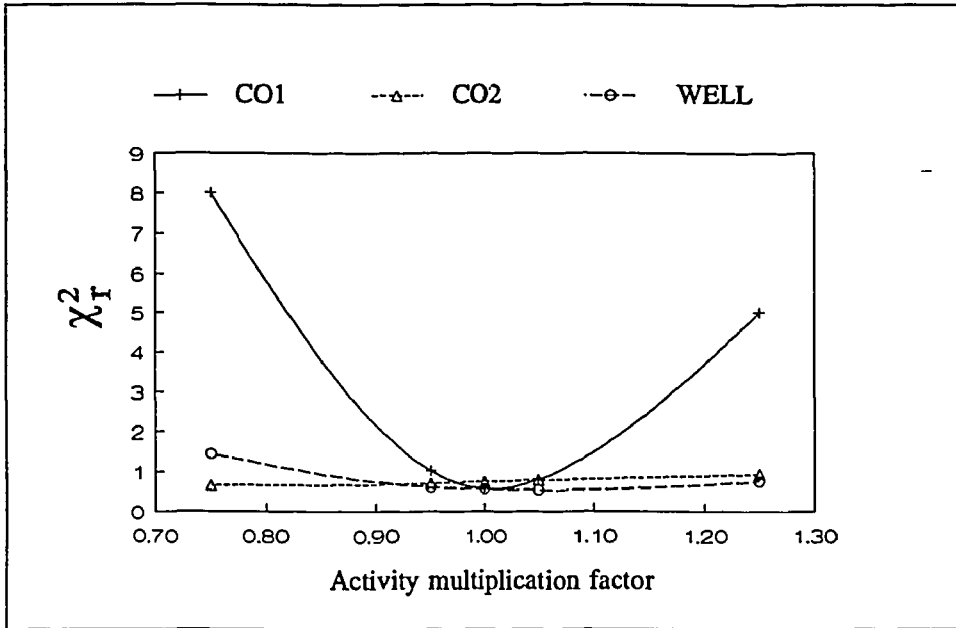
Fig.9.4: χ_r^2-values for the matches between measured and reproduced peak areas of ^{82}Br for different detectors and activity multiplication factors.

9.4.2.2. The CO1 detector

The χ_r^2-curve for the CO1 detector in Fig.9.4 shows a strong dependence on the source activity multiplication factor. This indicates that a detector as efficient as the CO1 detector cannot be used for activity measurements without applying coincidence corrections. Its absolute efficiency curves must therefore be known even for relative measurements. It is a common mistake to neglect coincidence effects in counting geometries such as used with this detector.

9.4.2.3. The WELL detector

Surprisingly, the χ_r^2-curve for the WELL detector in Fig.9.4 has a much less well defined minimum than the curve of the CO1 detector. Even though the coincidence effects are much stronger for the WELL than for the CO1 detector, the curve hardly shows any dependence on the activity multiplication factor. A possible explanation of this phenomenon is based on the behaviour of the efficiency multiplication factor of the WELL detector as shown in Fig.9.5. This factor also shows little sensitivity for the activity multiplication factor used. In other words, even when the fitting algorithms are misinformed about the source activity, the resulting efficiency curves lead to theoretical ^{152}Eu photopeak areas that are on average more or less correct. This may mean that the information in the sum peak areas of the ^{82}Br spectrum is much more
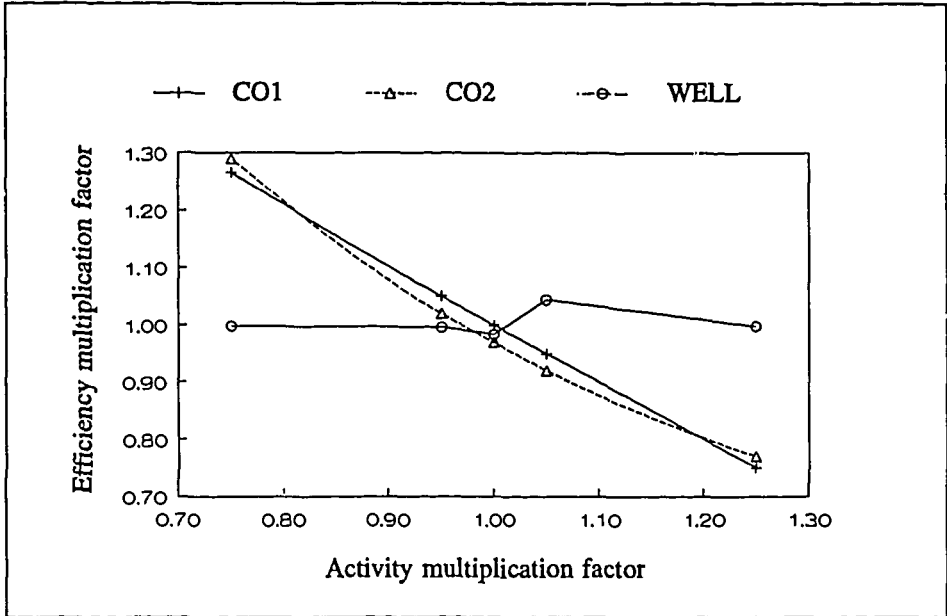
Fig.9.5: Efficiency multiplication factors for three detectors and different activity multiplication factors. Curves were drawn to guide the eye.

important to the fitting algorithm than the source activity.

The only indication, before testing the ^{152}Eu spectrum, that something is wrong with the source activity, when using activity multiplication factors other than unity, is given by the curve for the WELL detector shown in Fig.9.6. These curves however prove to be an unreliable test of the quality of the efficiency curves determined for the other two detectors.

The χ_r^2-values of the match between theoretical and measured ^{152}Eu photopeak areas are shown in Fig.9.7. Since the coincidence effects for ^{152}Eu are less pronounced than the effects for ^{82}Br, the independence of the χ_r^2-values of the activity multiplication factor is understandable in the cases of the CO1 and the CO2 detector. The match is worse for the CO1 than for the less efficient CO2 detector, possibly due to the angular correlation effects that were neglected in the computations. The χ_r^2-values of the match for the WELL detector demonstrate that the efficiency curves determined with activity multiplication factors other than unity are not realistic after all, even though they yield ^{152}Eu photopeak areas that are on average correct, as mentioned above. This may indicate that ^{152}Eu is more suitable for the determination of the efficiency curves of well-type detectors than ^{82}Br.
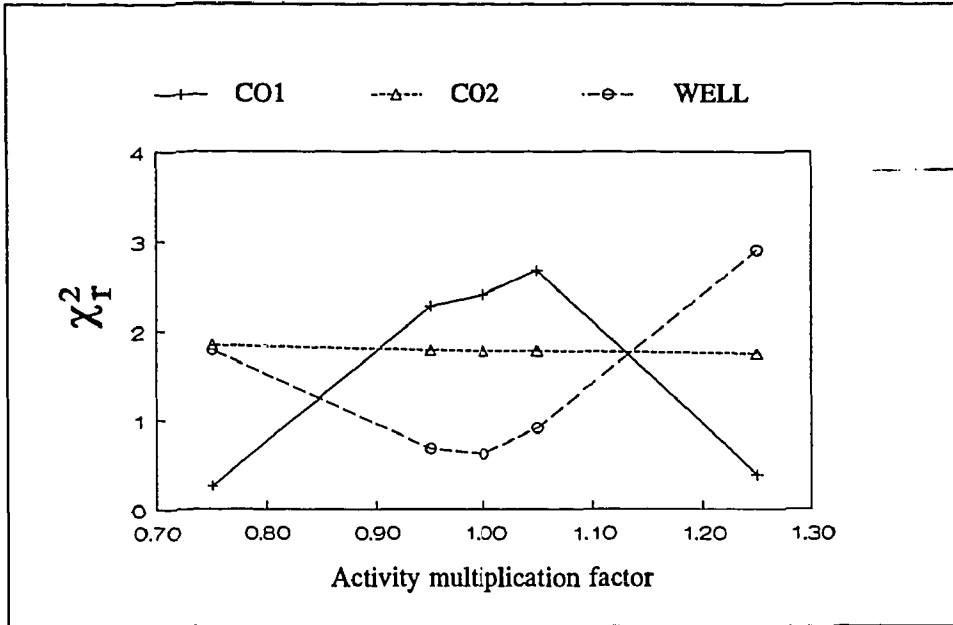
Fig.9.6: χ_r^2 values for the fourth-order polynomial fit to the fitted photopeak areas as a function of the activity multiplication factor. Curves were drawn to guide the eye.

9.5. Conclusions

It is possible to determine both absolute photopeak efficiency and total efficiency curves of a Ge detector from the spectrum of a single radionuclide. Moreover, no precise knowledge of the activity of the single radionuclide source used is required, if only the gamma-ray spectra obtained from the detector show significant coincidence effects. For detectors with intermediate efficiencies, [82]Br is a suitable radionuclide to use for this purpose. For highly efficient detectors such as well-types, [152]Eu may be more appropriate.

The method outlined in this work makes it possible to precisely measure efficiency curves in situations where coincidence effects cannot be avoided. The resulting efficiency curves cannot be used for activity calculations later on directly: They can only be used by way of the P values when measuring activities of radionuclides emitting coincident gamma-rays.

It is also possible to accurately compute the probability per disintegration P of obtaining a count in any photopeak to be expected in a gamma-ray spectrum, given the efficiency curves of the detector. This was already known with respect to moderately efficient detectors, but to my knowledge it has been shown for the first time for well-type detectors.
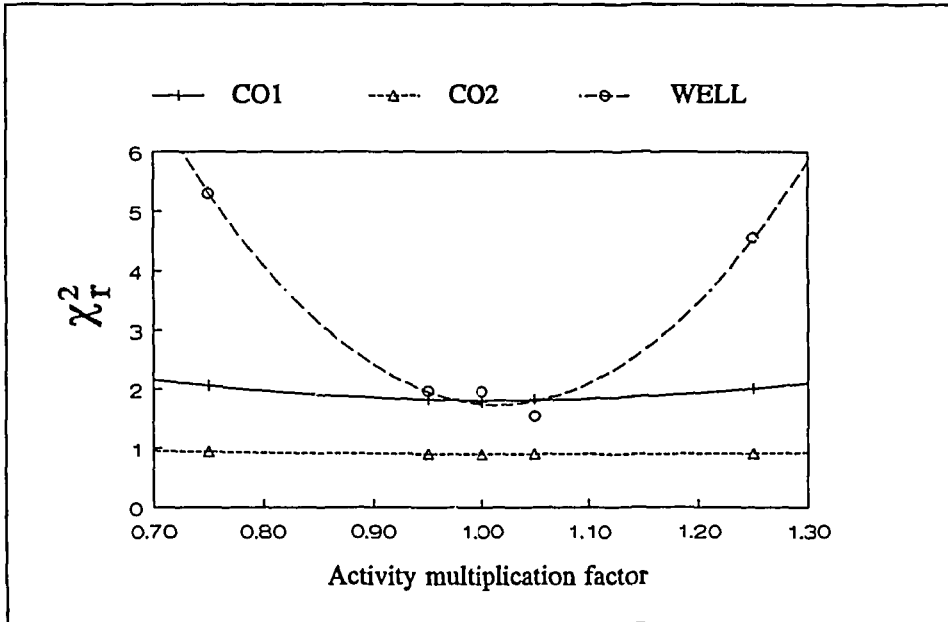
Fig.9.7: χ_r^2-values for the match between measured and computed ^{152}Eu photopeak areas. Curves were drawn to guide the eye.

The possibility of easily obtaining efficiency curves for highly efficient gamma-ray detectors, such as well-type detectors and spectrometers with a close source-to-endcap counting geometry, and of computing P values for other isotopes from these curves, facilitates the use of these detectors for e.g. single comparator INAA very much.

9.6. References

1. M.de Bruin, M.Blaauw, Analyst 117 (1992) 431-434
2. D.S.Andreev, K.I.Erokhina,V.S.Zvonov, I.Kh.Lemberg, Instr.Expt.Tech. 15 (1972) (USSR) (English.Transl.) 1358
3. G.J.McCallum, G.E.Coote, Nucl.Instr.Meth. 130 (1975) 189-197
4. R.Gunnink, Nucl.Instr.Meth. A299 (1990) 372-376
5. L.Moens, J.de Donder, Lin Xilei, F.de Corte, A.de Wispelaere, A.Simonits, J.Hoste, Nucl.Instr.Meth. 187 (1981) 451.
6. D.S.Andreev, K.I.Erokhina, V.S.Zvonov, I.Kh.Lemberg, Bull.Acad.Sci.USSR Phys.Ser. (English transl.) 37 (1973) 41-43
7. M.de Bruin, P.J.M.Korthoven, Radiochem.Radioanal.Letters 19/3 (1974) 153-156
8. T.M.Semkow, G.Mehmood, P.P.Parekh, M.Virgil, Nucl.Instr.Meth.in Phys.Res. A290 (1990) 437-444

9. G.A.Brinkman, A.H.W.Aten, J.Th.Veenboer, Int.J.appl.Rad.Isotopes <u>14</u> (1963) 153-157
10. M.Blaauw, M.J.J.Ammerlaan, P.Bode, Appl.Rad.Is. 1992 (in press)
11. K.Debertin, U.Schötzig, Nucl.Instr.Meth. <u>158</u> (1979) 471-477

Chapter 10

A Versatile Computer Algorithm for Linear First-order Equations Describing Compartmental Models with Backward Branching

10.1. Introduction

First-order linear equations can describe many systems, e.g. compartmental systems as used in biological modelling, radioactive decay chains, simultaneous activation and decay of radionuclides and simple chemical reactions. As a consequence, refined mathematical methods have been developed in the past to deal with these systems.

The behaviour of the contents N of a compartment in the systems considered here can always be described by the following differential equation:

$$\frac{dN}{dt} = \sum_i \lambda_i N_i - N(\sum_j \lambda_j) \tag{10.1}$$

where the λ are the time constants, the summation over i concerns compartments from which the contents flow into the compartment considered, and the summation over j concerns the compartments into which the contents of the compartment considered flows. Equations like this can be given for all compartments involved. The resulting system of equations becomes very hard to solve as the number of compartments increases. Even though solutions have been found for many commonly encountered situations, a general solution will be useful in many cases.

The general solution as given by Bateman[1] was further developed by Skrable[2], whilst independently, this solution was translated into recursive formulas by Hamawi[3]. Hamawi's recursive formulas were modified later by Scherpelz[4] to deal with the special problem of identical time constants within a single chain of compartments. Miles[5] generalized the recursive formulas for use in complex chains of compartments with branching.

One special case has been disregarded or specifically excluded by all these authors: Backward branching. Examples of backward branching are the pairs of compartments as found in biological models, where matter can flow from one compartment to the next just as well as the other way around (Fig.10.3), and complex activation as encountered sometimes in Neutron Activation Analysis (Fig.10.1).

Another problem is the computer implementation of formulas as mentioned. When the elapsed time is very small as compared to the time constants of (some of) the compartments, the calculation of the output of the compartments will involve the calculation of very small differences between very large numbers. Limited numerical
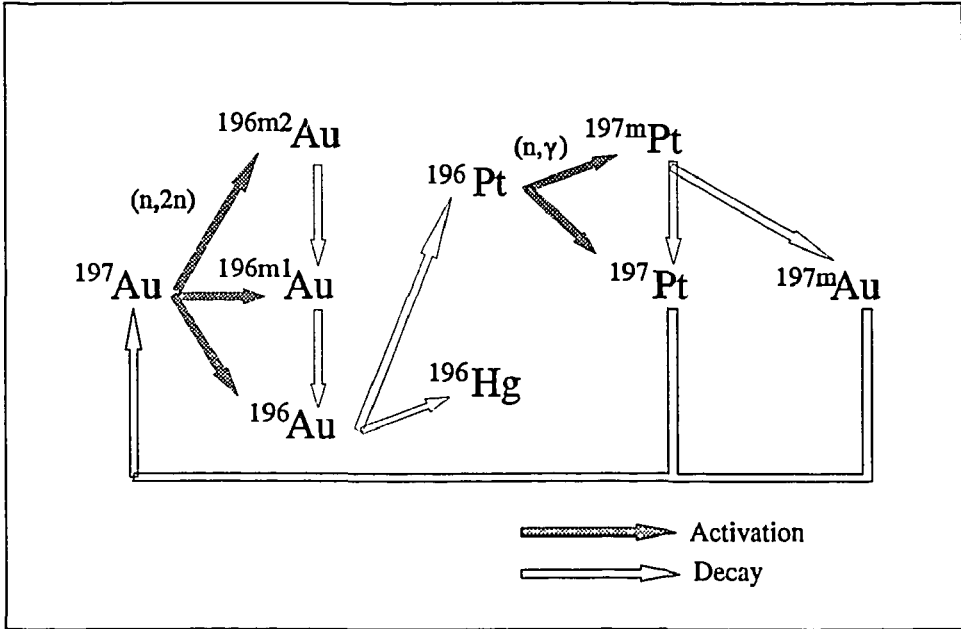
Fig.10.1: Part of the complex activation of gold. (n,γ) activation of ^{197}Au and ^{196}Hg has been omitted for clarity's sake.

precision will lead to unacceptable errors in this case.

In this chapter, formulas and a computer algorithm are presented which can handle backward branching (which also involves the case of equal time constants), or any other structure of interrelated compartments, to any required precision. The integrated output of the compartment in a time interval, which is the number of disintegrations in the case of radioactive decay chains, can also be calculated.

This is accomplished by decomposing the structure of interrelated compartments into a set of linear structures with an initial amount present only in the first compartment (Fig.10.2) as described in section 10.4. In the case of backward branching, such a structure will have infinite length. A general formula not unlike Hamawi's is derived in section 10.2 to describe the changes in contents of the compartments as a function of time. In section 10.3, the formulas are implemented as a computer algorithm that avoids the calculation of small differences between large numbers when the elapsed times are small as compared to the time constants in the compartments. In section 10.5, two examples of possible applications are given.

10.2. Derivation of a general formula for linear structures
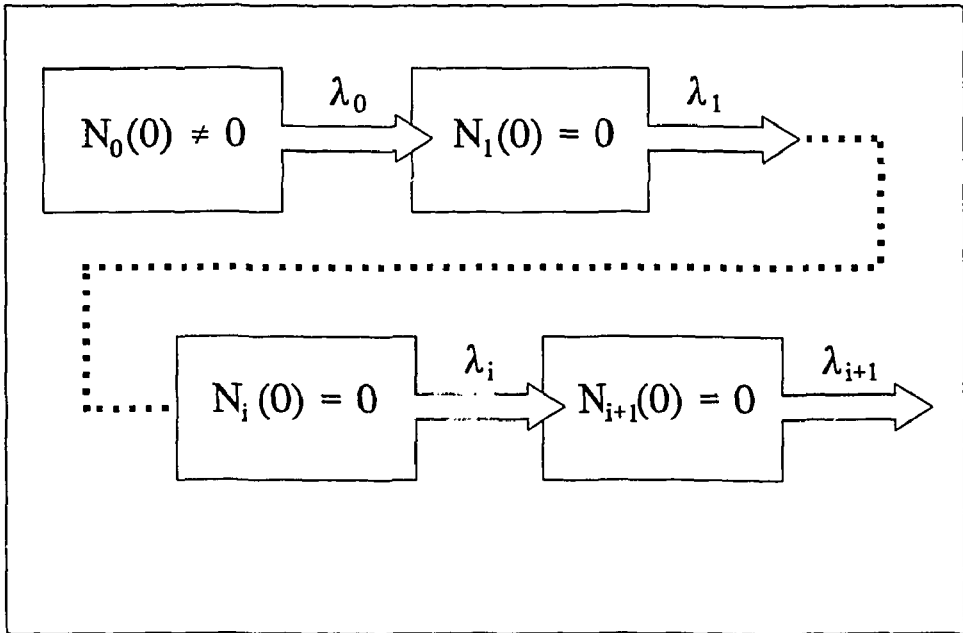
Fig.10.2: Simple, linear structure of compartments with initial content only in the first compartment.

The contents of any compartment i as shown in Fig.10.2 can be described by:

$$N_i(t) = \sum_{j=0}^{i} \sum_{k=0}^{i} C_{ijk} \, t^k e^{-\lambda_j t} \tag{10.2}$$

where:

t = time

$N_i(t)$ = contents of compartment i at time t

C_{ijk} = constant

λ_j = time constant of compartment j

k = parameter allowing for equal time constants in different compartments.

This will be proven using the principle of induction, i.e. by showing it is true for compartment 0, and by showing that if it is true for compartment i, it must also be true for compartment $i+1$. Furthermore, the relation between the C_{ijk} and the C_{i+1jk} will be determined.

The following is true for compartment 0:

$$\frac{dN_0}{dt} = -\lambda_0 N_0 \tag{10.3}$$

and the solution of this differential equation is:

$$N_0(t) = N_0(0) \, e^{-\lambda_0 t} \tag{10.4}$$

The general Eq.(10.2) transforms into eq.(10.4) with $C_{000} = N_0(0)$, which proves the validity of Eq.(10.2) for $i = 0$.

Assuming Eq.(10.2) is true for $N_i(t)$, the following differential equation can be written for compartment $i+1$:

$$\frac{dN_{i+1}}{dt} = -\lambda_{i+1} N_{i+1} + \lambda_i \sum_{j=0}^{i} \sum_{k=0}^{i} C_{ijk} \, t^k \, e^{-\lambda_j t} \tag{10.5}$$

This inhomogeneous equation can be solved by variation of the constant. First, the homogeneous part is solved:

$$N_{i+1}(t) = Ae^{-\lambda_{i+1} t} \tag{10.6}$$

Taking the first derivate to t yields:

$$\frac{N_{i+1}}{dt} = -\lambda_{i+1} Ae^{-\lambda_{i+1} t} + \frac{dA}{dt} e^{-\lambda_{i+1} t} \tag{10.7}$$

And comparison of eq.(10.7) and eq.(10.5) results in:

$$\frac{dA}{dt} = \lambda_i \sum_{j=0}^{i} \sum_{k=0}^{i} C_{ijk} t^k e^{-(\lambda_j - \lambda_{i+1})t} \tag{10.8}$$

Integration yields the following equation for A:

$$A(t) = B - \lambda_i \sum_{j=0, \lambda_j \neq \lambda_{i+1}}^{i} \sum_{k=0}^{i} \sum_{l=k}^{i} C_{ijl} \frac{l!}{k!} \frac{t^k}{(\lambda_j - \lambda_{i+1})^{l-k+1}} e^{-(\lambda_j - \lambda_{i+1})t}$$
$$+ \lambda_i \sum_{j=0, \lambda_j = \lambda_{i+1}}^{i} \sum_{k=0}^{i} C_{ijk} \frac{t^{k+1}}{k+1} \tag{10.9}$$

And substitution of this result in eq.(10.6) yields:

$$N_{i+1}(t) = B.e^{-\lambda_{i+1} t}$$
$$- \lambda_i \sum_{j=0, \lambda_j \neq \lambda_{i+1}}^{i} \sum_{k=0}^{i} \sum_{l=k}^{i} C_{ijl} \frac{l!}{k!} \frac{t^k}{(\lambda_j - \lambda_{i+1})^{l-k+1}} e^{-\lambda_j t}$$
$$+ \lambda_i \sum_{j=0, \lambda_j = \lambda_{i+1}}^{i} \sum_{k=0}^{i} C_{ijk} \frac{t^{k+1}}{k+1} e^{-\lambda_j t} \tag{10.10}$$

The initial condition $N_{i+1}(0) = 0$ determines the value of B:

$$B = \lambda_i \sum_{j=0,\lambda_j \neq \lambda_{i+1}}^{i} \sum_{k=0}^{i} C_{ijk} \frac{k!}{(\lambda_j - \lambda_{i+1})^{k+1}}$$

(10.11)

Substitution of this result in eq.(10.10) yields:

$$
\begin{aligned}
N_{i+1}(t) = &+ \lambda_i \sum_{j=0,\lambda_j \neq \lambda_{i+1}}^{i} \sum_{k=0}^{i} C_{ijk} \frac{k!}{(\lambda_j - \lambda_{i+1})^{k+1}} e^{-\lambda_{i+1} t} \\
&- \lambda_i \sum_{j=0,\lambda_j \neq \lambda_{i+1}}^{i} \sum_{k=0}^{i} \sum_{l=k}^{i} C_{ijl} \frac{l!}{k!} \frac{t^k}{(\lambda_j - \lambda_{i+1})^{l-k+1}} e^{-\lambda_j t} \\
&+ \lambda_i \sum_{j=0,\lambda_j \neq \lambda_{i+1}}^{i} \sum_{k=0}^{i} C_{ijk} \frac{t^{k+1}}{k+1} e^{-\lambda_j t}
\end{aligned}
$$

(10.12)

The constants $C_{i+1,jk}$ are defined as follows:
For $j=i+1$ and $k=0$:

$$C_{i+1,i+1,0} = \lambda_i \sum_{j=0,\lambda_j \neq \lambda_{i+1}}^{i} \sum_{k=0}^{i} C_{ijk} \frac{k!}{(\lambda_j - \lambda_{i+1})^{k+1}}$$

(10.13)

For $j = i+1$ and k values of 1 up to $i+1$:

$$C_{i+1,i+1,k} = 0$$

(10.14)

For values of j from 0 up to i and of k from 0 up to $i+1$:

$$
\begin{aligned}
C_{i+1,jk} &= -\lambda_i \sum_{l=k}^{i} C_{ijl} \frac{1}{(\lambda_j - \lambda_{i+1})^{l-k+1}} \frac{l!}{k!} \quad &&\text{if } \lambda_j \neq \lambda_{i+1}, \text{ else} \\
&= \lambda_i \frac{C_{ij,k-1}}{k} \quad &&\text{if } k > 0, \text{ else} \\
&= 0
\end{aligned}
$$

(10.15)

These definitions transform eq.(10.12) to:

$$N_{i+1}(t) = \sum_{j=0}^{i+1} \sum_{k=0}^{i+1} C_{i+1,jk} \, t^k e^{-\lambda_j t}$$

(10.16)

which proves the validity of eq.(10.2) for any compartment i.

10.3. Implementation of the general formula

The formulas derived in the previous paragraph are to be used for two purposes: To compute the final contents of each compartment at time t and to compute the total output of each compartment during this time. They should not be used directly in a computer implementation however, because the terms in eq.(10.2) may represent very large numbers as compared to their differences when the elapsed times are very small as compared to the time constants. Direct implementation would yield very imprecise results due to the finite precision of the computer representation of the very big numbers involved.

Eq.(10.2) can also be written as

$$N_i(t) = T1(t) + T2(t) \tag{10.17}$$

where:

$$T1(t) = \sum_{j=0}^{i} \sum_{k=0}^{i} C_{ijk} \, t^k \tag{10.18}$$

and

$$T2(t) = \sum_{j=0}^{i} \sum_{k=0}^{i} C_{ijk} \, t^k (e^{-\lambda_j t} - 1) \tag{10.19}$$

The sequence for $T1(t)$ in Eq.(10.18) contains the large numbers and the one in Eq.(10.19) for T2(t) the small ones, in those cases where t is small as compared to the half lives of (some of) the compartments. By computing the sum of the two sequences separately, and by using a suitable linear approximation for $(1-e^{-\lambda t})$ when λt gets very small, the precision of the final result will not deteriorate by the subtraction of very large numbers with small differences.

The expression for $T1(t)$ can be simplified even further, noting that

$$N_i(0) = \sum_{j=0}^{i} C_{ij0} \tag{10.20}$$

which is $N_0(0)$ for the first compartment and 0 for all others. This transforms Eq.(10.18) to

$$T1(t) = \sum_{j=0}^{i} \sum_{k=1}^{i} C_{ijk} \, t^k + N_0(0) \tag{10.21}$$

Eq.(10.17) yields the contents at time t. From this, the integrated output $O_0(t)$ can

be obtained as follows for compartment 0:

$$O_0(t) = N_0(0) - N_0(t) = (N_0(0) - T1(t)) - T2(t) \qquad (10.22)$$

where the brackets indicate the order in which to computate. For the other compartments, the total output $O_i(t)$ is

$$O_i(t) = O_{i-1}(t) - N_i(t) = (O_{i-1}(t) - T1_i(t)) - T2_i(t) \qquad (10.23)$$

```
main routine:
- make a copy of the original structure with all contents set to 0.
- create a linear structure.
- while a compartment with initial content > 0 can be found:
    - set the initial amount in the original structure to 0.
    - call the pathfinder routine with the non-empty compartment
      just found as the first and only compartment in the linear
      structure.
- replace the original structure by its copy.

pathfinder routine (recursive):
- compute both contents and integrated output of the last
  compartment in the linear structure at time t, using its total
  outflow rate as λ₁. Add these contents to the contents of the
  corresponding compartment in the copy of the original structure.
- if the integrated output of the current compartment is larger than
  the requested precision then:
    - for all compartments to which the contents of the last com-
      partment flow in the original structure:
      - add the compartment to the "tail" of the linear structure,
        using the outflow rate.
      - call the pathfinder routine.
      - remove the compartment just added to from "tail" again.
- return to caller
```

Text box 1.1: Recursive decomposition of complex structure

10.4. Decomposition of complex structures of interrelated compartments

Any complex structure can be decomposed into a set of structures as shown in Fig.10.2 by the recursive pseudocode in Text box 1.1. The number of resulting structures will be at least the number of compartments with initial contents > 0. The
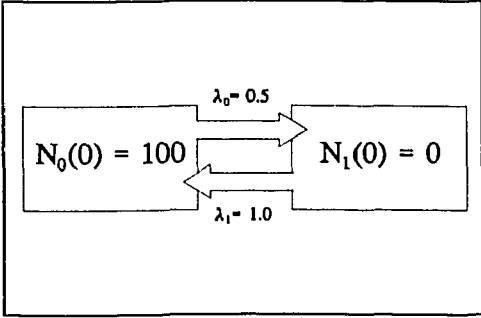
Fig.10.3: Compartmental model for the approach of dynamic equilibrium

resulting structures might get infinitely long and an infinite number of structures might result, if it weren't for the required precision test. The algorithm takes the initial contents from the compartment it starts with and then travels through the complex structure by all possible paths, leaving some of the initial contents of the first compartment behind in each compartment it passes. It stops travelling along a path when the amount that remains after all deposits has become smaller than the requested precision, or when the path ends.

10.5. Two examples

10.5.1. Dynamic equilibrium

An example of the transition to steady state as encountered when modelling tracer experiments used to study steady-state biological systems, as well as in simple chemical reactions was modelled as shown in Fig.10.3. The contents of the compartments shown were computed at different elapsed times, with the precision requested to be 10^{-5}. The results are shown in Table 10.10. They were verified using the direct solution of the differential equations and found to be correct.

t	N_0	$\dot{N}_1$
0	100.00	0.00
1	74.10	25.90
2	68.33	31.67
5	66.69	33.31
10	66.67	33.33

Table 10.10: Contents of two compartments after different elapsed times.

10.5.2. Secundary activation in Neutron Activation Analysis

For this example, the model shown in Fig.10.2 in combination with realistic parameters for NAA was used. Compartment 0 was set to contain 10^{22} atoms at $t=0$. The atoms have a neutron cross-section of 10^{-28} m^2 and are irradiated at a neutron flux of 5.10^{16} m^{-2}s^{-1}, resulting in $\lambda_0 = 5.10^{-12}$ s^{-1}. The halflife of the atoms in compartment 1 was set to 10 hours, so $\lambda_1 = 1.9254.10^{-5}$ s^{-1}. The atoms in compartment 2 have a relevant neutron cross-section of 10^{-25} m^2, so $\lambda_2 = 5.10^{-9}$ s^{-1}. Finally, the halflife of the

atoms in compartment 3 is 1 year, so $\lambda_3 = 2.1965.10^{-8}$ s^{-1}.

Compartment	Content
0	$1.000.10^{22}$
1	$2.105.10^{15}$
2	$2.215.10^{15}$
3	$3.576.10^{11}$
4	$1.116.10^{9}$

Table 10.10: Contents of five compartments after irradiation.

The contents of compartments 0 to 4 were computed for an irradiation time of 24 hours, with the precision requested to be 1. The results are shown in Table 10.10, and were found to be consistent with the results obtained using common approximations.

At IRI, the algorithm is routinely used in the system for Instrumental Neutron Activation Analysis. It works with the actual numbers of atoms and the required precision is set to 1000 atoms. Computing what happens during activation, decay and two measurements with all elements present in our nuclear catalogues (284 activation reactions and 333 decay relations) takes 9 seconds on a 25 MHz 68040 CPU.

10.6. References

1. H. Bateman, Proc. Cambridge Phil. Soc. 15 (1910) 423
2. K.W. Skrable, C. French, G. Chabot and A. Major, Health Phys. 27 (1974) 155
3. J.N. Hamawi, Nucl. Techn. 11 (1971) 84
4. R.I. Scherpelz, A.E. Desrosiers, Health Phys. 40 (1981) 905
5. R.E. Miles, Nucl. Sci. Eng. 79 (1981) 239

Part III

Holistic Interpretation
of
Gamma-ray Spectra
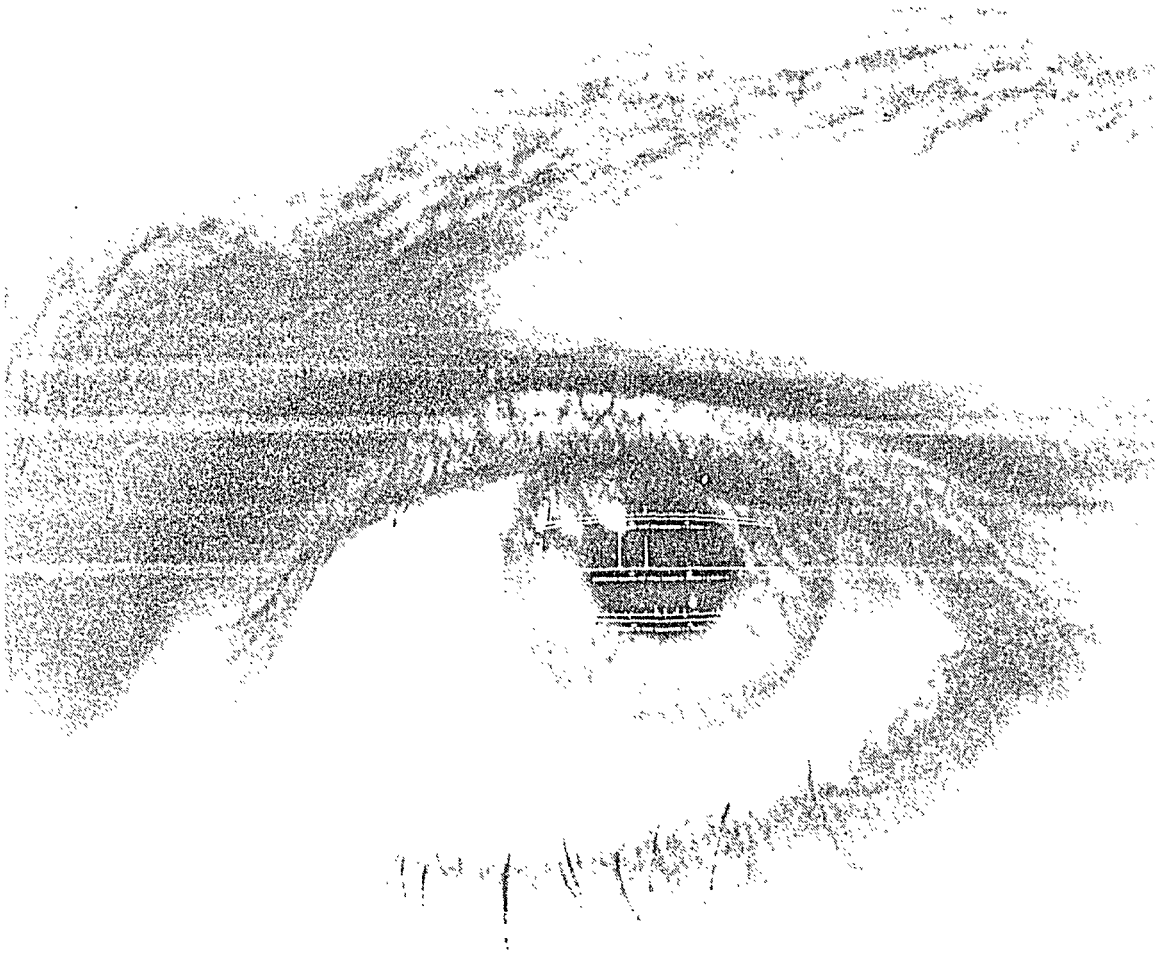
Chapter 11
Interpretation Techniques

11.1. Introduction

In the past, when only low-resolution NaI(Tl) detectors with their inherently low energy resolution were available for the measurement of gamma-ray spectra, it was generally considered to be possible only to reduce the measured spectrum if it was very simple. To interpret a complex spectrum, the channel contents in the measured spectrum were sometimes considered to be a linear sum of the spectra of the radio-nuclides, and linear least squares (LLS) methods were used to get at the radionuclide activities. Previously measured spectra of every expected radionuclide were required.

A complicating factor was the possibility that the gain of the amplifier could change between the measurement of the reference radionuclide spectra and the measurement of the sample. The radionuclide spectra had to be stored in a format independent of amplifier gain, and decisions about the energy-calibration of the sample spectrum had to be made in the interpretation stage.

Another complication was the influence of the matrix of the sample itself on the shape of the spectrum. Because of the low energy resolution, Compton edges hardly could be distinguished from photopeaks, and Compton scattering in the sample influenced these edges. LLS techniques therefore were not popular for interpretation purposes. Mostly, only the areas of clearly visible peaks were estimated and a concentration calculated from these single peaks. This "characteristic peak" method largely subsisted when the Ge detector became available.

As compared to peak fitting techniques, little attention has been paid in the past to the interpretation of gamma-ray spectra since the introduction of the high-resolution Ge detector. Most efforts were directed to the deconvolution of multiplets in an attempt to render the interpretation step trivial. Techniques were developed to interpret spectra without spectral interferences[1]. In the relative standardization method, standards of the elements of interest are co-irradiated and the concentrations are obtained from the ratios of the peak areas of the spectra of the standards and those of the sample. The SAMPO 90[2] spectrum interpretation code is based on this. It is a questionable practice however, because of possible spectral interferences with elements unexpectedly present in the sample[3]. In some cases, the risk can be reduced by measuring the sample more than once and comparing the half-life of the peak area in question to the half-life of the radionuclide supposedly yielding it.

A distinction is usually made between qualitative and quantitative interpretation of the spectrum. The qualitative interpretation consists of decisions about the

112

presence of radionuclides in the sample, the quantitative interpretation results in radionuclide activities. Generally, the qualitative interpretation is the most difficult part of the process.

All attempts previously made to automate the qualitative interpretation were based on the methods used by analysts with NaI(Tl) experience. The rules-of-thumb developed from experience were implemented in computer algorithms[4,5], even the deduction schemes as employed by the analysts were incorporated in the computer programs[6,7]. Some modern programs, like GAUSS VIII[8], leave the difficult decisions to be made up to the user. Accepting the human approach as unavoidable, and thinking of the interpretation process as being "by nature iterative", Aarnio et al.[9] resort to the so-called "expert system" to solve their problems for them. In the present study, an attempt was made to develop techniques that use no rules-of-thumb and are non-iterative. These techniques are described in Chapter 12.

All interpretation techniques mentioned above interpret the spectrum in terms of radionuclide activities first, and compute the concentrations of the elements from the activities later on. Since the radionuclide spectra can be considered to be the invariant basic components of the spectra, this seems to be the logical way to do it. In INAA, however, a single element may yield multiple radionuclides upon activation, and the relative abundances of these radionuclides after irradiation and decay are all known. *The newly developed technique described in the next chapter therefore interprets the spectra in terms of elemental concentrations right away.* Moreover, all spectra obtained from a single sample are interpreted simultaneously. The extra information thus coming into play may render the deconvolution of multiplets superfluous, maybe even disadvantageous. The results of an experimental test of this hypothesis are presented in Chapter 14.

At first sight, the quantitative interpretation is much more straightforward than the qualitative interpretation. However, remarkably few authors regard the reduced spectra as a linear sum of basic components and solve the resulting system of linear equations by LLS methods[5]. Most, like Korthoven[6,7], persist in using subjective techniques to get the activities of the radionuclides.

The technique described in Chapter 12 does interpret using LLS methods. All information present in the reduced spectra is used. Inconsistent information is detected, any uninterpreted information shows up.

The quality of any analytical technique is not only determined by the accuracy and precision of the actual value of a single analytical result, but also by the estimation of its accuracy and precision. To correctly estimate these, all sources of random and systematic variation in the technique must be known quantitatively. Heydorn[10] describes how to test the adequacy of the estimation of this precision.

In the literature, differences can be found in the details of error propagation. No technique described gives a correct approach to the propagation of the errors to the

final concentrations. Neither does the technique described in this thesis, but a description is given in Chapter 12 of the sources of error, how they should ideally be propagated and how they are in fact propagated.

The results of a comparison of the new, holistic method of interpreting reduced gamma-ray spectra and Korthoven's method are presented in Chapter 13. In Chapter 15, the results of a similar comparison of the holistic analysis method, not deconvoluting multiplets included, and Korthoven's method as a whole are presented. The quality of the results are compared both with respect to the reported concentrations and with respect to their reported uncertainties.

11.2. References

1. R.MacDonald, A.Robertson, T.J.Kennett, W.V.Prestwich, J.Radioanal.Chem. 23 (1974) 123-130.
2. P.A.Aarnio, M.T.Nikkinen, J.T.Routti, "Automated gamma spectrum analysis for NAA with PC-based SAMPO 90", Proc. 8th Conf. Modern Trends in Activation Analysis, to be published, J.Radioanal.Nucl.Chem.
3. R.R.Greenberg, D.A.Becker, R.M.Lindstrom, "A retrospective look at γ-ray interferences in neutron activation analysis", Proc. 8th Conf. Modern Trends in Activation Analysis, to be published, J.Radioanal. Nucl.Chem.
4. R.Dams, F.Adams, J.Radioanal.Chem. 4 (1970) 311-323
5. R.Gunnink, J.B.Niday, "Computerized quantitative analysis by γ-ray spectroscopy (program GAMANAL), UCRL-51061, vols 1-2 (1972).
6. P.J.M.Korthoven, J.Radioanal.Chem. 15 (1973) 675-682
7. P.J.M.Korthoven, M.de Bruin, J.Radioanal.Chem. 35 (1977) 127-137
8. R.G.Helmer, M.H.Putnam, C.M.McCullagh, Nucl.Instr.Meth. A242 (1986) 427-436
9. P.A.Aarnio, T.T.Hakulinen, "Expert system identification for gamma spectrum analysis", Proc. 8th Conf. Modern Trends in Activation Analysis, to be published, J.Radioanal.Nucl.Chem.
10. K. Heydorn, K. Norgard, Talanta 20 (1973) 835-842

Chapter 12
The Holistic Interpretation of Reduced Gamma-ray Spectra

12.1. Introduction

A reduced gamma-ray spectrum can be regarded as the linear sum of the possible basic components. These components can be radionuclide spectra (when activities are to be result of the interpretation) or combinations of radionuclide spectra (when fluxes or concentrations of elements are to be the result). The resulting set of equations can be written as

$$a_i = \sum_j c_j M_{ij} \tag{12.1}$$

or in vector-matrix notation

$$\vec{a} = M\vec{c} \tag{12.2}$$

where

a_i = the area of the ith observed peak area
M_{ij} = the contribution to the area of the ith observed peak from entity j
c_j = the value of entity j (concentration or flux)

If as many peak areas as concentrations are involved, the set of equations can simply be solved by

$$\vec{c} = M^{-1} \vec{a} \tag{12.3}$$

where M^{-1} is the inverse of the square matrix M. If more entities are involved than independent peak areas, no unique solution can be found. This situation can usually be avoided by identifying the undistinguishable entities and removing them from the set of equations. If more peak areas than entities are involved, linear least squares (LLS) methods are used to find the optimal solution for the set of equations. If only the a_i have known uncertainties, the LLS solution is given by

$$\vec{c} = (M'WM)^{-1} M' W \vec{a} \tag{12.4}$$

where M' is the transpose of M, and W is a diagonal matrix containing the uncertainties in the a_i.

The uncertainties σ_j in the resulting c_j are given by

$$\sigma_j^2 = (M'WM)_{jj}^{-1} \tag{12.5}$$

In the interpretation of a typical INAA sample at IRI, two irradiations, three spectra containing up to 200 peaks each and some 70 element concentrations are involved. Not all peaks theoretically present in the spectra will be observed in practice. These "missing" peaks must be dealt with in order to construct the set of equations. The resulting set will be huge and usually cannot be solved because of ambiguities caused by spectral interferences and/or different elements yielding the same radionuclides upon activation. In this chapter, the steps taken to construct the set of equations, to divide it in as many independent subsets as possible, the solution to the ambiguities and the propagation of errors to the final results are described.

The first step in constructing the set of linear equations is the computation of the basic spectra to be expected, using an arbitrary value for the entities to be determined. Next, the peaks in the expected spectra are assigned to the peaks in the measured spectra. The maximal amount of each entity j present in the sample can now be calculated. Both observed peak areas and upper limits for areas of "missing" peaks are used for this. Knowing the maximal amounts, it is possible to check for each observed peak whether the entities, of which a peak was assigned to it, could have contributed significantly to its area. If not, the corresponding M_{ij} can be set to 0.

In case of "missing" peaks, just setting the corresponding M_{ij} value to 0 will not do: The absence of a peak, or rather the upper limit of its area, may be valuable information. If this is the case, an artificial entry is inserted in the list of observed peak areas.

Subsets of equations that can be solved independently of other subsets can be extracted. Solving or fitting such a subset is only possible if the expected spectra contained in it are independent. Undistinguishable entities must be taken care of, and reported later as such.

The end result of all this is a group of manageable subsets of equations that can be solved or fitted to find the best c_j values.

All parameters and values used in this chapter have uncertainties. All of these should be propagated to the final results.

12.2. Computation of basic spectra

In part II of this thesis, all the tools needed for the computation of the basic spectra have been described. The procedure is different for fluxmonitors and samples. In both cases however, the number of disintegrations per radionuclide per measurement to be expected is computed for each entity from rough estimations of its value. Knowing the P values of all peaks in counts/disintegration for each spectrometer, peak areas can be computed. With each peak area, the name of the radionuclide in question is stored.

12.2.1. Computation of basic spectra of the elements for fluxmonitors

A fluxmonitor is a sample of known composition, usually containing only a few target nuclides. The entities to be determined from the spectra of a fluxmonitor are the flux parameters Φ_t, f, α and Φ_f/Φ_t, or a subset of these (Φ_t in the current implementation of the analysis).

Using reasonable estimates for the flux parameters and the known experimental parameters in the history of the fluxmonitor, such as the spectrometer used, irradiation, decay and measurement times, the spectra that are expected as a result of each activation reaction in the flux monitor are computed. The c_j values obtained from the solution of the system of equations indicate to what degree the actual flux differed from the estimated flux. This difference may not be equal for all reactions, because the activation rates may depend on the flux parameters f and α differently. In that case, f and α can be extracted from the c_j values. In the current implementation of the analysis, the use of effective k_1-values necessitates the determination of Φ_t (as defined in Chapter 6) only. The flux parameters f, α and Φ_f/Φ_t are considered to be constant in time. Only the total flux Φ_t is therefore determined from the c_j.

12.2.2. Computation of basic spectra of the elements for samples

Knowing all experimental parameters (i.e. flux parameters, spectrometers used, irradiation, decay and measuring times), it is possible to compute the basic spectrum for each element in the periodic system. The estimated value of the concentration of each element is set to 1. After interpretation, the c_j values will directly represent concentrations.

12.3. Assignment of peaks

As described in part I of this thesis, the final result of the reduction of the gamma-ray spectra is a list of peak energies, energy ranges, areas and uncertainties of the areas (Chapter 4). A compressed version of the channel contents in the spectrum remaining after removal of the photopeaks is also available.

For each peak expected, a matching peak in the measured spectrum is searched for. A match is found if the theoretical energy of the expected peak falls within the energy range of a observed peak. Each expected peak gets a pointer referring to the observed peak, or is tagged if no matching peak was found.

Some peaks with small energy separations within the basic spectrum of a single element or radionuclide may be assigned to the same peak in the measured spectrum. In this case, the areas of the expected peaks are added and the expected peaks merged to a single expected peak.

12.4. Determination of maximal amounts

From each match between an expected and an observed peak, a c_{ij} value and its uncertainty σ_{ij} can be calculated based on the assumption that only entity j contributes to the area a_i of the observed peak.

If no match was found for the expected peak, estimates for the μ and σ (both expressed as peak areas) of the error function describing the probability of detecting the peak at that position in the spectrum can be obtained as described in Chapter 3. This μ and σ are now used as peak area and uncertainty to obtain a c_{ij} value and its uncertainty. In this way, the c_{ij} values with their uncertainties obtained from each peak can be interpreted in the same way: The probability of the actual amount of the entity exceeding $x_{ij} = c_{ij} + 2.\sigma_{ij}$ is 2.5% for each peak. The minimum of all x_{ij} values found for entity j is defined as its maximal amount, and the corresponding c_{ij} and σ_{ij} values are stored for future use.

The algorithm finding these maximal amounts uses different initial maximal amounts in different cases. For flux monitors it is set to 1, which corresponds to the estimated flux parameters. For INAA samples, the initial value depends on available information on sample composition. This information is usually absent, in which case the initial maximal amount is set to 1, which corresponds to a concentration of the element of 100%.

12.5. Elimination of insignificant contributions

Now that maximal amounts are known for each entity j, maximal contributions of the entities to the observed peak areas can be computed. If this maximal contribution is less than the (Poisson) uncertainty of the observed peak area, the contribution is considered insignificant. It is also considered insignificant if the contribution is less than 1% of the observed peak area. This decision is based on the fact that virtually no k_1-values (describing the activation rate) are known with better accuracy than 1% and few P values (describing the detector efficiency in counts/disintegration) are known better than that either. Expected peak areas therefore have an uncertainty that always exceeds 1%.

The M_{ij} values corresponding to the insignificant contributions are set to 0. This may lead to entities j with all M_{ij} values set to 0. For these entities, only the maximal amount x_j is reported as the upper limit of the c_j value, and the entity will neither be considered in the following steps, nor in the solving or fitting of the sets of equations finally obtained.

12.6. Insertion of missing peaks in the measured spectra

The absence of expected peaks in the measured spectrum was already used in the computation of the maximal amounts. Now it must be decided whether to set the corresponding M_{ij} value to 0 or to insert artificial peaks in the list of observed peaks.

Setting the M_{ij} value to 0 corresponds to a loss of information which could only deteriorate the final interpretation results. It would not bias the interpretation results however. Insertion of peaks in the list of observed peaks will bias the interpretation result. This bias can be suppressed setting the uncertainty in the area of the inserted peak to some high value. However, the absence of peaks in the measured spectrum should pull the final c_j values down if the absence of the peak is statistically improbable.

The problem is solved by using the μ and σ of the peak search error function also applied in the determination of maximal amounts as the area and uncertainty of the peak to be inserted. Here, μ is the area of a peak with a probability of 50 % to be detected, and $\mu + 2\sigma$ is the area of a peak with a probability of 97.5 % to be detected. Now, the maximal contribution of entity j to this hypothetical peak is calculated. If this contribution is less than the uncertainty σ of the peak to insert, it is considered insignificant, is not inserted and the corresponding M_{ij} value is set to 0. If the maximal contribution is significant, the peak is inserted in the measured spectrum, tagged as artificially inserted.

12.7. Extraction of independent subsets of equations

The first peak not artificially inserted is taken from the list of observed peak areas. Next, all entities contributing to this peak are collected. The procedure is repeated for all peaks these entities contribute to, as long as they are not artificially inserted peaks. The procedure as a whole is recursive and ends when no new peaks and entities are added in a single run. All peaks included in the subset of equations thus found are removed from the list of observed peaks, so after a series of calls, the list will be empty and no more subsets are left to be extracted. The exceptions for artificially inserted peaks are made to avoid the linking of essentially independent subsets.

12.8. Identification of undistinguishable entities

Sometimes, it is impossible to distinguish between elements by their basic gamma-ray spectrum. It may be that the two elements yield the same radionuclide

when activated, or that they may yield radionuclides with undistinguishable gamma-ray energies. The presence of such elements renders the finding of a solution to the set of equations ambiguous. In the process of finding a LLS fit to the equations, a non-invertible matrix is encountered. To avoid this, undistinguishable entities must be removed from the set of equations before attempting to find a solution for it.

For each pair of entities a and b, the basic spectra as contained in the M matrix are compared. It is decided that the entities are undistinguishable if all remaining expected peaks stem from the same radionuclide. If this is not the case, the ratios r_i of the expected peak areas M_{ia} and M_{ib} of the two entities are calculated. Next, all ratios are compared. If any two ratios are statistically different with a reliability of 95%, the entities a and b are considered distinguishable. This is also the case if one of the two expected peak areas is 0.

After the decision of undistinguishability has been made, the average ratio between the expected peak areas is calculated and stored. One of the two entities is removed from the matrix. In the end, the two entities will be reported as undistinguishable but concentrations can be given for both using the average ratio. The analyst will have to interpret such a pair of concentrations as ambiguous: It is either entity a being present with amount c_a, or entity b being present with amount c_b, or a situation in between.

The procedure outlined here only removes halves of pairs of undistinguishable items from the matrix. If the spectra of three or more entities are dependent, the solution will be ambiguous also. This is a very rare situation, but when it occurs, the c_j values determined in the procedure for the determination of maximal amounts are reported for all entities in the matrix, with flags indicating the ambiguity of the results.

12.9. Solving or fitting the subsets of equations

Each subset of equations obtained as described above could simply be solved or fitted using Eq.(12.3), or Eq.(12.4) and Eq.(12.5), if the observed peak areas a_i had uncertainties only. The M_{ij}, however, also have estimated uncertainties, as will be elaborated further in the next section. These uncertainties are propagated to the c_j by computing a first solution as given by Eq.(12.3) or Eq.(12.4). Afterwards, using the c_j just determined, the uncertainties in the M_{ij} can be propagated to the a_i using Eq.(12.1), adding to the uncertainties they already had. Finally, Eq.(12.3) or Eq.(12.4) can be used again to calculate a second solution and Eq.(12.5) to calculate the new uncertainties in the c_j, now including the uncertainties in the M_{ij}. This technique is commonly used when fitting curves to a set of (x,y) data, if both the x and the y values have uncertainties. If the uncertainties in the M_{ij} were too large, it would be

necessary to repeat the process until some convergence criterion is satisfied. In practice, the second set of c_j values is virtually the same as the first. Only the uncertainties finally found in the c_j are larger after the second step. The χ_r^2-value of the second least squares solution, if it exceeds unity, is propagated to the uncertainties of the c_j.

If a single sample was counted twice, the estimated uncertainties in the peak areas a_i should cover the random variation in them. In the first set of concentration uncertainties σ_j, only these peak area uncertainties are accounted for. This means that the first σ_j can be identified as a measure of the reproducibility or precision of a final result c_j. In the second step, systematic errors are accounted for. The second set of σ_j can therefore be regarded as an estimate of the accuracy of the result c_j. Both uncertainties are stored. The accuracy is used when reporting concentrations. The precision is used when comparing results obtained from duplicate samples to test if the results are in control statistically.

It must be said that the recipe for error propagation given above theoretically should only be used when the uncertainties in the M_{ij} are uncorrelated. They are not, and the calculated accuracies σ_j are therefore subject to error. On the other hand, it would be far worse to only report the uncertainties based on the uncertainties in the observed peak areas, as is often done in INAA, because these are generally much smaller than the accuracy of the result. In the next paragraph, this subject is elaborated further.

12.10. Sources of error and their propagation

Each parameter used in the calculation of concentrations has its uncertainty. A discussion of how these uncertainties should be propagated to the M_{ij} and, in the end, to the final concentration, and of how they are in fact currently propagated is given for each parameter.

12.10.1. The effective k_1-constant
The effective k_1-constant actually used in the analysis, defined by

$$k_{1,eff} = \frac{M_c \theta_a \sigma_{eff,a}}{M_a \theta_c \sigma_{eff,c}} \qquad (12.6)$$

consists of atomic mass, isotopic abundance and effective neutron capture cross-section for the activation reaction of interest. Errors in this constant are systematic for each activation reaction. Estimates of these errors are propagated to the uncertainties of the expected peak areas when computing the basic spectra.

If an element can be determined through multiple activation reactions, a weighted average of the concentrations obtained from different reactions should be reported. This is what currently happens if the different activation reactions each yield one photopeak in the spectrum. If a produced radionuclide yields more than one photopeak however, the uncertainty in the k_1-constant is propagated directly to each expected peak area, and the concentration finally reported will be a weighted average of the concentrations that may be calculated from each peak area. The resulting uncertainty in the weighted average will be too small in this case. On the other hand, if there are different activation reactions leading to a concentration and the resulting concentrations disagree, the use of the χ_r^2-value to enlarge the reported uncertainty will correct for this.

12.10.2. f, α, Q_0', and E_r

Since the current system works with effective k_1 values, measured in our own irradiation facilities, these parameters would play a role only if the flux parameters changed and new effective k_1 values would have to be calculated from the old values. When this happens, the uncertainties in Q_0' and α will be propagated to the new k_1 constants.

On the other hand, not monitoring these flux parameters is a source of error in itself.

12.10.3. Half lives

The uncertainties in the tabulated half lives are considered to be negligible as compared to all other sources of error. It is true that a small uncertainty in a half life will become a large uncertainty in the expected peak area after many half lives have elapsed, but the observed area of such a peak will usually have a large uncertainty also. The latter uncertainty will be large enough to render the first negligible. Uncertainties in half lives are therefore not propagated to the final concentrations.

12.10.4. The P value

Two kinds of P values, denoting the probability of detecting a count in the photopeak per disintegration of the radionuclide, are in use in the system.

The first kind, used for coaxial detectors with negligible coincidence summing, is calculated from the gamma-ray abundance of the peak and the photopeak efficiency of the detector. In the past, the gamma-ray abundance was established by calibration using the same photopeak efficiency curve as was used later on to obtain a P value. If the P values are to be calculated for a new coaxial detector, however, published gamma-ray abundances will be used and both the uncertainties in these abundances and the uncertainties in the photopeak efficiency curve must be propagated to the P values.

The second kind is used for well-type detectors. These P values have all been measured directly on the detector of interest. The uncertainties in the P values result from the experimental parameters involved in their determination. It will be very difficult to obtain good estimates for the uncertainties of P values calculated from the efficiency curves of the detector and the decay scheme of the radionuclide as described in Chapter 9. Especially the uncertainties of the established decay scheme itself are a source of error. As yet, no attempt has been made to deal with these uncertainties.

The P value uncertainties are propagated to the final concentrations as described in the preceding section. They are thus, incorrectly, considered to be uncorrelated.

12.10.5. Neutron flux

A total neutron flux is calculated from the spectrum of each comparator irradiated along with the samples. The only uncertainties propagated to this flux are the uncertainty in the P values of the observed peaks and the uncertainty in the observed peak area. The effective k_1-constant of the comparator is no source of error because all other k_1-constants have been measured relative to this k_1-constant.

When a sample is to be interpreted, the flux values of the comparators positioned in the same column of the irradiation container are used to obtain an estimate of the neutron flux the sample was irradiated with. Polynomial fitting is used for this[1]. The unexplained variation in the measured comparator flux values is used as an estimate for the uncertainty in the flux value to be used for the analysis of the sample.

An exception is made when too few comparators have been irradiated along with the sample. In this case, the average observed flux and its standard deviation are used for the analysis of the sample. If only one comparator was irradiated, the uncertainty in the flux is set to 15 %, corresponding to the maximal variations normally found within an irradiation container.

The uncertainty in neutron flux is propagated to the final concentrations just as the uncertainties in the effective k_1-constants. As is the case with the k_1 uncertainties, this leads to a slight underestimation of the concentration uncertainties. It would be better to add the flux uncertainty to the concentration uncertainties in a final step, but this becomes a complicated task if more than one irradiation was performed. Furthermore, the flux uncertainty is usually less than 1 % and therefore not a predominant source of variation.

12.10.6. Observed peak area

The observed peak area uncertainty consists of two parts: The counting geometry variation and the Poisson variation. The second is obtained in the spectrum reduction. Counting geometry variation will have the same effect on all observed peak areas, the Poisson variation affects each peak individually. Currently, only the Poisson

uncertainty is propagated to the final concentrations. If a sample has been counted only on one detector, this may lead to an underestimation of the concentration uncertainties. If the sample has been counted on more than one detector, and the concentrations that could be obtained from each spectrum disagree, the χ_r^2-mechanism will compensate for the omission.

12.11. References

1. M.Blaauw, M.J.J.Ammerlaan, P.Bode, Int.J.Appl.Rad.Is. <u>44</u> (1993) 547-551

Chapter 13
Experimental Comparison of Two Interpretation Techniques

13.1. Introduction

In this chapter, an experimental comparison is made between the results of the holistic approach for the interpretation of INAA gamma-ray spectra and the "characteristic peak" approach. To this end, the results obtained for characteristic samples with the INTERPRET program, described in the previous chapter, were compared to the results obtained with the ICPEAX[1,2] program.

Because the ICPEAX program is an integrated package that unavoidably performs spectrum reduction as well as interpretation, the reduced spectra as obtained from ICPEAX were submitted to the INTERPRET program. The nuclear catalogues used with the two programs were identical. Any difference in interpretation results must therefore be attributed to the interpretation algorithms themselves.

13.2. Experimental

13.2.1. Sample preparation

Four samples were prepared by weighing amounts of approximately 100 mg of the certified reference materials Buffalo River Sediment (NBS-2704) and Coal Fly Ash (NBS-1633a), 200 mg of Citrus Leaves (NBS-1572) and 150 mg of Pig Kidney (BCR-186) in high density polyethylene capsules (diameter 8 mm, height 10 mm, manufacturer Free University of Amsterdam). The snap-on lids were heat sealed to the capsules. It was experimentally verified that the capsules had negligible blank values; they contained a significant amount of chrome of 0.67 μg only. Four zinc flux monitors of 2 mg each were also prepared.

Each sample was paired to a fluxmonitor, the pairs were stacked in a column, and wrapped in heat-sealed plastic foil. The column of capsules was packed in a high density polyethylene irradiation container.

13.2.2. Irradiation and measurement

The irradiation was performed in the BP3 pneumatic irradiation facility of the Hoger Onderwijs Reactor of the Interfaculty Reactor Institute. The irradiation end of this facility is located aside the reactor core in the water reflector. Thermal neutron flux in this facility is in the order of $4.5 * 10^{16}$ $s^{-1}.m^{-2}$ and an irradiation time of 1.5

hours was applied.

After about 6 days decay time, the gamma-ray spectra of the irradiated samples were measured during 1 hour on a coaxial Ortec Ge(Li) detector, absolute photopeak efficiency $2.8*10^{-3}$ for the 1332 keV photopeak of ^{60}Co, in a vertical dipstick configuration. The sources were placed above the detector, in a 4 cm source to end-cap geometry. The bottom of the capsules was facing the detector. After 35 days decay time, the samples were measured again during 30 minutes using a well-type Philips Ge(Li) detector, with an absolute photopeak efficiency of 4.5 % for the 1332 keV photopeak of ^{60}Co. The samples were placed directly on the bottom of the cryostat well.

The spectrometers were equipped with a computer controlled automatic sample changers. To monitor deadtime and pile-up, a 25 Hz pulser was used to generate a peak in the high energy part of the spectra where background is negligible.

13.2.3. Spectrum analysis

The gamma-ray spectra of both samples and fluxmonitors were reduced by the ICPEAX program. The reduced spectra were interpreted both by the ICPEAX and by the INTERPRET program, using identical information, such as nuclear catalogues and efficiency curves. Both programs are based on the single-comparator method, both can use zinc as the comparator element.

The ICPEAX program cannot interpret more than one reduced spectrum at a time. The results obtained from the interpretation of the two spectra of each sample were therefore combined afterwards. If a specific element was reported for one of the spectra only, the corresponding concentration was used. If an element was reported from both spectra, the value with the smallest reported uncertainty was used. The INTERPRET program interpreted the two spectra of each sample simultaneously.

The concentrations reported were compared with the certified concentrations in two ways. The ratio r of measured and certified concentrations was calculated with

$$r = \frac{c_m}{c_c} \tag{13.1}$$

where c_m and c_c are the measured and the certified concentration, resp.

The standardized difference z was computed with

$$z = \frac{c_m - c_c}{\sqrt{\sigma_m^2 + \sigma_c^2}} \tag{13.2}$$

where σ_m and σ_c are the absolute uncertainties (one standard deviation) in measured and certified concentration, resp. If the certificate listed a concentration without an

uncertainty, the relative uncertainty in the certified concentration was set to 25 %.

Both ICPEAX and INTERPRET reported copper in all reference materials. Copper always is a difficult element to determine using the protocol as described, because the longer lived radionuclide resulting from the activation of copper only contributes to the annihilation photopeak, to which many other elements contribute as well. The problem resides in the P value (see Chapter 7) catalogues. Annihilation P values have never been measured at IRI for many radionuclides, and the presence of any of these nuclides will therefore interfere with the copper determination. As a result, the results for copper were all nonsensical and were therefore disregarded.

Finally, a χ_r^2-value was calculated for each sample and each interpretation program as the average squared z value of the certified elements.

13.3. Results

13.3.1. Citrus Leaves (NBS-1572)

The results obtained for the certified elements from the Citrus Leaves sample are shown in Fig.13.1. The χ_r^2-values for ICPEAX and INTERPRET are 17.9 and 3.9, resp. The very high value for ICPEAX is mainly due to the erroneous europium concentration reported by this program. This concentration was obtained from the observed, as yet unidentified 1408 keV photopeak erroneously assigned to ^{152}Eu, even though the much more intense 122 keV photopeak of the same radionuclide was not found in the spectrum.

Apart from the certified elements shown in Fig.13.1, the INTERPRET program reported Cu, Ge, Ru, Ta and Th for a total of 22 elements (the presence of Ge and Ru, however, is dubious), whereas the ICPEAX program also reported Cu, Ge and Th, for a total of 15 (Ge dubious). The Ge concentrations stem from the possibly incorrect deconvolution of the La-Ba multiplet at 242 keV.

Apart from europium, the two programs performed approximately equally well for the 15 elements reported by both programs.

13.3.2. Buffalo River Sediment (NBS-2704)

The results obtained from this material are shown in Fig.13.2. The χ_r^2-values for ICPEAX and INTERPRET are 1.9 and 1.4, resp. The ICPEAX program reported 22 elements, the INTERPRET program 26. Apart from the certified elements shown, both program reported Cu, Ge and Yb. INTERPRET was able to solve the Sc-Cr-Ti and the Sm-Gd interference, ICPEAX was not.

13.3.3. Pig Kidney (BCR-186)

The results obtained from this material are shown in Fig.13.3. The χ_r^2-values for
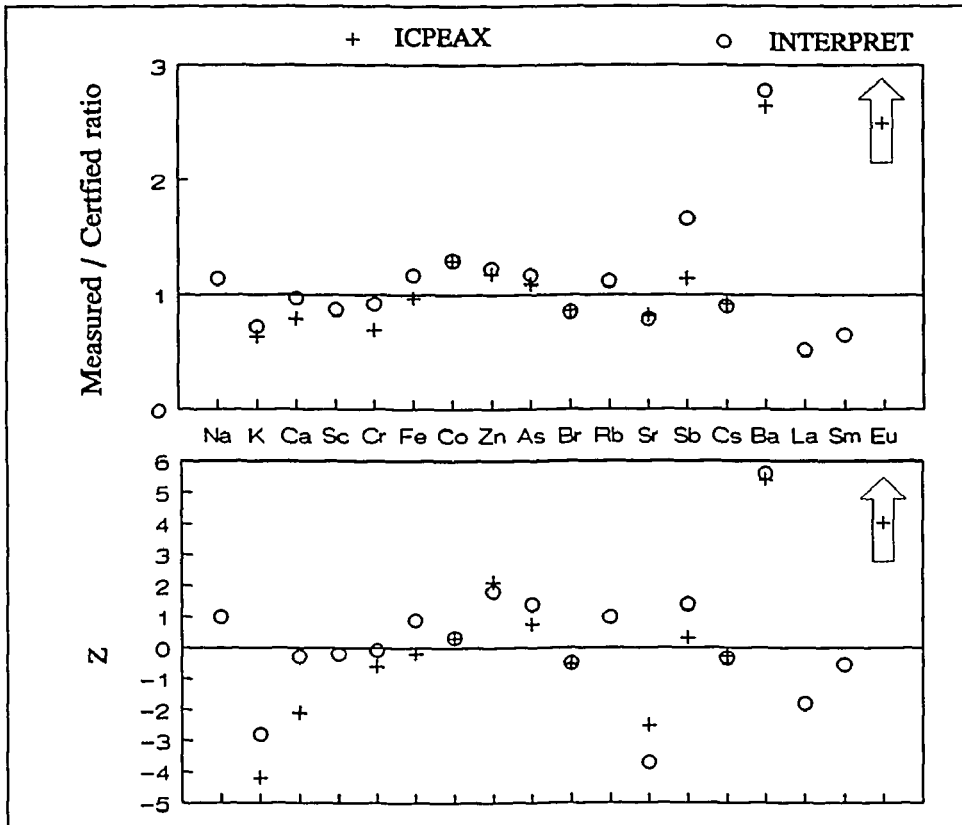
Fig.13.1: Results from the two interpretation programs for Citrus Leaves. The arrows indicate the ICPEAX results for europium: The ratio was 58, the standardized difference 13.

ICPEAX and INTERPRET are 1.1 and 0.3, resp. Apart from the certified elements shown, the ICPEAX program reported K, Co, Cu, Ge, Br, Rb, Eu and Ir for a total of 12 elements (the presence of Ir and Ge, however, is dubious: only one peak of each was observed, both probably being background peaks), the INTERPRET program also reported K, Co, Cu, Br, Rb, and Eu for a total of 10.

13.3.4. Coal Fly Ash (NBS-1633a)

The results obtained from this material are shown in Fig.13.4. The χ_r^2-values for ICPEAX and INTERPRET are 2.5 and 1.0, resp. The high Ge and W concentrations reported by ICPEAX stem from the possibly incorrect deconvolution of the La-Ba-Eu multiplet at 242 keV. ICPEAX reported 24 elements, INTERPRET 26. Again, INTERPRET solved the Sc-Ti-Cr and the Sm-Gd interference.
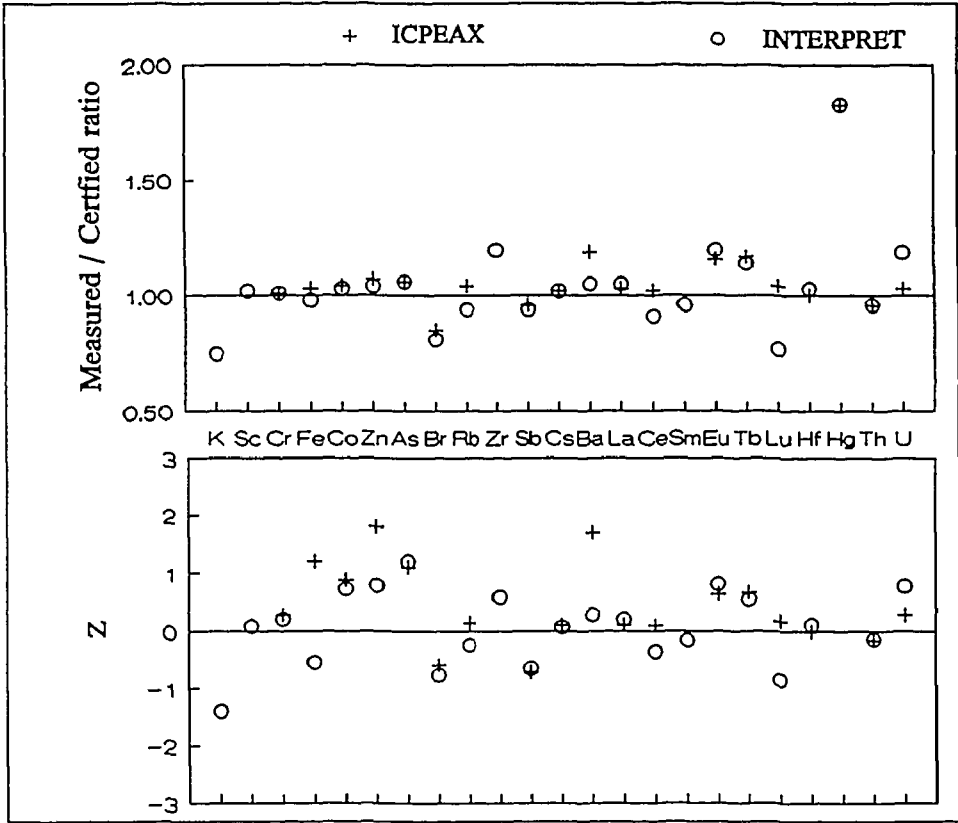
Fig.13.2: Results from the two interpretation programs for Buffalo River Sediment.

13.4. Discussion

The ratios between measured and certified concentrations are approximately equally good for both programs. The ICPEAX program however sometimes reports very high concentrations (Eu in Citrus Leaves, Ge in Coal Fly Ash). These concentrations are based on one observed peak each. The absence of other expected peaks from these elements in the respective spectra was used by INTERPRET to declare these elements undetected, demonstrating the advantage of the holistic approach.

The χ_r^2-values of the INTERPRET program are better because it does not only propagate the statistical uncertainty of the photopeak areas to the element concentrations, as ICPEAX does, but also other uncertainties as described in Chapter 12. Even when reporting exactly the same concentrations, the larger uncertainties as reported by INTERPRET will lead to a better χ_r^2-value. The χ_r^2-values from both programs are not good for Citrus Leaves. Apart from the Eu problem mentioned before, this may be the result of incorrect spectrum reduction results, which were the input for
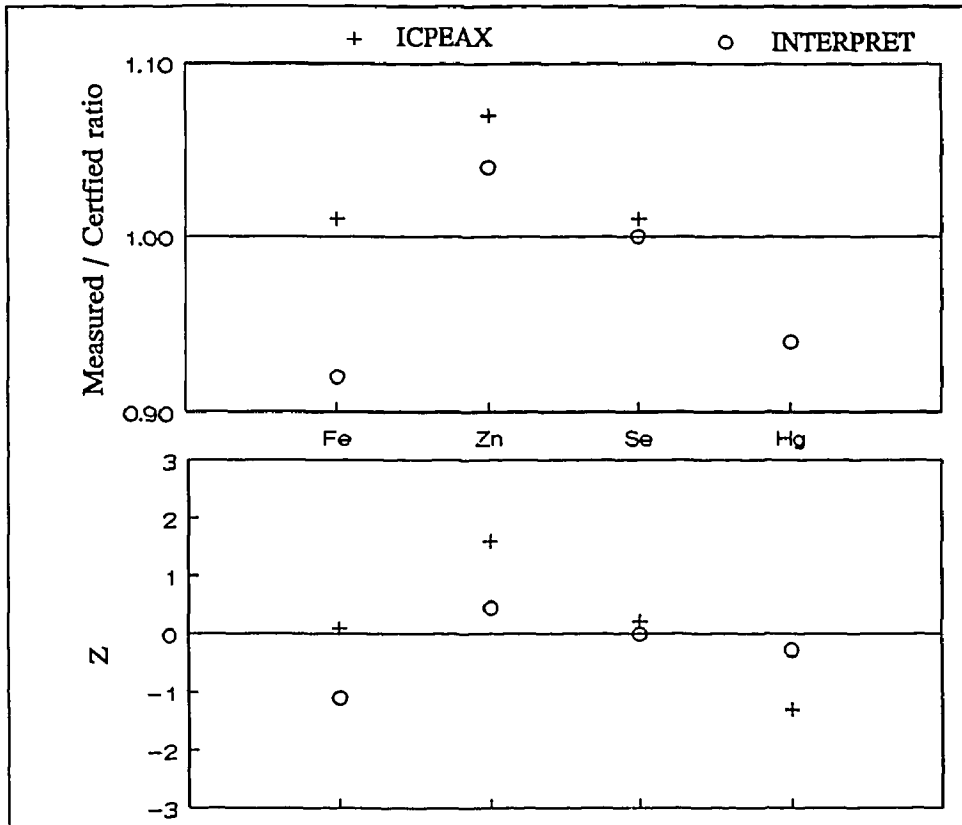
Fig.13.3: The results from the two interpretation programs for Pig Kidney.

both programs.

The INTERPRET program usually reports more elements than the ICPEAX program. Because it interprets two spectra simultaneously, the INTERPRET program can sometimes solve e.g. the Sc-Ti-Cr interference, which the ICPEAX program cannot.

13.5. Conclusions

The holistic INTERPRET approach, where multiple gamma-ray spectra are interpreted simultaneously in terms of element concentrations, makes it possible to automatically solve complex interferences as between scandium, titanium and chromium. A program like ICPEAX, which uses the characteristic peak approach to interpret single spectra in terms of radionuclide activities first and calculate concentrations only later, cannot solve these interferences on its own.
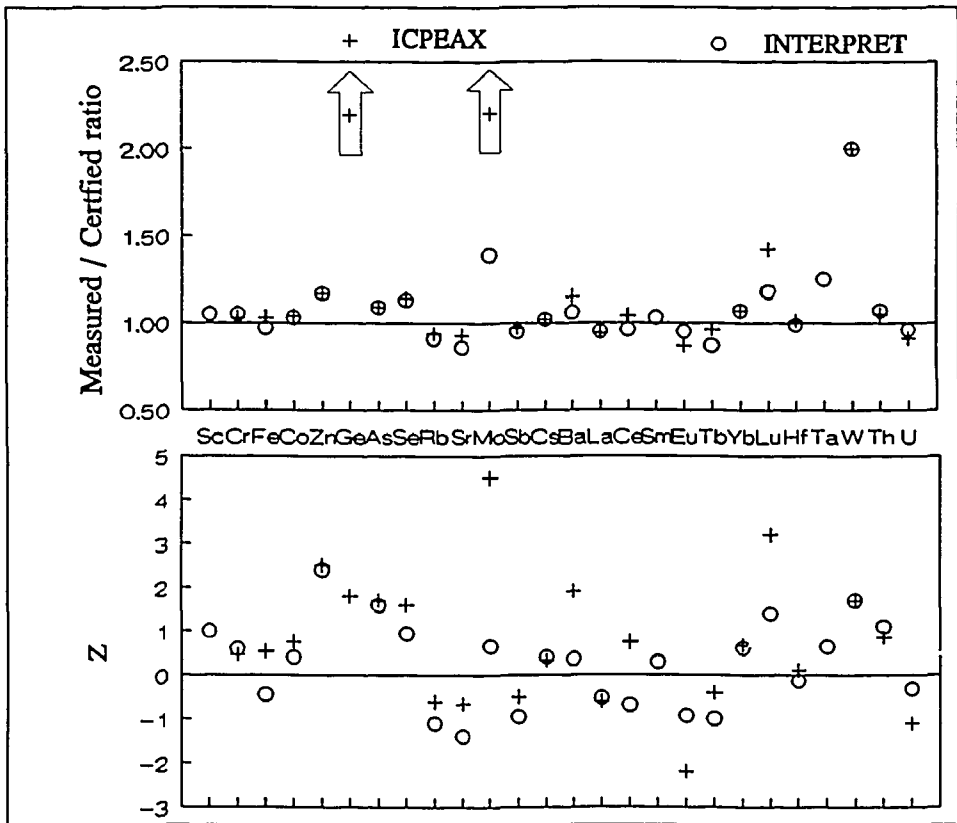
Fig.13.4: The results from the two interpretation programs for Coal Fly Ash. Not shown is are germanium ratio of 130, and the Mo ratio of 5 of ICPEAX.

Moreover, the holistic approach is more robust with respect to spurious peaks: the absence of other peaks expected from the element corresponding to such a peak is used to decide about the presence of the element in the sample.

The better error propagation of the INTERPRET program is clearly demonstrated by the χ_r^2-values of the two programs: Except for Citrus Leaves, these values prove INTERPRET to be in better statistical control.

13.6. References

1. P.J.M.Korthoven, J.Radioanal.Chem. 15 (1973) 675-682
2. P.J.M.Korthoven, M.de Bruin, J.Radioanal.Chem. 35 (1977) 127-137

Chapter 14

Multiplet Deconvolution as a Cause of Unstable Results in Gamma-ray Spectrometry for INAA

14.1. Introduction

As was explained in Chapter 3, multiplet deconvolution may be an inherently unstable process. Minor differences in sample composition might therefore lead to major differences in the analysis results if multiplet deconvolution is applied in the reduction of the gamma-ray spectra obtained from the samples. In this chapter, the hypothesis is tested that integrating multiplets and subsequently treating them as single peaks improves the reproducibility of the analysis results as compared to the results obtained with multiplet deconvolution, for characteristic samples as encountered in practice.

To this end, duplicate samples of two reference materials known to yield complex gamma-ray spectra were measured on a well-type detector. The coincidence summing effects and relatively bad peak resolution of a well-type detector increase the complexity of the gamma-ray spectrum even more.

All spectra were reduced by the SPECFIT program, described in Part I of this thesis, and by the ICPEAX[1,2] program, which deconvolutes multiplets. All reduced spectra were interpreted by the INTERPRET program.

The results were compared to the certified concentrations. The results obtained from the duplicate samples were also compared.

14.2. Multiplet deconvolution algorithms and the SPECFIT alternative

All computer algorithms performing multiplet deconvolution perform in similar ways. To begin with, peak positions are located using some peak search algorithm (SPECFIT and SAMPO 90 both use the Routti-Prussin peak search algorithm). The photopeak width and the two tail parameters are taken from a shape calibration previously made. The peak area and the background parameters are estimated from the measured channel contents. If the peaks constituting a multiplet are separated well enough, the peak positions indicated by the peak search algorithm already reveal the presence of the multiplet. In other cases, the decision that more peaks are present in a peak region than were found by the peak search algorithm is made when fitting the multiplet.

In conventional software, such a SAMPO 90[2] and ICPEAX, the multiplet is fitted first with the peaks as found by the peak search algorithm, and afterwards the residuals of the fit are subjected to secondary peak search algorithms. SAMPO 90 uses auto-correlation techniques for this[3], ICPEAX sums the standardized residuals in subsequent channels and decides that an extra peak must be present in the multiplet if the sum exceeds a threshold value. The sequence of fitting and examining the residuals is repeated until the residuals of the fit no longer indicate the presence of undetected peaks.

The SPECFIT program does not detect extra peaks in a multiplet when fitting. This means that a multiplet is fitted as such only if the separate peaks have been observed by the peak search algorithm. The peak width is adjusted in the fit to allow for doublets with very small peak separations. If the χ_r^2-value of the fit exceeds a threshold, the program flags the fit as "bad" and leaves it to the user to determine the combined net area of all peaks in the possible multiplet interactively, as described in Chapter 4.

14.3. Experimental

14.3.1. Sample preparation

Two pairs of duplicate samples were prepared by weighing amounts of approximately 100 mg of the certified reference materials Buffalo River Sediment (NBS-2704) and Coal Fly Ash (NBS-1633a) in high density polyethylene capsules, as descibed in Chapter 13.

14.3.2. Irradiation and measurement

Irradiations conditions were as described in Chapter 13. After about 35 days decay time, the gamma-ray spectra of the activated samples were measured using a well-type Philips Ge(Li) detector, with an absolute photopeak efficiency of 4.5 % for the 1332 keV peak of ^{60}Co, and a resolution of 2.3 keV at that energy.

14.3.3. Spectrum analysis

The gamma-ray spectra of both samples and fluxmonitors were reduced by the SPECFIT program. Multiplet fits in sample spectra flagged as "bad" by the program were integrated manually. The gamma-ray spectra of the samples were also reduced by the ICPEAX program. In the output of this program, peaks constituting multiplets can be recognized.

The reduction results of SPECFIT were interpreted by the INTERPRET program. To eliminate the effects of other differences between the reduction programs than the multiplet deconvolution, the lists of peak positions and areas of the samples

as obtained from SPECFIT were edited: The total areas determined by user interaction were replaced by the deconvolution results of ICPEAX. The resulting lists were interpreted again by INTERPRET.

The concentrations reported were compared with the certified concentrations in two ways. The ratio r of measured and certified concentrations, and the standardized difference z were computed as in Chapter 13. Uncertified elements were not considered.

To compare the results obtained from duplicate samples, the ratios of the concentrations reported for each pair of samples were calculated.

14.4. Results

14.4.1. Buffalo River Sediment (NBS-2704)

In the gamma-ray spectrum of the first sample of this material, six multiplets were deconvoluted by the ICPEAX program and integrated manually in the SPECFIT session. A total of 98 peaks was detected by SPECFIT. The INTERPRET program reported the same elements with and without deconvolution, except for a few elements reported with inaccuracies in excess of 100 %. The interpretation results from the two lists of peak areas and positions, as compared to the certified concentrations, are shown in Fig.14.1. It can be seen that the results obtained for iron, antimony and europium with multiplet deconvolution are less good than those obtained with user multiplet integration.

In the gamma-ray spectrum of the second sample, the same multiplets were found by ICPEAX, and the same elements were again reported by INTERPRET. A comparison of the results obtained from the first and the second sample, both with and without multiplet deconvolution, is shown in Fig.14.2. It can be seen that the reproducibility of the results for antimony and cerium is better when not deconvoluting multiplets.

14.4.2. Coal Fly Ash (NBS-1633a)

In the gamma-ray spectrum of the first sample of this material, eight multiplets were deconvoluted by the ICPEAX program and integrated manually in the SPECFIT session. A total of 129 peaks was detected by SPECFIT. The INTERPRET program reported the same elements with and without deconvolution, except for a few elements reported with inaccuracies in excess of 100 %. The interpretation results from the two lists of peak areas and positions, as compared to the certified concentrations, are shown in Fig.14.3. It can be seen that the results obtained for cobalt, cerium and terbium with multiplet deconvolution are less good than those obtained with user multiplet integration.

Fig.14.1: Measured concentrations obtained with and without multiplet deconvolution as compared to the certified concentrations, both on an absolute and on a standardized scale.

In the gamma-ray spectrum of the second sample, the same multiplets were found by ICPEAX, and the same elements were again reported by INTERPRET, except for antimony, which was not reported with multiplet deconvolution. A comparison of the results obtained from the first and the second sample, both with and without multiplet deconvolution, is shown in Fig.14.4. It can be seen that the reproducibility of the results for zinc, antimony, barium, europium and terbium is better when not deconvoluting multiplets. Antimony was not observed with multiplet deconvolution in the second spectrum because the ^{124}Sb-^{134}Cs doublet at 603 keV was not recognized as a doublet by ICPEAX, and subsequently completely attributed to
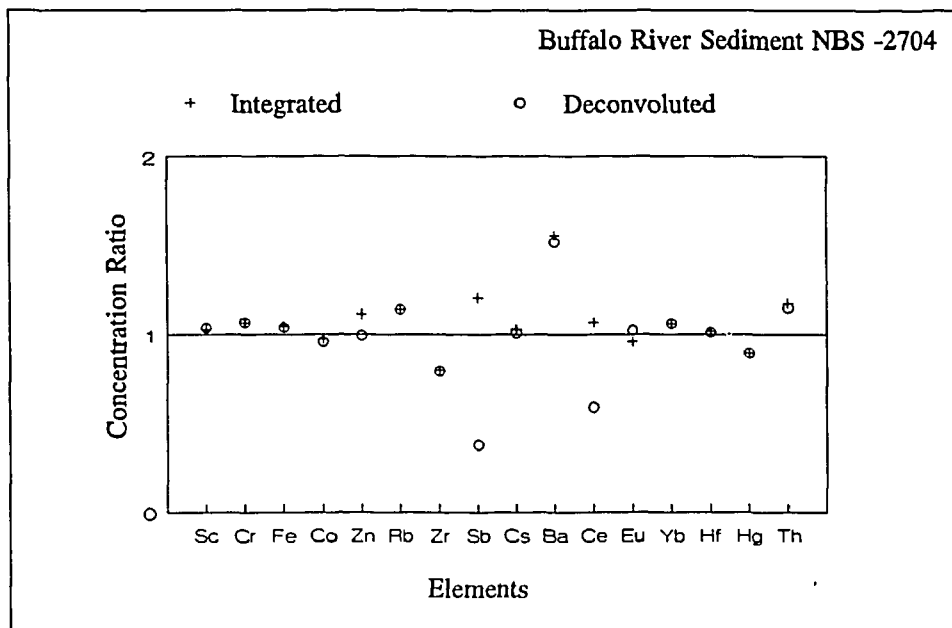
Fig.14.2: Comparison of results obtained from two samples of the same material, both with and without multiplet deconvolution.

cesium by INTERPRET.

14.5. Discussion

The results clearly indicate that user multiplet integration yields better results than multiplet deconvolution in the experimental set-up used. This might be explained by improper functioning of the deconvolution algorithm of ICPEAX, but this improper functioning should lead to high χ_r^2-values of the fits in the multiplet regions, which were not reported by the program. Also, visual inspection of the multiplet regions involved did not indicate erroneous fitting by ICPEAX.

Noise amplification probably is the cause of the trouble, so criteria are clearly needed to decide at what peak separation multiplet deconvolution can safely be attempted. The criterion used in these experiments by SPECFIT *in retrospect* was the detection of the separate peaks by the peak search algorithm: If the peaks constituting a multiplet were separately detected by the peak search algorithm, it was considered to be safe to fit the multiplet as such. If they were not detected separately, they were integrated by the user in the end. The criterion involves both the peak separation and the peak areas, and even though it may not be the optimal criterion, it
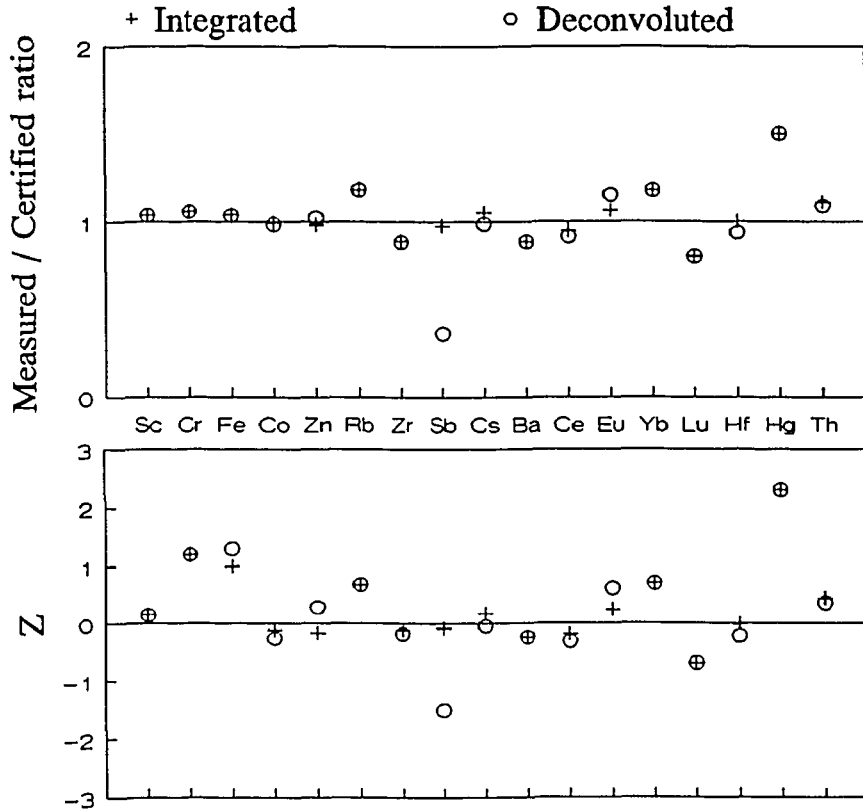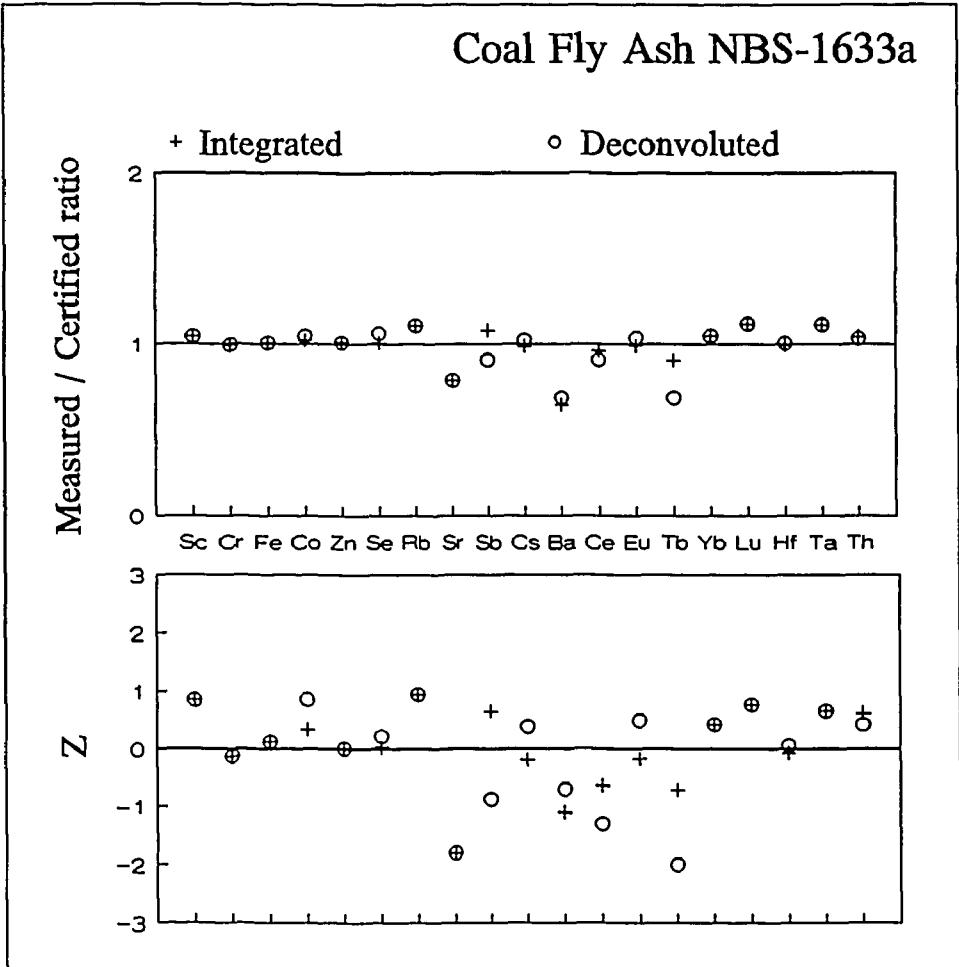
Fig.14.3: Measured concentrations obtained with and without multiplet deconvolution as compared to the certified concentrations, both on an absolute and on a standardized scale.

seems to work well.

Information is lost when a multiplet is integrated by hand and subsequently treated as a single peak. The results demonstrate, however, that the holistic interpretation approach amply compensates for the loss of information resulting from not deconvoluting multiplets.

It is important to note that the INTERPRET program, when interpreting in terms of concentrations, needs less information than programs which must interpret in terms of isotope activities. Only some 70 elements could possibly be seen in a gamma-ray spectrum obtained with INAA, whereas hundreds of radionuclides can be
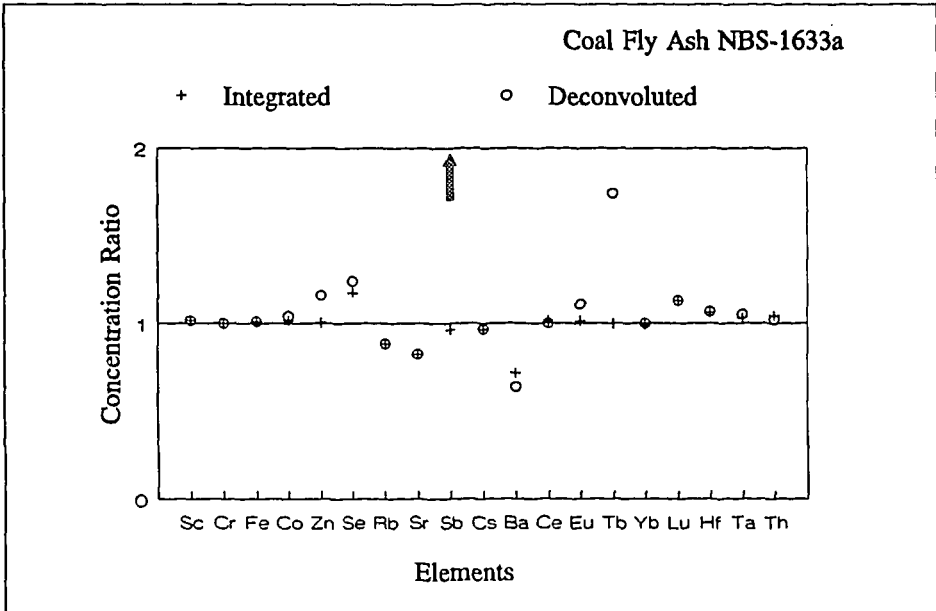
Fig.14.4: Comparison of results obtained from two samples of the same material, both with and without multiplet deconvolution.

measured in general. This means that an INAA gamma-ray spectrum constitutes a system of equations with only 70 unknowns, whereas a gamma-ray spectrum that is to be interpreted in terms of radionuclide activities corresponds to hundreds of unknowns. In INAA, the analysis software can therefore afford to reduce the number of equations by treating multiplets as single peaks. On the other hand, the commercially available software packages all have options limiting the number of radionuclides possibly present in a spectrum. If this option is used, the results of these experiments might apply to gamma-ray spectrometry in general instead of gamma-ray spectrometry for INAA only.

14.6. Conclusions

Probably due to noise amplification, multiplet deconvolution may lead to unstable final interpretation results of INAA if attempts are made to separate peaks which are too close together.

Better results are obtained when determining the total area of the multiplets by user integration, and making the decisions about the division of the area between different elements or radionuclide activities when interpreting. The loss of informa-

tion in the reduced spectrum that results from user integration does not seem to lead to deterioration of the final interpretation results.

A practical criterion to decide whether to deconvolute or not may be the detectability of the separate peaks constituting a multiplet to the Routti-Prussin peak search algorithm.

14.7. References

1. P.J.M.Korthoven, J.Radioanal.Chem. 15 (1973) 675-682
2. P.J.M.Korthoven, M.de Bruin, J.Radioanal.Chem. 35 (1977) 127-137
3. P.A,Aarnio, M.J.Koskelo, P.Zombori, Nucl.Instr.Meth. 184 (1981) 487-492

Chapter 15
Experimental Comparison of Two INAA Software Packages

15.1. Introduction

In this chapter, an experimental comparison is made between the holistic analysis of INAA gamma-ray spectra, including spectrum reduction as well as interpretation, and the characteristic peak method combined with multiplet deconvolution as employed by the ICPEAX program.

The new software consists of separate programs for spectrum reduction (SPECFIT), energy conversion (ENERGY) and interpretation (INTERPRET). The complete new package is called the APOLLO package. Multiplets are not deconvoluted by SPECFIT, and the reduced spectra are interpreted using the holistic method by INTERPRET.

This package has been extensively discussed in the previous chapters, the ICPEAX program has been described by Korthoven et al[1,2].

Four certified reference materials were irradiated, measured twice and the spectra subsequently handled by both packages. The nuclear catalogues used by the two programs were identical. Any difference in results must therefore be attributed to the software packages themselves.

The only difference between the comparison presented in Chapter 13 and the comparison in this chapter is that, in Chapter 13, ICPEAX reduced the spectra to be interpreted by the INTERPRET program, and in this chapter the SPECFIT program was used in combination with the INTERPRET program.

15.2. Experimental

15.2.1. Sample preparation, irradiation and measurement

Four samples were prepared by weighing amounts of approximately 100 mg of the certified reference materials Buffalo River Sediment (NBS-2704) and Coal Fly Ash (NBS-1633a), 200 mg of Citrus Leaves (NBS-1572) and 150 mg of Pig Kidney (BCR-186) in high density polyethylene capsules as described in Chapter 13. Irradiation and measurement conditions were also as described in Chapter 13.

15.2.2. Spectrum analysis

The gamma-ray spectra of both samples and fluxmonitors were reduced and interpreted both by the new software package and by ICPEAX. The packages used

identical information, such as nuclear catalogues and efficiency curves.
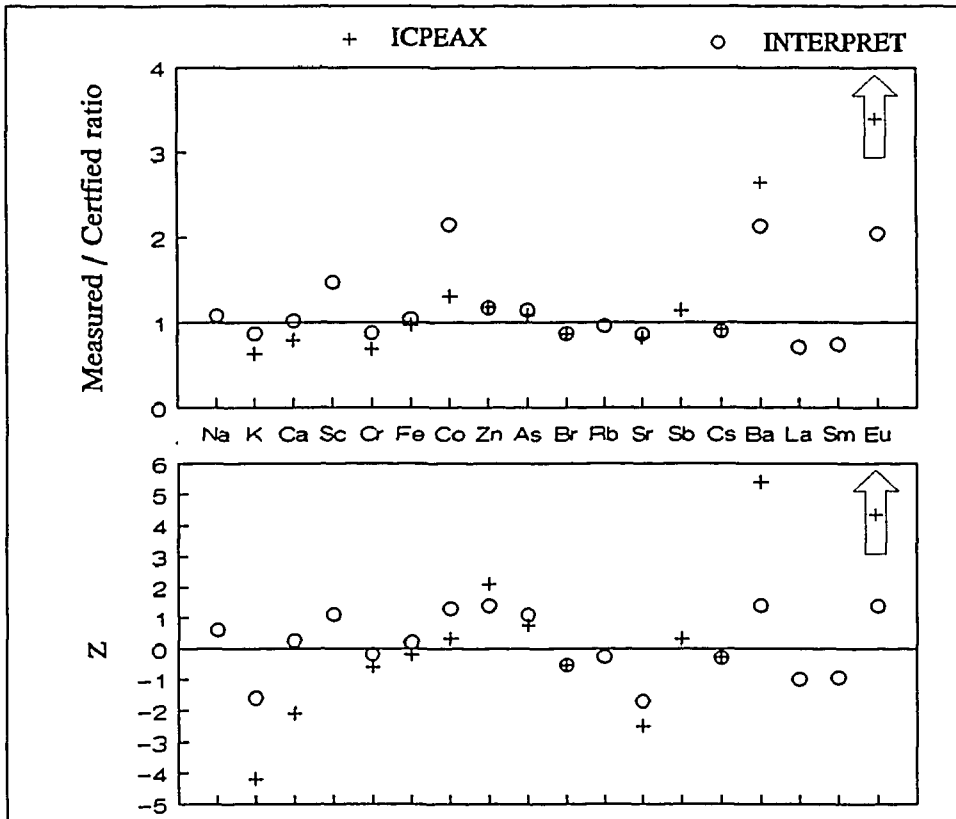
Fig.15.1: Results from the two software packages for Citrus Leaves. Not shown are the ICPEAX results for europium: The ratio was 58, the standardized difference 13.

The ICPEAX program cannot interpret more than one reduced spectrum at the same time. The results obtained from the interpretation of the two spectra of each sample were therefore combined as descibed in Chapter 13. The INTERPRET program interpreted the two spectra of each sample simultaneously.

The concentrations reported were compared with the certified concentrations in two ways. The ratio r, the standardized difference z and the overall χ_r^2 of measured and certified concentrations were calculated as described in Chapters 13 and 14. Copper was reported in all samples by the two software packages, but the results were excluded from this test as explained in Chapter 13.

15.3. Results

15.3.1. Citrus Leaves (NBS-1572)

The results obtained from the Citrus Leaves sample are shown in Fig.15.1. The χ_r^2-values for ICPEAX and the APOLLO package are 17.9 (5.25 if the Eu result is omitted) and 1.1, resp.

Apart from the certified elements, the APOLLO package reported Th and U for a total of 20 elements, whereas the ICPEAX program also reported Ge and Th for a total of 15 (the presence of Ge, as mentioned in Chapter 13, is dubious).

15.3.2. Buffalo River Sediment (NBS-2704)
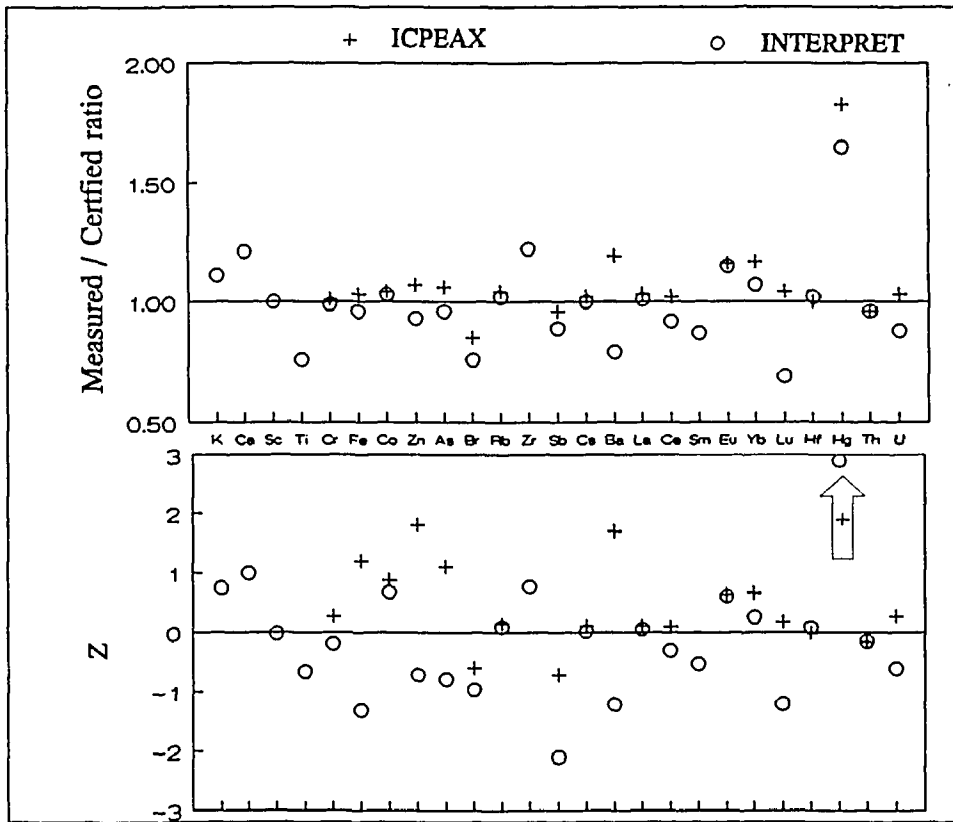
Fig.15.2: Results from the two software packages for River Sediment. Not shown is the ICPEAX standardized difference of 4.9 for molybdenum.

The results obtained from this material are shown in Fig.15.2. The χ_r^2-values for ICPEAX and the APOLLO package are 1.9 and 1.0, resp. Both programs have problems with mercury. Both packages also reported Ge and Tb, for a total of 22

elements for ICPEAX and 27 for the APOLLO package.

15.3.3. Pig Kidney (BCR-186)
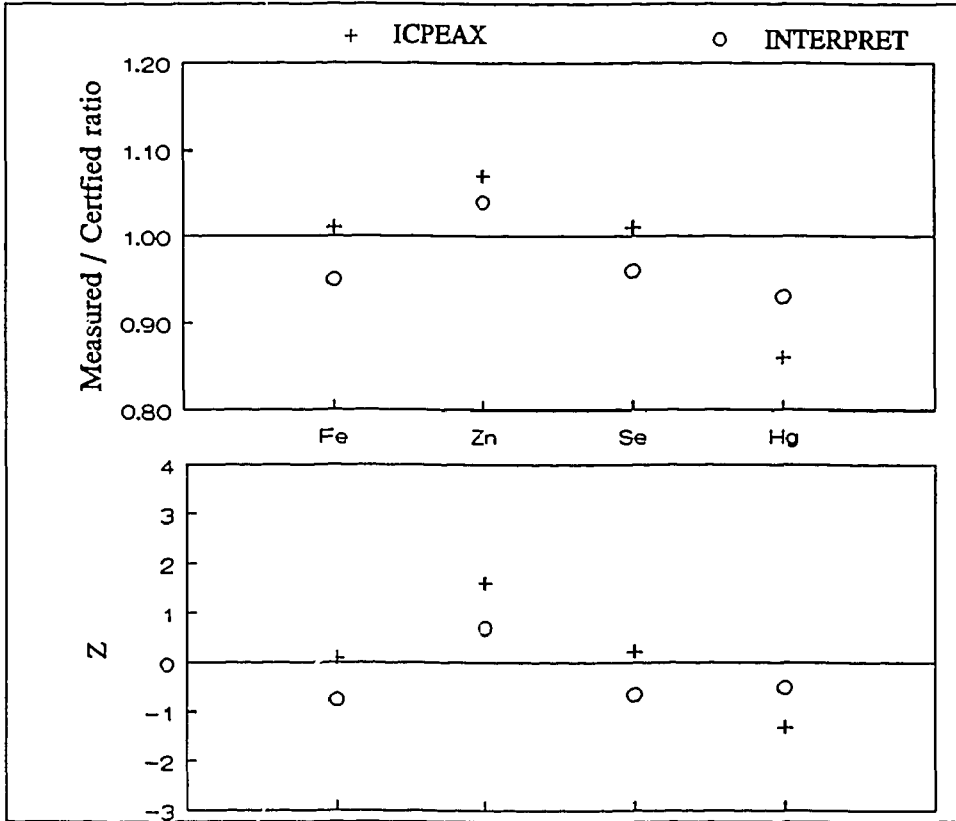
Fig.15.3: The results from the two software packages for Pig Kidney.

The results obtained from this material are shown in Fig.15.3. The χ_r^2-values for ICPEAX and the APOLLO package are 1.1 and 0.4, resp. Apart from the certified elements, the APOLLO reported Na, K, Co, Br, Rb, Cs and Eu for a total of 11 elements, whereas ICPEAX also reported K, Co, Ge, Br, Rb, Eu and Ir for a total of 12 elements (the presence of Ir and Ge, as mentioned in Chapter 13, is dubious).

15.3.4. Coal Fly Ash (NBS-1633a)

The results obtained from this material are shown in Fig.15.4. The χ_r^2-values for ICPEAX and the APOLLO package are 2.5 and 0.7, resp. ICPEAX reported 24 elements, the APOLLO package 30.
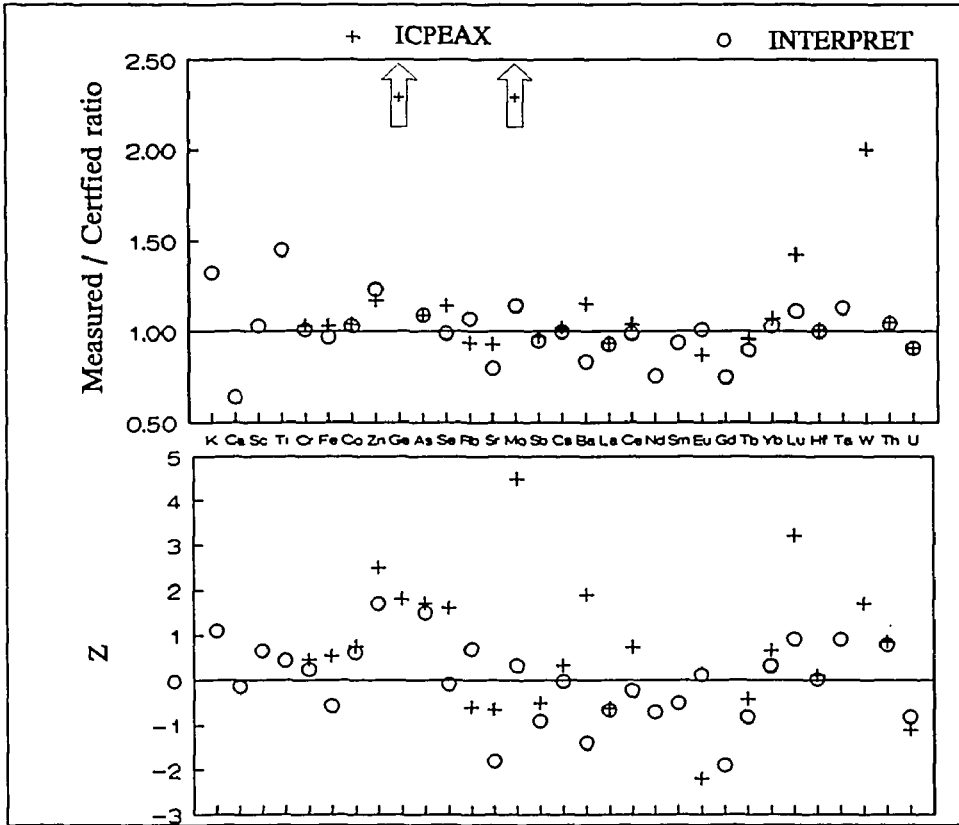
Fig.15.4: The results from the two software packages for Fly Ash. Not shown are the ICPEAX ratios of 130 for germanium and 5 for molybdenum.

15.4. Discussion

When inspecting the results presented in the previous paragraphs, it is obvious that they are similar to the results shown in Chapter 13. The discussion from that chapter also applies here. In Chapter 13 all spectrum reduction was performed by ICPEAX, in this chapter SPECFIT reduced the spectra to be interpreted by INTER-PRET. The ICPEAX final results have remained the same as described in Chapter 13, the APOLLO results have improved. The results therefore indicate that the spectrum reduction components of the two software packages are not equivalent.

The extra influence of noise amplification by multiplet deconvolution in ICPEAX can be observed when comparing the overall χ_r^2 values of the APOLLO results in the two comparisons. These χ_r^2 values, as well as the numbers of elements reported, are shown again in Table 15.1. Moreover, the two dubious elements only found by INTERPRET in conjunction with ICPEAX in Citrus Leaves, i.e. Ge and Ru, may

144   15. Experimental Comparison of Two INAA Software Packages

	NBS-1572 Citrus Leaves	NBS-2704 Buffalo River Sediment	BCR-186 Pig Kidney	NBS-1633a Coal Fly Ash
ICPEAX χ_r^2	17.9	1.9	1.1	2.5
ICPEAX + INTERPRET χ_r^2	3.9	1.4	0.3	1.0
APOLLO χ_r^2	1.1	1.0	0.4	0.7
ICPEAX N	14 (1)	22	10 (2)	24
ICPEAX + INTERPRET N	20 (2)	26	11	26
APOLLO N	20	27	12	30

Table 15.1: χ_r^2 values and numbers of elements reported by the ICPEAX program, the combination of ICPEAX and INTERPRET, and the APOLLO package. Reported elements of which the presence is dubious are listed between brackets.

indicate that multiplet deconvolution can lead to detection of elements not present in the sample. In conjunction with SPECFIT, the APOLLO package proves to be in as good as complete statistical control, as demonstrated by the χ_r^2 values, showing the computed concentrations with their estimated accuracies to agree with the certified concentrations, wheras in conjunction with ICPEAX spectrum reduction, this control was less good.

As will be clear from Chapter 12, error propagation in the interpretation stage is performed only roughly at the moment. As the results in this chapter demonstrate, the system is nevertheless in control statistically where the reported accuracies for reference materials are concerned, as shown by the χ_r^2 values. The error propagation rules used are therefore good enough.

The APOLLO package as a whole generally reports more element concentrations than either the ICPEAX program or the combination of ICPEAX spectrum reduction and the INTERPRET program. This is probably a result of the peak search algorithm being tuned to the peak width more precisely than is the case in the ICPEAX program, as indicated in Chapters 3 and 4.

15.5. Conclusions

The combination of a good peak search algorithm, not deconvoluting multiplets

and the holistic interpretation approach can lead to analysis results that are in complete statistical control, without the loss of results that might be expected from treating the integrated multiplets as single peaks.

As was already concluded in Chapter 13, the holistic interpretation approach allows for the automatic solution of spectral interferences not solved by the ICPEAX program.

15.6. References

1. P.J.M.Korthoven, J.Radioanal.Chem. 15 (1973) 675-682
2. P.J.M.Korthoven, M.de Bruin, J.Radioanal.Chem. 35 (1977) 127-137

Epilogue
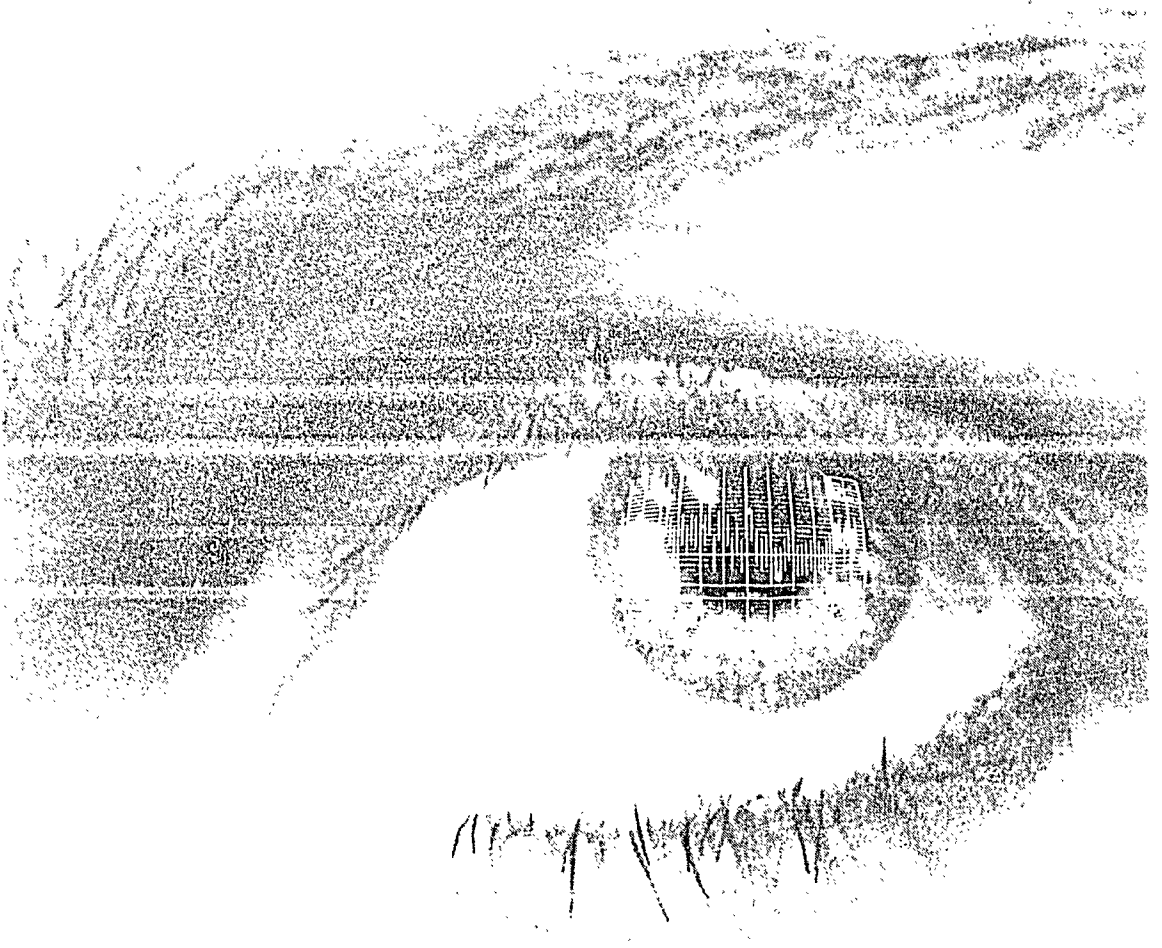
Chapter 16
General Discussion

In this thesis, a holistic approach for the automated analysis of gamma-ray spectra in INAA is presented. This approach was attempted because it was expected to yield better results than interpretation methods based on the use of characteristic peaks only, both quantitatively (more elements reported) and qualitatively (better precision and accuracy). It was even expected to render deconvolution of multiplets superfluous. From the results presented in Chapter 13, 14 and 15, it can be concluded that all this is in fact the case.

The key elements of the holistic approach with respect to precision are the knowledge of the properties of the peak search algorithm, the decision not to deconvolute multiplets (both presented in Part I of the thesis) and the use of all measured net peak areas in the interpretation stage.

The gain in accuracy mainly results from the development and use of the k_1 single comparator method for quantification of the results, as presented in Part II. The holistic interpretation method, yielding mathematically optimal results in case of spectral interferences, also contributes to the overall accuracy.

The increase in the number of reported elements can be attributed to the simultaneous interpretation of multiple spectra, directly in terms of element concentrations, as presented in Part III.

The overall accuracy of the method is estimated to be better than 5 %. This accuracy could be further improved by implementing methods to correct for self-shielding and self-absorption, by improving the accuracy of the data in the catalogues of the k_1-method, and by finding better ways to propagate errors in the interpretation stage. On the other hand, it would be very difficult to establish the accuracy obtained after these improvements: Few elements in reference materials are certified at this level of accuracy, and sample homogeneity will become the limiting factor when testing the reproducibility of the results.

Part I: Reduction of gamma-ray spectra

The physical impossibility of meaningfully deconvoluting multiplets consisting of gaussians that overlap too much, as explained in Chapter 2, is well known. This fact is important in e.g. optics, image restoration techniques and statistical mechanics. Apparently, none of the authors working on gamma-ray spectrum reduction software noticed its importance in the context of gamma-ray spectrometry. In Chapter 14, it is

demonstrated that multiplet deconvolution is not just superfluous: it can lead to unstable results in INAA. The integration method as described in Chapter 3, combined with the interpretation method as described in Chapter 12, yields better results.

The stability of the results of multiplet deconvolution might be improved by the introduction of more knowledge about the spectrum, such as the positions of the peaks to be expected, in the fitting algorithms. The feasibility of this approach has been demonstrated by van Espen et al.[1] for XRF spectra, and by Gunnink for gamma-ray spectra obtained from mixtures of plutonium isotopes[2]. It might be worthwhile to attempt to fit the multiplets in INAA gamma-ray spectra after a preliminary interpretation in terms of element concentrations. The resulting knowledge of the peaks possibly present in the spectrum might reduce the family of solutions available for a multiplet deconvolution to a unique solution.

On the other hand, now that the sources of error mentioned in the introduction of the thesis have been dealt with, the spectrum reduction probably no longer is a predominant source of error. Other sources of error, such as self-shielding and self-absorption, will require attention first.

Part II: Quantification

The k-factor based single comparator methods for INAA were developed to circumvent the imprecise knowledge of physical parameters: The detector efficiency ϵ, the gamma-ray abundance γ and the effective neutron capture cross section σ_{eff}. In the original method, the constant constituted by these parameters, the atomic mass M and the isotopic abundance θ was determined experimentally relative to that of the comparator nuclide for a specific irradiation facility, detector and counting geometry. High accuracy was achieved at the cost of little versatility. Versatility with respect to spectrometers was partly obtained by the introduction of the detector efficiency curve and the removal of ϵ from the k-factor. The k_{Zn} is an example of such a k-factor. Versatility with respect to irradiation facilities was achieved by the introduction of parameters characterizing the neutron flux energy distribution, and the replacement of σ_{eff} by the thermal neutron capture cross section σ_0. The result is the k_0-factor. Even more versatility with respect to spectrometers was obtained using the decay scheme of the radionuclides in conjunction with multiple detector efficiency curves to describe the coincidence summing effects, and the removal of γ from the k_0. The result is the k_1-factor, as described in Chapter 7.

Each time the k-factor lost a parameter, a loss of accuracy might have been the result. To prevent this, methods were specified to accurately determine the stand-alone parameters as well as the remainder of the k-factor. De Corte and his co-workers have been carrying out measurements of the k_0 parameters since 1975. The

definition of the k_0-factor, however, allows for interlaboratory comparison of k-factors. Such a comparison has been carried out for the first time in Chapter 8 of this thesis. The completion of the catalogue of k_0 parameters would be greatly facilitated if more laboratories would carry out comparisons like this and report their findings.

The k_1-method presented in the second part of the thesis is versatile both with respect to irradiation facilities and to spectrometers, even if the spectrometer comprises a highly efficient detector such as a well-type detector. The ease with which well-type detectors can be calibrated using the techniques presented in Chapter 9 may promote their use for single comparator INAA in years to come. The same techniques may also prove useful when correcting for self-absorption of gamma-rays in the sample. The transmission probability as a funtion of photon energy can be determined even in the presence of severe coincidence effects.

The accuracy of the γ values as computed from the decay schemes of the nuclides can be checked using highly efficient detectors. Well-type detectors are especially suited for this purpose because of their insensitivity with respect to counting geometry and angular correlations between photons emitted in cascade. Once these checks have been carried out, the k_1 will be as accurate as the k_0 now is.

The parameters M and θ are generally well known. The only other parameter remaining in the k_1 is σ_0. This implicates that accurate knowledge of k_1-factors results in accurate knowledge of σ_0 values.

The catalogues of k-method parameters can be regarded as a set of relations between the nuclear parameters involved. These relations or constraints can be used to determine a new set of nuclear parameters, optimized in the least squares sense. The intention to carry out this enterprise was announced by Fleming at the international k_0 users workshop in October 1992[3].

The pattern emerging from the history of the k-factor leads to the prediction that, in the future, maximum versatility will be achieved by abandoning the k-factor methods in favour of the absolute standardization method. By that time, the determinations carried out by the INAA community will have contributed to a knowledge of the nuclear parameters involved as complete as required to make the absolute standardization method for INAA as accurate as the relative standardization method is now.

Part III: Holistic interpretation of gamma-ray spectra

The simultaneous, holistic interpretation of multiple spectra allows for the resolution of interferences like the Sc-Cr-Ti interference, as demonstrated in Chapter 13. The results presented in Chapter 15 proves the combination of the holistic approach and not deconvoluting multiplets to be in control statistically.

150

The linear least squares method mathematically is the only correct way to find a solution for the system of linear equations as represented by a reduced gamma-ray spectrum in INAA. The LLS approach was already implemented by Gunnink as early as 1972, only a few years after the Ge detector had allowed for the reduction of gamma-ray spectra[4].

Some of the reasons why other scientists working on INAA failed to adopt this approach may be the following: The methods developed for the analysis of NaI gamma-ray spectra tended to persist. INAA by the relative standardization method, which still is frequently used, allowed for the computation of element concentrations from the ratio of two peak areas. Correction for interference was necessary only rarely and performed by *ad hoc* methods. The characteristic peak method for the interpretation of gamma-ray spectra obtained in multi-element INAA was a logical extension of the algorithms applied in the relative standardization method. Also, knowledge of the gamma-ray spectra of the radionuclides, their relations and half lives was insufficient. The interpretation of all peaks in the spectrum was therefore practically impossible. The treatment of undetected peaks when setting up the system of linear equations in Gunnink's method was primitive, as was the virtually absent error propagation of the uncertainties in the expected peak areas to the final element concentrations.

The results obtained using the holistic approach demonstrate that the currently available knowledge of the gamma-ray spectra of the radionuclides, as well as the knowledge of activation reactions and activation rates is now complete enough to make the approach work. Other key factors are the mathematical modelling of the properties of the peak search algorithm as presented in Chapter 4, and the methods for error propagation as described in Chapter 12.

Implementation

The software described in this thesis was implemented on nine networked Hewlett-Packard/Apollo workstations[5]. UNIX Sys5.3 was selected as the operating system and C as the programming language. The software consists of 6.10^4 lines of source code, divided in approximately a hundred modules performing specific tasks. Some modules have already been ported to IBM PC compatibles.

Several programs in the software package have not been described in this thesis. These programs mostly perform administrative and quality control related tasks, such as comparisons of results obtained from reference materials. All programs use the same menu-based user interface. Most information can be obtained from the system in graphical form.

The system became operational in 1991. It services nine spectrometers, four comprising coaxial gamma-ray detectors, three comprising well-type gamma-ray detectors and two comprising α-ray detectors. Several thousands of samples haven been analyzed since, mostly by analysts after a software training period of just one day. In the near future, the system will also control a new gamma-ray spectrometer for very big samples and analyze the spectra obtained from these samples. This will involve large self-shielding and self-absorption corrections.

The system has proved to be highly reliable. Early in 1993, the independent Dutch STERLAB certification institute considered it to satisfy the criteria specified in the European norm EN 45001 for quality assurance, accrediting the INAA group at IRI as the first universitary analytical laboratory in The Netherlands, possibly the first INAA laboratory in the world.

References

1. P. van Espen, H. Nullens, F. Adams, Nucl.Instr.Meth. 142 (1977) 243-250
2. R.Gunnink, "MGA: A Gamma-Ray Spectrum Analysis Code for Determining Plutonium Isotopic Abundances", UCRL-LR-103220, Vol.1 (1990).
3. R.F.Fleming, "Least Squares Evaluation of a Complete and Consistent Set of k_0 Factors", Proc.Int.k_0 Users Workshop, Ghent (1993).
4. R.Gunnink, J.Niday, "Computerized Quantitative Analysis by γ-Ray Spectroscopy (program GAMANAL), UCRL-51061, vols 1-2 (1972)
5. M.Blaauw, R.M.Lindstrom, J.Radioanal.Nucl.Chem. 169 (1993) 443-452

Summary

Neutron activation analysis (NAA) allows for the determination of a large number of chemical elements with a high degree of sensitivity and accuracy in a variety of materials. By irradiation with neutrons, radionuclides are formed from most of the elements. When measuring the activated sample using gamma-ray spectrometry, the nature of the induced radioactivity yields qualitative information on the composition of the sample. The activities of the individual radionuclides are a measure of the amounts of the related elements.

Until the mid-sixties, the limited energy resolution of the available gamma-ray detectors allowed for selective measurement of individual radionuclides only after the sample had been subjected to chemical separations. The introduction of the germanium semiconductor detector around 1965 offered the possibility of spectrometric separation of the radionuclides. Such instrumental neutron activation analysis (INAA) involves only the irradiation of the sample, the measurement of one or more gamma-ray spectra and the analysis of the spectra.

The subject of this thesis is the computerized analysis of the gamma-ray spectra in INAA. This analysis can be separated in three parts: the conversion of the spectra to information on gamma-ray energies and their relative intensities (spectrum reduction), the determination of the relation between the intensity of a gamma-ray energy and the amount of the corresponding element present in the sample (standardization) and the attribution of the gamma-ray energies to the elements, including the subsequent computation of the amounts of the elements (interpretation).

A gamma-ray spectrum can be considered to be the linear sum of the gamma-ray spectra of the individual radionuclides present in the sample. Knowing the relative activities of the different radionuclides that may be produced by activation of a single element, a gamma-ray spectrum in INAA can also be considered to be the linear sum of the spectra of the elements. This principle has hitherto not been used in INAA to analyze the spectra by linear least squares methods, using all gamma-ray energies observed in the spectrum. The implementation of this "holistic" approach required that attention be paid to both spectrum reduction, standardization and interpretation. This thesis describes the methods developed for the holistic analysis of gamma-ray spectra in INAA, and presents results of experimental comparisons between the holistic and other approaches.

In the General Introduction, a survey is made of the theoretical basis and the historical development of instrumental neutron activation analysis. Also, the necessity of developing better methods for the analysis of the gamma-ray spectra is discussed.

In Part I, the reduction of the spectra is described. In Chapter 2, a general description of the reduction problem and ways to solve it is presented. The reduction

process consists of the search for peaks in the spectrum and the subsequent determination of their intensities. The statistical characteristics of the peak search algorithm must be known to estimate the detection limits of the method as a whole, and also to make correct decision about the presence of elements in the sample in the spectrum interpretation stage. In Chapter 3, several peak search algorithms are compared and measurements of the characteristics of the selected algorithm are described. In Chapter 4, the techniques used to determine the gamma-ray intensities are described. It is hypothesized that the deconvolution of multiplets (i.e. groups of overlapping peaks) in the spectrum is no longer necessary, or maybe even disadvantageous, when using the holistic approach.

In Part II, the standardization is described. For this, the k_1-method was developed from the k_0-method. The k_0-method is a "single comparator" method, prescribing the irradiation and measurement of the sample together with a single element standard. It also provides a nuclear catalogue specifying the rates of most activation reactions relative to the comparator reaction, as a function of parameters describing the neutron flux energy distribution. Moreover, the k_0-method provides methods to determine the relations between the activities of the radionuclides present in the sample and the gamma-ray intensities observed in the spectrum for moderately efficient detectors. In Chapter 6, a survey is given of the theoretical basis and the history of single comparator methods. In Chapter 7, an alternative for the Høgdahl convention, used in the k_0-method to specify the relation between activation rates and neutron flux parameters, is presented. In Chapter 8, the k_1-constant is presented as an alternative for the k_0-constant. As opposed to the k_0-constant, the k_1-constant allows for the standardization of so-called "sum" peaks often observed in spectra obtained with well-type or other highly efficient germanium detectors. In Chapter 9, a comparison is made between the experimentally determined nuclear catalogue of the single comparator method previously in use at IRI and the nuclear catalogue of the k_0-method. In Chapter 10, novel methods are described to determine the relations between the radionuclide activities and the gamma-ray intensities in the spectrum for highly efficient detectors. In Chapter 11, a newly developed algorithm to compute the relation between the number of disintegrations of a radionuclide during measurement and irradiation time, decay time and measuring time is presented.

In Part III, the holistic interpretation method is described and the results of experimental comparisons with the commonly used "characteristic peak" method are presented. In Chapter 12, a survey is given of the historical development of interpretation methods. In Chapter 13, the holistic method is described. In Chapter 14, a comparison is made between the results obtained with the holistic interpretation method and with the commonly used "characteristic peak" method. In Chapter 15, the results of experimental tests prove the hypothesis to be true that multiplet deconvolution is both unnecessary and disadvantageous when using the holistic approach. In

Chapter 16, a comparison is made between the holistic method for analysis of gamma-ray spectra, as implemented in the new automated system for INAA at IRI, and the method previously employed at IRI. It is concluded that the holistic method can yield analysis results that are in complete statistical control. Also, the holistic approach allows for the automatic solution of spectral interferences, especially when interpreting multiple spectra of a single sample simultaneously.

In the General Discussion, general considerations and future prospects are discussed. It is stated that, to increase the precision of INAA, it will be necessary to correct for self-shielding and self-absorption. Also, it may be worthwhile to deconvolute multiplets after a first interpretation of the spectrum has been made. It is predicted that single comparator methods will transform into absolute standardization methods in the future.

Samenvatting

Met neutronen activeringsanalyse (NAA) kan een groot aantal chemische elementen bepaald worden, met een hoge gevoeligheid en juistheid, in een verscheidenheid aan materialen. Door bestraling met neutronen worden radionucliden gevormd uit de meeste elementen. Bij meting van de activiteit van het bestraalde monster met gamma-spectrometrie geeft de aard van de straling kwalitatieve informatie over de samenstelling van het monster. De activiteiten van de individuele radionucliden zijn een maat voor de hoeveelheid van de corresponderende elementen.

Tot in de zestiger jaren was het alleen mogelijk de activiteit van een specifiek radionuclide te meten na het uitvoeren van chemische scheidingen, omdat de beschikbare gamma-detectoren een te lage energie-resolutie hadden. De komst van de germanium halfgeleiderdetector met zijn hoge energie-resolutie maakte het rond 1965 mogelijk de activiteiten van de verschillende radionucliden spectrometrisch te onderscheiden. Deze instrumentele neutronen activeringsanalyse (INAA) wordt verricht door het bestralen van het monster, het meten van een of meer gamma-spectra en het analyseren van de spectra.

Het onderwerp van dit proefschrift is de gecomputeriseerde analyse van de gamma-spectra voor INAA. Deze analyse kan in drieën gedeeld worden: het omzetten van de spectra in informatie over de gamma-energieën en hun relatieve intensiteiten (spectrum reductie), het bepalen van het verband tussen de gamma-intensiteiten en de hoeveelheid van het overeenkomstige element in het monster (kwantificering), en het toekennen van de gamma-energieën aan de elementen, inclusief het berekenen van de hoeveelheden van de elementen (interpretatie).

Een gamma-spectrum kan beschouwd worden als de lineaire som van de gamma-spectra van de individuele radionucliden in het monster. Als de relatieve activiteiten van de verschillende radionucliden die kunnen ontstaan bij bestraling van één element bekend zijn, kan het spectrum zelfs gezien worden als de lineaire som van de spectra van de elementen. Dit uitgangspunt werd niet eerder toegepast in INAA om, gebruik makend van alle waargenomen gamma-energieën in de spectra, de spectra met lineaire kleinste kwadraten methodes te analyseren. Om deze "holistische" methode te implementeren bleek het noodzakelijk te zijn aandacht te besteden aan zowel de spectrum reductie, als de kwantificering, als de interpretatie. In dit proefschrift worden de methodes beschreven die ontwikkeld werden voor de holistische analyse van gamma-spectra in INAA. Ook worden resultaten gegeven van tests waarin de holistische methode vergeleken werd met andere methodes.

In de Algemene Inleiding wordt een overzicht gegeven van de theoretische basis en de geschiedenis van de INAA. Ook wordt de noodzaak om betere methodes te vinden voor de analyse van de gamma-spectra besproken.

156

In Deel I wordt het reduceren van de spectra beschreven. In Hoofdstuk 2 worden het probleem als geheel en de bekende methodes om het op te lossen geschetst. Het reduceren wordt gedaan in twee stappen: Eerst worden de pieken in het spectrum opgespoord, daarna worden de piekintensiteiten bepaald. De statistische eigenschappen van het algoritme dat de pieken zoekt moeten bekend zijn om de detectiegrenzen van de techniek als geheel te kunnen schatten, en ook om goede beslissingen te kunnen nemen over de aanwezigheid van elementen in het monster bij het interpreteren. In Hoofdstuk 3 worden verscheidene algoritmen vergeleken en de eigenschappen van het gekozen algoritme beschreven. In Hoofdstuk 4 wordt beschreven hoe de intensiteiten van de pieken worden bepaald. Er wordt gesteld dat het deconvolueren van multipletten (groepen overlappende pieken) niet langer nodig is, en misschien zelfs ongewenst, bij het gebruik van de holistische methode.

In Deel II wordt het kwantificeren beschreven. Hiertoe werd de k_1-methode ontwikkeld uit de k_0-methode. De k_0-methode is een zogenaamde "monostandaard" methode die het bestralen van monsters samen met een standaard van een enkel element voorschrijft. De methode verschaft ook een catalogus die het mogelijk maakt te berekenen hoe snel de andere activeringsreacties verlopen ten opzichte van de reactie in de standaard, als functie van parameters die de neutronen energieverdeling beschrijven. Bovendien geeft de k_0-methode technieken om de verbanden tussen de activiteiten van de radionucliden in het monster en de intensiteiten van de pieken in het gamma-spectrum te bepalen, voor niet al te efficiënte detectoren. In Hoofdstuk 6 wordt een overzicht gegeven van de theoretische basis en de geschiedenis van de monostandaard-methodes. In Hoofdstuk 7 wordt een alternatief beschreven voor de Høgdahl conventie, die in de k_0-methode gebruikt wordt om het verband tussen de activeringssnelheden en de fluxparameters te beschrijven. In Hoofdstuk 8 wordt de k_1-constante gedefiniëerd. In tegenstelling tot de k_0-constante maakt de k_1-constante de kwantificering mogelijk van de zogenaamde sompieken die optreden in gamma-spectra die gemeten werden met zeer efficiënte detectoren (bijvoorbeeld putdetectoren). In Hoofdstuk 9 worden de nucleaire catalogi vergeleken van de k_0-methode en van de monostandaard-methode die voorheen op het IRI gebruikt werd. In Hoofdstuk 10 wordt een innovatieve methode beschreven om voor efficiënte detectoren het verband tussen de activiteiten van de radionucliden in het monster en de intensiteiten van de pieken in het gamma-spectrum te bepalen. In Hoofdstuk 11 wordt een computeralgoritme beschreven dat het verband tussen de activiteit van de radionucliden en de bestralings-, wacht- en meettijd kan berekenen.

In Deel III wordt de holistische interpretatie beschreven, en worden de resultaten van experimentele vergelijkingen met de algemeen gebruikte "karakteristieke piek" methode gepresenteerd. In Hoofdstuk 12 wordt een overzicht gegeven van de historische ontwikkeling van de interpretatiemethodes. In Hoofdstuk 13 wordt de holistische methode voor interpretatie beschreven. In Hoofdstuk 14 worden resultaten

die verkregen werden met de holistische methode voor interpretatie vergeleken met die van de "karakteristieke piek" methode. In Hoofdstuk 15 wordt met experimentele resultaten de stelling bewezen dat de deconvolutie van multipletten zowel onnodig als ongewenst is binnen de holistische methode. In Hoofdstuk 16 worden experimentele resultaten, verkregen met de volledige holistische methode als geïmplementeerd in het nieuwe, geautomatiseerde systeem voor INAA van het IRI, vergeleken met resultaten die verkregen werden met het systeem dat er voorheen in gebruik was. Er wordt geconcludeerd dat de holistische methode resultaten op kan leveren die statistisch onder controle zijn. Ook maakt de holistische benadering het mogelijk automatisch interferenties op te lossen, in het bijzonder als meerdere spectra van één monster tegelijkertijd geïnterpreteerd worden.

In de Algemene Discussie worden algemene overwegingen en toekomstperspectieven besproken. Er wordt gesteld dat het nodig zal zijn om te corrigeren voor zelfafscherming en zelfaborptie om de precisie van INAA te verhogen. Ook zou het de moeite waard kunnen zijn om multipletten te deconvolueren nadat een eerste interpretatie van het spectrum gemaakt is. Er wordt voorspeld dat monostandaardmethodes in de toekomst over zullen gaan in absolute methodes voor standaardizering.

List of publications

The following publications correspond to chapters of this thesis:

Chapter 3: M.Blaauw, "*Statistical Properties of a Peaksearch Algorithm for γ-Ray Spectrometry as related to Currie's Detection Limits*", in press, Nucl.Instr.Meth.

Chapter 6: M.Blaauw, P.Bode, M. de Bruin, "*An alternative convention describing the (n, γ)-reaction rate suited for use in the k_0 method of NAA*", J.Radioanal.Nucl.Chem. 152 (1991) 435-445

Chapter 7: M.Blaauw, P.Bode, "*Introduction of the k_f-concept for the Interpretation of Artificial Peaks in k_0 based NAA*", J.Radioanal.Nucl.Chem. 169 (1993) 201-208

Chapter 9: M.Blaauw, "*The Use of Sources Emitting Coincident γ-Rays for Determination of Absolute Efficiency Curves of Highly Efficient Ge Detectors*", Nucl.Instr.Meth. A332 (1993) 493-500

Chapter 10: M.Blaauw, "*A Versatile Computer Algorithm for Linear First Order Equations*", Appl.Radiat.Isot. 44 (1993) 1225-1229

Chapter 14: M.Blaauw, "*Multiplet Deconvolution as a Cause of Unstable Results in INAA*", Nucl.Instr.Meth. A333 (1993) 548-552

The following publications are related to the subject of this thesis:

1. M. de Bruin, M.Blaauw, "*Sources of Error in Analytical Gamma-Ray Spectrometry*",Analyst 117 (1992) 431-434
2. I.Obrusnik, M.Blaauw, P.Bode, "*Comparison of Routine INAA Procedures Based on k_0 and k_{Zn} Standardizations*", J.Radioanal.Nucl.Chem. 152 (1991) 507-518
3. P.Bode, M.Blaauw, I.Obrusnik, "*Variation of Neutron Flux and Related Parameters in an Irradiation Container, in use with k_0-based Neutron Activation Analysis*", J.Radioanal.Nucl.Chem. 157 (1992) 310-312
4. M.Blaauw, R.M.Lindstrom, "*Local Area Networks in NAA: Advantages and Pitfalls*", J.Radioanal.Nucl.Chem. 169 (1993) 443-452
5. M.Blaauw, M.J.J.Ammerlaan, P.Bode, "*Quantification of Sources of Variation in Neutron Activation Analysis*", Appl.Radiat.Is. 44 (1993) 547-551

Acknowledgements

Several persons contributed to this thesis. Some of the chapters are adapted versions of publications written in cooperation with others.

Chapter 6, "The alternative Høgdahl convention", as a publication was written in cooperation with Peter Bode en Marcel de Bruin.

Chapter 7, the "Introduction of the k_1-concept", as a publication was written together with Peter Bode.

Frans de Corte and Luc Moens were so kind as to provide me with their nuclear databases on magnetic media. Jeroen de Goeij was an invaluable, very critical aid in preparing the manuscripts of the thesis and the corresponding publications.

Dankwoord

Hoe meer mensen genoemd worden in een dankwoord, hoe meer er zich gekwetst zullen voelen omdat ze er niet in voorkomen. Ik zal me dus tot het minimum beperken.

Zeergeleerde vader, beste Oebele, en zeergeleerde moes, beste Gertie, jullie zijn het geweest die mij van jongs af aan geleerd hebben systematisch te denken en mij voorzien hebben van een kritische zin en een hardnekkige eigenwijsheid die velen tot wanhoop gedreven moeten hebben, maar een prima basis bleken te zijn voor het in dit proefschrift beschreven werk.

Hooggeleerde promotor, beste Marcel, jij redde mij van een lot als systeemprogrammeur en gaf me een rol in de wetenschappelijke wereld. Ik hoop dat dit proefschrift aan je hooggespannen verwachtingen voldoet.

Hooggeleerde promotor, beste Wim, de relatief weinige uren die wij samen doorbrachten werden ruimschoots goedgemaakt door de baudrate van het door jou te berde gebrachte. Niet gehinderd door een overmaat aan kennis van de INAA wees je feilloos de plekken aan waar ik teveel voorkennis bij de lezer veronderstelde in de vakspecifieke hoofdstukken. En als het over gamma-spectrometrie ging was jij degene die mijn bevindingen in het grote geheel van de signaalverwerking wist te plaatsen.

Hooggeleerd afdelingshoofd, beste Jeroen, waar de heren promotoren mijn verrichtingen soms alleen van grote hoogte volgden en zich meer bezig hielden met de specificaties van het eindprodukt, was jij het die de schroeven en moeren in de gaten hield. Dankzij jou werden de meeste van mijn publicaties voetstoots geaccepteerd. Ik heb veel van je geleerd, en hoop dat je dat ook gemerkt hebt.

Zeergeleerde begeleider, beste Peter, de snelheid waarmee jij de vinger op de zwakke plek wist te leggen als mijn kwadratische optelsommen weer eens niet uit wilden komen zal me altijd blijven verbazen. Je was onmisbaar.

Waarde collega's, jullie gezelligheid en jullie tolerantie als ik weer eens iets veranderd had in de software - wat niet altijd tot betere resultaten leidde - hebben mijn promotietijd tot een zeer aangename periode in mijn leven gemaakt. Ik hoop dat jullie collegialiteit ook in de toekomst zo zal blijven.

Technische Universiteit Delft

Mekelweg 15
2629 JB Delft
Telefoon (015) 78 50 52
Telefax (015) 78 64 22
Telex 38151 butud nl

Aan de leden van de Wetenschappelijke Raad,
Instituutsbestuur en
Interuniversair Overlegorgaan IRI

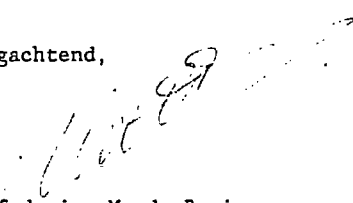| Uw kenmerk en datum	Ons kenmerk	Doorkiesnummer	Datum
—	772-0Z/93u/nb	015-786712	27 oktober 1993
Onderwerp		Onderdeel	
—		directie	

Bij deze doe ik u toekomen een exemplaar van het proefschrift van
drs. M. Blaauw getiteld: The Holistic Analysis of Gamma-ray Spectra in
Instrumental Neutron Activation Analysis.

De verdediging van dit proefschrift zal plaatsvinden op:

Datum: maandag 15 november
Tijd: 16.00 uur
Plaats: Aula van de Technische Universiteit Delft.

Uw aanwezigheid bij de promotie wordt uiteraard zeer op prijs gesteld.

Hoogachtend,

prof.dr.ir. M. de Bruin
wetenschappelijk directeur

STELLINGEN

behorende bij het proefschrift

The Holistic Analysis of Gamma-ray Spectra in Instrumental Neutron Activation Analysis

1. The deconvolution of multiplets in gamma-ray spectrometry is an inherently unstable process due to noise amplification.

   This thesis, Chapter 14

2. The combination of a good peak search algorithm, multiplet integration and the holistic interpretation approach can lead to analysis results that are in complete statistical control, without the loss of results that might be expected from treating the integrated multiplets as single peaks.

   This thesis, Chapter 15

3. The habit of incorrectly regarding the k_0 method of INAA as a single comparator method correctly reflects the commonly incorrect application of this method.

   This thesis, Chapter 5

4. De Corte's decision to determine k_0 constants for elements with very high neutron absorption cross sections such as gadolinium and cadmium using isotopically enriched compounds is in conflict with the basic philosophy of the k_0 method.

   F. De Corte, thesis, Rijksuniversiteit Gent 1987
   This thesis, Chapter 8

5. The IUPAC definition of the absolute photopeak efficiency of a gamma-ray detector as "the ratio between the number of particles or photons counted with a radiation counter and the number of similar particles or photons emitted by the radiation source", "when only considering the events recorded in the photopeak" should be replaced by "the probability of a photon emitted by the source depositing all its energy in the detector crystal".

   M. de Bruin, Pure and Appl. Chem. 54 (1982) 1534
   This thesis, Chapter 9

6. When applying Stuart's formula for neutron self-shielding corrections in neutron activation experiments in the presence of neutron scattering the factor f_0 should be computed using the total neutron cross section instead of the absorption cross section.

   G.W. Stuart, Nuc.Sci and Eng. 2 (1957) 617
   J.C. Stewart, P.F. Zweifel, in "Proceedings of the Second International Confererence on the Peaceful Uses of Atomic Energy", United Nations, New York 16 (1958) 650
   P.F. Zweifel, Nucleonics 18 (11) (1960) 174
   R.F. Fleming, Int.J.Appl.Radiat.Isot 33 (1982) 1263

7. Inelastic collisions between electrons cannot exist except perhaps in high-energy physics. Price's statement that beta-radiation interacts with matter by "inelastic collisions leading to excitation and ionization" is therefore misleading, and De Bruin's statement that beta-radiation interacts with matter by "inelastic collisions with losely bound electrons" incorrect. Instead, one should speak of inelastic collisions between electrons and atoms.

W.J. Price, Nuclear Radiation Detection, McGraw-Hill, 1958
M. de Bruin, P.P. van Rijk (ed.), in "Nuclear Techniques in Diagnostic Medicine",
Martinus Nijhoff Publ., Dordrecht 1986

8. There is no physical explanation for Liz Mackey's experimental results, where the sensitivity for both hydrogen and samarium in PGAA experiments increases with samarium concentration. Her results must therefore be artefacts.

E.A.Mackey, G.E. Gordon, R.M. Lindstrom, D.L. Anderson, Anal.Chem. 64 (1992) 2366

9. The Brookhaven National Laboratory computer database containing evaluated nuclear data (ENDF/B-VI) is outdated and incomplete. To prevent researchers from using these data, the database must be made inaccessible or clearly labelled as unreliable.

10. The ten commandments are in fact only nine.

Exodus 20; Deuteronium 5

11. It is an oversimplification to say that the high speeds achieved in ice skating as compared to running speeds are due to the lesser friction on ice.

12. The claims that oral sex without protection is risky and actual intercourse with a condom is safe, leads to HIV contamination of people believing themselves to be safe.

T. McIlvenna (ed.) "The Complete Guide to Safer Sex", Barricade Books, N.Y. 1992

13. The inability of most human beings to perfectly reproduce a simple act is of vital importance to the acquisition of knowledge.

14. A common photocamera in daylight operation is operated by setting three variables: Shutter speed, diaphragm and focus. Therefore, any computerized camera with more than three variables to be set is user unfriendly.

15. The Groninger intelligentietest (GIT) - the standard intelligence test in the Netherlands - measures the intelligence of men and women on diferent scales. The apparent equality of the intelligence of men and women as observed using this test is therefore fictional.

De Groninger intellingentie test

The author of this thesis was employed by the Interfaculty Reactor Institute of the Technical University Delft in order to give the automated system for Instrumental Neutron Activation Analysis that was previously developed over a period of twenty years a complete overhaul. He Managed to eliminate the need for user interaction in the interpretation stage by developing an all-embracing or "holistic" interpretation approach.

"The combination of a good peak search algorithm, not deconvoluting multiplets and the holistic interpretation approach can lead to analysis results that are in complete statistical control, without the loss of information that might be expected from treating the integrated multiplets as single peaks"

(This thesis, Chapter 15)